

AD-A057 325 DAVID W TAYLOR NAVAL SHIP RESEARCH AND DEVELOPMENT CE--ETC F/G 21/5  
AN INVESTIGATION OF THE PERFORMANCE OF A J52-P-8A ENGINE OPERAT--ETC(U)  
AUG 77 R A HEMMERLY

UNCLASSIFIED

DTNSRDC/ASED-387

NL

1 of 2  
AD  
A057 325



AU No.

DDC FILE COPY

AD A057325

(11) LEVEL II

(9) Final rept. Apr 76-Aug 77



(6) AN INVESTIGATION OF THE PERFORMANCE OF A J52-P-8A  
ENGINE OPERATING UNDER THE INFLUENCE OF  
HIGH BLEED FLOW EXTRACTION RATES

by

(10) Rodney A. Hemmerly

APPROVED FOR PUBLIC RELEASE:  
DISTRIBUTION UNLIMITED

AVIATION AND SURFACE EFFECTS DEPARTMENT

(14) DTNSRDC/ASED-387

(12) 99P

(11) August 1977



(16) F414001

(17) ZF41400001

78 07 28 015  
387 695 JOB

DAVID  
W.  
TAYLOR  
NAVAL  
SHIP  
RESEARCH  
AND  
DEVELOPMENT  
CENTER

BETHESDA  
MARYLAND  
20084

**UNCLASSIFIED**

**SECURITY CLASSIFICATION OF THIS PAGE (When Data Entered)**

REPORT DOCUMENTATION PAGE		READ INSTRUCTIONS BEFORE COMPLETING FORM										
1. REPORT NUMBER <b>DTNSRDC ASED-387</b>	2. GOVT ACCESSION NO.	3. RECIPIENT'S CATALOG NUMBER										
4. TITLE (and Subtitle) <b>AN INVESTIGATION OF THE PERFORMANCE OF A J52-P-8A ENGINE OPERATING UNDER THE INFLUENCE OF HIGH BLEED FLOW EXTRACTION RATES</b>		5. TYPE OF REPORT & PERIOD COVERED <b>Final, Apr 76 - Aug 77</b>										
7. AUTHOR(s)  <b>Rodney A. Hemmerly</b>		6. PERFORMING ORG. REPORT NUMBER										
9. PERFORMING ORGANIZATION NAME AND ADDRESS  <b>David W. Taylor Naval Ship R&amp;D Center Aviation and Surface Effects Department Bethesda, Maryland 20084</b>		10. PROGRAM ELEMENT, PROJECT, TASK AREA & WORK UNIT NUMBERS  <b>Program Element 62241N Project ZF41.400.001 Work Unit 1660-605</b>										
11. CONTROLLING OFFICE NAME AND ADDRESS  <b>Naval Material Command MAT 08T23 Washington, D.C. 20360</b>		12. REPORT DATE  <b>August 1977</b>										
14. MONITORING AGENCY NAME & ADDRESS (if different from Controlling Office)		13. NUMBER OF PAGES  <b>105</b>										
		15. SECURITY CLASS. (of this report)  <b>UNCLASSIFIED</b>										
		15a. DECLASSIFICATION/DOWNGRADING SCHEDULE										
16. DISTRIBUTION STATEMENT (of this Report)  <b>APPROVED FOR PUBLIC RELEASE: DISTRIBUTION UNLIMITED</b>												
17. DISTRIBUTION STATEMENT (of the abstract entered in Block 20, if different from Report)  <b>D D C R E P O R T I P A U G 10 1978 B U N L I M I T E D</b>												
18. SUPPLEMENTARY NOTES												
19. KEY WORDS (Continue on reverse side if necessary and identify by block number)  <table> <tr> <td><b>Uninstalled Engine Performance</b></td> <td><b>Fuel Control System</b></td> </tr> <tr> <td><b>Corrected Engine Data</b></td> <td><b>Engine Acceleration Performance</b></td> </tr> <tr> <td><b>Bleed Flow Extraction</b></td> <td><b>Endurance</b></td> </tr> <tr> <td><b>Thrust Loss</b></td> <td><b>Hot Section Inspection</b></td> </tr> <tr> <td><b>Turbine Temperature Limits</b></td> <td></td> </tr> </table>			<b>Uninstalled Engine Performance</b>	<b>Fuel Control System</b>	<b>Corrected Engine Data</b>	<b>Engine Acceleration Performance</b>	<b>Bleed Flow Extraction</b>	<b>Endurance</b>	<b>Thrust Loss</b>	<b>Hot Section Inspection</b>	<b>Turbine Temperature Limits</b>	
<b>Uninstalled Engine Performance</b>	<b>Fuel Control System</b>											
<b>Corrected Engine Data</b>	<b>Engine Acceleration Performance</b>											
<b>Bleed Flow Extraction</b>	<b>Endurance</b>											
<b>Thrust Loss</b>	<b>Hot Section Inspection</b>											
<b>Turbine Temperature Limits</b>												
20. ABSTRACT (Continue on reverse side if necessary and identify by block number)  <p>The uninstalled performance characteristics of a J52-P-8A engine operating under the influence of bleed flow extraction rates in excess of the standard specification limits were experimentally evaluated. This investigation was undertaken as part of the Circulation Control Wing Flight Demonstrator Program to <del>to</del> assess engine capability of supplying airflow to power the high-lift aerodynamic system incorporated on the Flight</p>												

(Continued on reverse side)

**UNCLASSIFIED**

SECURITY CLASSIFICATION OF THIS PAGE (When Data Entered)

(Block 20 continued)

Demonstrator and (2) define a data base from which higher confidence level analytical short takeoff and landing performance evaluations could be obtained. Results of the investigation indicate that bleed flow extraction rates significantly greater than the standard specification limits are obtainable. An endurance evaluation of the engine operating under the influence of the high bleed flow extraction rates indicates that these extraction rates do not adversely affect the J52-P-8A engine. The results of the endurance evaluation should serve to qualify the J52-P-8A engine for the proposed Flight Test Program.

ADDRESSEES		
NTIS	4-119	<input checked="" type="checkbox"/>
EDD	4-119	<input type="checkbox"/>
TRANSMISSION		<input type="checkbox"/>
AUST		
BY		
DISTRIBUTION BY SECURITY CODES		
Dist.	AVAIL. AND OR SPECIAL	
A		

**UNCLASSIFIED**

SECURITY CLASSIFICATION OF THIS PAGE (When Data Entered)

## TABLE OF CONTENTS

	<u>Page</u>
LIST OF FIGURES.....	iv
LIST OF TABLES.....	vi
NOTATION.....	vii
ABSTRACT.....	1
ADMINISTRATIVE INFORMATION.....	1
INTRODUCTION.....	1
BACKGROUND INFORMATION AND TEST SETUP.....	4
BASIC J52-P-8A ENGINE CALIBRATION RESULTS.....	6
ROTOR SPEED PERFORMANCE.....	7
AIRFLOW AND FUEL FLOW PERFORMANCE.....	8
HIGH PRESSURE COMPRESSOR DISCHARGE CHARACTERISTICS.....	9
BURNER PERFORMANCE.....	9
TURBINE EXHAUST CHARACTERISTICS.....	10
BLEED FLOW CALIBRATION RESULTS.....	12
ROTOR SPEED PERFORMANCE.....	13
AIRFLOW AND FUEL FLOW PERFORMANCE.....	14
HIGH PRESSURE COMPRESSOR DISCHARGE CHARACTERISTICS.....	14
BURNER PERFORMANCE.....	15
TURBINE EXHAUST CHARACTERISTICS.....	15
THRUST PERFORMANCE.....	16
BLEED FLOW QUALITY.....	17
TURBINE INLET AND EXHAUST TEMPERATURE LIMITATIONS.....	19
FUEL CONTROL SYSTEM PERFORMANCE AND OPERATION.....	22
ENGINE ACCELERATION PERFORMANCE.....	24

	<u>Page</u>
<b>ENDURANCE EVALUATION.....</b>	26
<b>HOT SECTION INSPECTION RESULTS.....</b>	28
<b>FIRST INSPECTION REPORT.....</b>	28
<b>SECOND INSPECTION REPORT.....</b>	30
<b>THIRD INSPECTION REPORT.....</b>	32
<b>CONCLUSIONS.....</b>	34
<b>REFERENCES.....</b>	36
<b>APPENDIX - EXPERIMENTAL APPARATUS, INSTRUMENTATION AND TECHNIQUE.....</b>	85

#### LIST OF FIGURES

1 - Schematic of J52-P-8A Engine and Station Notation.....	37
2 - Rear View of Engine Showing Turbine Blades.....	39
3 - Front-Left Side View of Engine Showing Bellmouth Inlet.....	41
4 - Front-Right Side View of Engine Showing General Layout of Bleed Manifold System.....	43
5 - Closeup View of Bleed Manifold System Showing Reducer Pipe, Butterfly Valve and Measuring Nozzle.....	45
6 - Closeup View of Static Tap Installed on Bleed Manifold.....	47
7 - Closeup View of Butterfly Valve, Measuring Nozzle and Collector Pipe.....	49
8 - Low Pressure Compressor-Turbine Unit Speed as a Function of Net Thrust.....	51
9 - High Pressure Compressor-Turbine Unit Speed as a Function of Net Thrust.....	52
10 - Engine Airflow as a Function of Net Thrust.....	53
11 - Fuel Flow Rate as a Function of High Pressure Compressor- Turbine Unit Speed.....	54

	<u>Page</u>
12 - High Pressure Compressor Discharge Pressure Ratio as a Function of High Pressure Compressor-Turbine Unit Speed.....	55
13 - High Pressure Compressor Discharge Temperature as a Function of High Pressure Compressor-Turbine Unit Speed.....	56
14 - Burner Static Pressure Ratio as a Function of High Pressure Compressor-Turbine Unit Speed.....	57
15 - Turbine Exit Pressure Ratio as a Function of Net Thrust.....	58
16 - Turbine Exit Temperature as a Function of Net Thrust.....	59
17 - Low Pressure Compressor-Turbine Unit Speed as a Function of Bleed Flow Extraction Rate.....	60
18 - High Pressure Compressor-Turbine Unit Speed as a Function of Bleed Flow Extraction Rate.....	61
19 - Engine Airflow as a Function of Bleed Flow Extraction Rate.....	62
20 - Fuel Flow Rate as a Function of Bleed Flow Extraction Rate.....	63
21 - High Pressure Compressor Discharge Pressure Ratio as a Function of Bleed Flow Extraction Rate.....	64
22 - High Pressure Compressor Discharge Temperature as a Function of Bleed Flow Extraction Rate.....	65
23 - Burner Static Pressure Ratio as a Function of Bleed Flow Extraction Rate.....	66
24 - Turbine Exit Pressure Ratio as a Function of Bleed Flow Extraction Rate.....	67
25 - Turbine Exit Temperature as a Function of Bleed Flow Extraction Rate.....	68
26 - Net Thrust as a Function of Bleed Flow Extraction Rate.....	69
27 - Bleed Flow Rate as a Function of Net Thrust.....	70
28 - Average Bleed Port Total Pressure Ratio as a Function of Bleed Flow Extraction Rate.....	71

	<u>Page</u>
29 - Individual Bleed Port Total Pressure Ratio and Total-to-Static Pressure Ratio as a Function of Bleed Flow Extraction Rate at Military Thrust.....	72
30 - Individual Bleed Port Total Pressure Ratio and Total-to-Static Pressure Ratio as a Function of Bleed Flow Extraction Rate at 20.3-percent NRT.....	73
31 - Average Bleed Port Temperature as a Function of Bleed Flow Extraction Rate.....	74
32 - Turbine Exit Temperature as a Function of Net Thrust for Various Values of Bleed Flow Extraction Rate.....	75
33 - Turbine Inlet Temperature as a Function of Net Thrust for Various Values of Bleed Flow Extraction Rate.....	76
34 - Steady State Operating Line Performance as a Function of Bleed Flow Extraction Rate.....	77
35 - Speed Governer Droop Slope Performance.....	78
36 - J52-P-8A Engine Acceleration Performance with Zero and Maximum Bleed Flow.....	79
A.1 - Detailed Schematic of the Compressor Bleed Manifold.....	94
A.2 - Detailed Schematic of One of the Individual Bleed Port Collectors.....	95
A.3 - Isentropic Bleed Flow Ratio as a Function of Isentropic Mach Number.....	96
A.4 - Cross-Section Views of the Small and Large Diameter Measuring Nozzles.....	97

#### LIST OF TABLES

1 - General Information for the First Calibration.....	80
2 - General Information for the Second Calibration.....	80
3 - General Information for the Bleed Flow Calibration.....	81

## NOTATION

$A_{bl}$	Bleed port area, in. <sup>2</sup> (cm <sup>2</sup> )
$A_1$	Bellmouth inlet area, in. <sup>2</sup> (cm <sup>2</sup> )
$A_n$	Measuring nozzle area, in. <sup>2</sup> (cm <sup>2</sup> )
$C_1$	Bellmouth inlet pressure recovery factor
$C_n$	Measuring nozzle discharge coefficient
$D_s$	Speed governer droop slope, in. <sup>2</sup> /sec rpm (cm <sup>2</sup> /sec rpm)
$F_n$	Net thrust, lb (nt)
$F_{nm}$	Measured net thrust, lb (nt)
$g$	Gravitational constant = 32.174 ft/sec <sup>2</sup> (9806.65 cm/sec <sup>2</sup> )
$h$	Specific enthalpy, Btu/lb (Btu/kg)
LHV	Lower heating value (JP-5 fuel), Btu/lb (Btu/kg)
$M_i$	Isentropic Mach number
$N_1$	Low pressure compressor-turbine unit rotational speed, rpm
$N_2$	High pressure compressor-turbine unit rotational speed, rpm
PLA	Power level angle, deg
$P_{s_2}$	Bellmouth inlet static pressure, lb/in. <sup>2</sup> (nt/cm <sup>2</sup> )
$P_{s_b}$	Burner static pressure, lb/in. <sup>2</sup> (nt/cm <sup>2</sup> )
$P_{s_{bl}}$	Individual bleed port static pressure (1 through 4), lb/in. <sup>2</sup> (nt/cm <sup>2</sup> )
$\bar{P}_{s_{bl}}$	Average bleed port static pressure, lb/in. <sup>2</sup> (nt/cm <sup>2</sup> )
$P_{t_{bl}}$	Individual bleed port total pressure (1 through 4), lb/in. <sup>2</sup> (nt/cm <sup>2</sup> )
$\bar{P}_{t_{bl}}$	Average bleed port total pressure, lb/in. <sup>2</sup> (nt/cm <sup>2</sup> )

$P_{t_n}$	Measuring nozzle total pressure, lb/in. <sup>2</sup> (nt/cm <sup>2</sup> )
$P_{t_2}$	Bellmouth inlet total pressure, lb/in. <sup>2</sup> (nt/cm <sup>2</sup> )
$P_{t_4}$	High pressure compressor discharge total pressure, lb/in. <sup>2</sup> (nt/cm <sup>2</sup> )
$P_{t_7}$	Turbine exit total pressure, lb/in. <sup>2</sup> (nt/cm <sup>2</sup> )
R	Universal gas constant = 53.3 ft-lb/lb R (191,168 cm-nt/kg R)
$T_{accel}$	Acceleration time to 95.0 percent Military Thrust, sec
$T_{t_{bl}}$	Average bleed port total temperature (R)
$T_{t_n}$	Measuring nozzle total temperature (R)
$T_{t_2}$	Bellmouth inlet total temperature (R)
$T_{t_4}$	High pressure compressor discharge total temperature (R)
$T_{t_5}$	Turbine inlet total temperature (R)
$T_{t_7}$	Turbine exit total temperature (R)
$W_a$	Engine airflow rate, lb/sec (kg/sec)
$W_b$	Bleed flow rate, lb/sec (kg/sec)
$W_{b_i}$	Isentropic bleed flow rate, lb/sec (kg/sec)
$W_f$	Fuel flow rate, lb/sec (kg/sec)
$W_{t_{ca}}$	Turbine cooling airflow rate, lb/sec (kg/sec)
$\Delta F_n$	Test cell thrust correction increment, lb (nt)
$\delta_{t_2}$	Inlet total pressure ratio = $P_{t_2} / 14.696$ lb/in. <sup>2</sup> ( $P_{t_2} / 10.13$ nt/cm <sup>2</sup> )
$\eta_b$	Burner efficiency
$\gamma$	Ratio of specific heats
$\theta_{t_2}$	Inlet total temperature ratio = $T_{t_2} / 519.68$ R

## ABSTRACT

The uninstalled performance characteristics of a J52-P-8A engine operating under the influence of bleed flow extraction rates in excess of the standard specification limits were experimentally evaluated. This investigation was undertaken as part of the Circulation Control Wing Flight Demonstrator Program to (1) assess engine capability of supplying airflow to power the high-lift aerodynamic system incorporated on the Flight Demonstrator and (2) define a data base from which higher confidence level analytical short takeoff and landing performance evaluations could be obtained. Results of the investigation indicate that bleed flow extraction rates significantly greater than the standard specification limits are obtainable. An endurance evaluation of the engine operating under the influence of the high bleed flow extraction rates indicates that these extraction rates do not adversely affect the J52-P-8A engine. The results of the endurance evaluation should serve to qualify the J52-P-8A engine for the proposed Flight Test Program.

## ADMINISTRATIVE INFORMATION

The work reported herein was sponsored by the Naval Material Command (MAT 08T23). Funding was provided under Project ZF41.400.001, Program Element 62241N and Work Unit 1660-605. Engine preparation and testing occurred during the time period November 1976 through January 1977.

## INTRODUCTION

In recent years considerable interest has been given to high-lift technology for fixed wing aircraft. This technology has significant application in carrier-based operations offering such benefits as short takeoff and landing (STOL) overload capability and reduced takeoff and landing distances and associated velocities. Increased pilot visibility, maneuverability, and safety can be achieved by the proper use of high-lift technology. In essence, high-lift technology offers a more reasonable compromise in the area of aircraft design to the problems of high wing loadings required for cruise efficiency and reduced loadings for the low speed flight regime.

One high-lift aerodynamic concept offering considerable promise is the circulation control wing (CCW) which employs the Coanda principle for the simultaneous generation of high lift and drag (References 1-3). The CCW concept involves the conversion of the sharp trailing edge of a cruise configured airfoil into a rounded surface from which a relatively high energy jet sheet of air is blown tangentially from the upper surface. CCW achieves its high-lift potential as the jet sheet adheres to the rounded surface and gives considerable control over the airfoil stagnation points. At higher blowing rates, it has been verified by wind tunnel investigations that the jet sheet can turn nearly 180 deg around the trailing edge before detachment occurs. Viscous mixing of the jet with the lower surface free stream provides negligible thrust recovery and offers significantly higher drag levels than do the blown or jet flap concepts. This characteristic offers considerable advantage during a power approach.

The CCW concept is currently scheduled for full-scale flight evaluation by modifying an A-6A aircraft to accommodate the CCW system (References 4-5). This Circulation Control Wing Flight Demonstrator Program is a joint effort involving the Navy and the Grumman Aerospace Corporation as prime contractor. The objective of this program will be to demonstrate STOL capability of the A-6A CCW aircraft to prove the operability and advantages of this high-lift system.

One important basic requirement for the Flight Demonstrator aircraft is that the CCW system be powered by air from the two existing J52-P-8A engines currently installed in the aircraft. Considerable research has been done in the area of analyzing various blowing air supply concepts using engine bleed flow to power the CCW system. These concepts include, but are not limited to, the use of direct bleed, or the use of bleed flow to power turbocompressors or flow multipliers to generate the blowing air required by the CCW system. On the basis of performance, simplicity, and cost effectiveness the direct bleed concept was chosen as the most viable approach (Reference 5).

As the Flight Demonstrator aircraft will derive its STOL potential by direct bleed flow from the J52-P-8A engines, a large amount of bleed flow is certainly desirable. Unfortunately, information relevant to high bleed flow extraction rates from existing engines has not been available as conventional aircraft operations require only minimal bleed flow extraction rates to power such items as the Environmental Control System (ECS) and the Constant Speed Drive (CSD). The J52-P-8A currently has been qualified for bleed flow extraction rates up to 5.0 percent of the total engine airflow at thrust levels of Normal Rated or less and up to 2.5 percent at the Military Thrust condition (Reference 6). These existing bleed flow extraction rates allow a moderate STOL potential for the Flight Demonstrator (a portion of the allowable bleed flow still must be available to power the CSD and ECS); however, a more substantial performance improvement could be realized if larger bleed flow extraction rates could be obtained. An engine evaluation was thus undertaken to determine if the existing standard bleed flow extraction rate limits were conservative and to verify that higher bleed flow extraction rates, if obtained, do not adversely affect the J52-P-8A engine operation.

This investigation was conducted during December 1976 and January 1977 in Test Cell 2W at the Naval Air Propulsion Center in Trenton, New Jersey. The program was structured into two major phases. The first phase was the bleed flow calibration which enabled a determination of the bleed flow quantity and quality along with mapping the engine operating parameters with bleed flow extraction. These results will be used not only as design input for the bleed flow manifold and ducting system required to deliver the bleed flow to the wing plenums of the Flight Demonstrator, but also as a data base from which higher confidence level analytical STOL performance estimates can be derived. The second phase was a 50-hr endurance evaluation designed primarily to qualify the J52-P-8A engine operating under the influence of high bleed flow extraction rates for the proposed 50-hr flight evaluation of the Flight Demonstrator. In addition to the two major phases of the program, a preliminary investigation of the engine acceleration performance while operating at high bleed flow extraction rates was undertaken to aid in assessing wave-off maneuver capability. Hot section

inspections were performed at various phases of these investigations to document the condition of the engine. This report documents the results of these evaluations and presents background information relevant to measurement and evaluation technique.

#### BACKGROUND INFORMATION AND TEST SETUP

The Pratt and Whitney Aircraft J52-P-8A engine is a dual stage compressor-turbine unit turbojet rated at uninstalled thrust levels of 8,200 lb (36,473 nt) and 9,300 lb (41,366 nt) for Normal Rated Thrust (NRT) and Military Thrust, respectively. These values are referenced to static, sea level, standard day conditions. The engine generates a turbine exhaust temperature of 1180 F (1240 R) at a corresponding turbine exhaust pressure of 2.7 atmospheres at the Military Thrust condition (Reference 6). Figure 1 presents a schematic of the engine showing major components and station identification. The engine used for the investigation is shown installed in the test cell in Figures 2-5. Figure 2 presents a rear view of the engine where the low pressure compressor-turbine unit turbine blades can be seen. The low pressure compressor consists of five stages of rotor blades. This compressor can be seen in Figures 3-4 as located between the shiny aft part of the bellmouth inlet and the row of poppet valves located radially about the engine. These poppet valves are used for compressor stall relief at higher Mach number operation. The high pressure compressor consists of seven stages of rotor blades and is located between the poppet valves and the high pressure compressor discharge area. This discharge area is where the high pressure bleed ports are located and can be seen in Figures 4-6 where the four individual corrugated flexible metal tubing bleed port collectors mate with the engine. The two compressors in unison can develop a pressure of 13.8 atmospheres at a temperature on the order of 760 F (1220 R).

The J52-P-8A has four high pressure bleed ports from which bleed flow can be extracted. These ports are located radially around the engine as shown in Figures 2-5. Three of these ports have diameters of 2.25 in. (5.715 cm); the fourth port, which is a fuel heater port commonly not in use, has a somewhat smaller diameter of 1.25 in. (3.175 cm). To measure

the amount of bleed flow, a manifold system was designed and constructed to commonly collect the individual bleed flows from each of the ports. Various components of the manifold system are shown in Figures 2-7. The manifold system incorporated two supply lines. Each of the supply lines was equipped with a reducer pipe, an electrically actuated butterfly valve, and a measuring nozzle located downstream of the valve. The butterfly valves regulated manifold backpressure and therefore the amount of bleed flow delivered to the measuring nozzles. Figure 7 is a photograph of one of the butterfly valves and measuring nozzles. Two large 3.1 in. (7.874 cm) diameter and one small 1.875 in. (4.673 cm) diameter measuring nozzles were manufactured to accommodate the expected bleed flows. These nozzles were required to be operated at nozzle pressure ratios of three or more for proper bleed flow measurement (Reference 7). This aspect is discussed in further detail in the Appendix. It should be noted that these nozzles were oriented 90 deg to the engine thrust axis to eliminate the thrust effects of the exiting bleed flow from the engine thrust. Also shown in Figure 7 is one of the collector pipes which gathered and redirected flow from the nozzles out the rear of the test cell to avoid possible damage to the test cell structure, which could occur if the bleed flow were allowed to impinge directly onto the test cell floor.

Each individual bleed port was instrumented with a thermocouple, a total pressure probe, and a static tap. The information gathered from these devices defines the bleed flow quality. Because flow characteristics in the bleed port vicinity could be quite difficult to measure accurately due to the possibilities of a highly distorted pressure distribution, high flow angularity, and local flow separation, a static tap was located on the main body of the compressor bleed manifold downstream of each of the bleed ports. These taps located in this manner provided backup information to the total pressure measurements taken at the bleed ports. One of these static taps is shown installed into the main body of the manifold in Figure 6. Further details relevant to the geometry and design rationale of the more important aspects of the compressor bleed manifold and measuring nozzles are presented in the Appendix.

The standard engine characteristics recorded during this investigation were measured by off-the-shelf instrumentation specifically designed for engine performance evaluations. The most noticeable of these devices in the engine photographs is the bellmouth inlet used to measure engine air-flow ( $W_a$ ). This bellmouth can be seen in Figures 2-4. Other engine characteristics measured include, but are not limited to, power lever angle (PLA), fuel flow ( $W_f$ ), low and high pressure compressor-turbine unit speeds ( $N_1$  and  $N_2$ , respectively), high compressor discharge pressure ( $P_{t_4}$ ) and temperature ( $T_{t_4}$ ), burner static pressure ( $P_{s_b}$ ), turbine exhaust pressure ( $P_{t_7}$ ) and temperature ( $T_{t_7}$ ), and net thrust ( $F_n$ ). The low pressure compressor inlet total pressure ( $P_{t_2}$ ) and temperature ( $T_{t_2}$ ) were measured to evaluate the corrected performance of the engine performance parameters. Further details associated with the engine instrumentation are discussed in the Appendix.

#### BASIC J52-P-8A ENGINE CALIBRATION RESULTS

Prior to the bleed flow calibration, a calibration of the uninstalled performance and operating characteristics of the unmodified J52-P-8A engine was undertaken. The J52-P-8A engine used for the investigation had a total running time of 820 hrs since new, of which 110 hrs were accumulated since last engine overhaul. For this reason some degradation in engine performance might be anticipated. The primary purpose of this calibration was to insure the validity of the results of the bleed flow calibration by verifying that the engine used for the investigation exhibited performance characteristics comparable to those of a typical J52-P-8A engine. The results of this calibration are presented in Figures 8-16. Appropriate performance levels are given in Reference 6 and are shown in these figures for comparison. To insure that no major deficiencies in performance occurred during the bleed flow calibration and endurance evaluation, a second calibration of the engine was undertaken at the end of the endurance evaluation. The data taken during this calibration are also included in the figures for comparison. It should be mentioned that both of these calibrations were

made with the compressor bleed manifold removed from the engine. The figures also present the data taken during the bleed flow calibration with the compressor bleed manifold installed but with no bleed flow. Any deviations of these data from the basic engine calibrations should be attributable to the presence of the compressor bleed manifold.

The corrected engine data taken from Reference 6 (herein referred to as the baseline data) are estimated performance levels. As these performance levels are estimated, total agreement with the calibration data is not expected. Another contributing factor resulting in some deviation between the performance levels given in Reference 6 and the calibration data is that corrected engine data are somewhat dependent on inlet conditions. This deviation occurs due to changes in viscosity with inlet temperature and changes in the engine component efficiencies with both inlet temperature and pressure. These secondary effects are not accounted for in either the baseline or calibration performance levels. The inlet conditions for the calibration data are summarized in Tables 1, 2, and 3. These tables also present the nominal thrust setting for the data. As shown, most of the data were taken at inlet pressures less than the standard day reference pressure, and all of the data were taken at inlet temperatures less than the corresponding reference temperature.

#### ROTOR SPEED PERFORMANCE

Figures 8 and 9 present the corrected low and high pressure compressor-turbine-unit speeds, respectively, as a function of corrected net thrust. The calibration data indicate a higher  $N_1$  and a lower  $N_2$  in the moderate and high thrust range in comparison to the baseline performance levels. It is suspected that a slightly deficient low pressure compressor unit could cause the increase in  $N_1$ , and possible degraded efficiencies of the high pressure compressor exit guide vanes and/or turbine inlet guide vanes could cause the decrease in  $N_2$ . The deviations from the baseline data of the compressor-turbine unit speeds are felt to reflect a minimal amount of engine wear. At the Standard Day Military Thrust condition ( $F_n / \delta_{t_2} = 9,300 \text{ lb} = 41,366 \text{ nt}$ ) the calibration data indicate a 280-rpm increase in

$N_1$  and a 140-rpm decrease in  $N_2$  in comparison to the baseline performance levels. Based on the baseline data these values correspond to a 2.7-percent increase and a 1.2-percent decrease in  $N_1$  and  $N_2$ , respectively. These deviations are within acceptable levels.

#### AIRFLOW AND FUEL FLOW PERFORMANCE

The corrected airflow performance is shown in Figure 10 as a function of  $F_n/\delta_{t_2}$ . Agreement between the airflow data obtained from the calibrations and the baseline data is quite good at the low and high thrust levels. In the moderate thrust range the airflow data from the calibrations are slightly lower than the baseline performance levels. At  $F_n/\delta_{t_2} = 3,147 \text{ lb}$  (14,000 nt) the calibration and baseline airflows are  $W_a \sqrt{\theta_{t_2}}/\delta_{t_2} = 86.4 \text{ lb/sec}$  (39.2 kg/sec) and  $84.2 \text{ lb/sec}$  (38.2 kg/sec), respectively. Relative to the baseline performance levels, these values correspond to a 2.6-percent reduction in airflow for the specific thrust condition. This deviation in airflow is most likely attributable to the slightly degraded efficiencies of the low pressure compressor and/or guide vanes.

The performance of the corrected fuel flow parameter is shown in Figure 11 as a function of  $N_2/\sqrt{\theta_{t_2}}$ , since  $N_2$  is the primary parameter regulated by the fuel controller during steady state operation. The baseline fuel flow data, derived from specific fuel consumption data taken from Reference 6, are in agreement with the calibration data. It should be noted that the baseline fuel flow data represent the maximum fuel flow values to be expected from an operational J52-P-8A. At the Standard Day Military Thrust condition ( $N_2/\sqrt{\theta_{t_2}} = 12,060 \text{ rpm}$ ) the calibration and baseline data show  $W_f \theta_{t_2}^{0.68}/\delta_{t_2} = 2.194 \text{ lb/sec}$  (0.995 kg/sec) and  $2.238 \text{ lb/sec}$  (1.015 kg/sec), respectively. This corresponds to a 2.0-percent reduction in fuel flow at this condition. These results indicate that the fuel control system was performing adequately in steady state operation and confirms, to some degree, that its performance during engine transients should be in order.

Further details relevant to the fuel control system are given in the Fuel Control System Performance and Operation section.

#### HIGH PRESSURE COMPRESSOR DISCHARGE CHARACTERISTICS

The high pressure compressor discharge pressure ratio characteristics are shown in Figure 12 as a function of  $N_2/\sqrt{\theta t_2}$ . As can be seen in the figure, the pressure ratio characteristics in the moderate  $N_2$  range are slightly greater than the baseline performance levels. The deviation of the two curves in this region might possibly be explained by noting that, for the same  $N_2$ , the  $N_1$  associated with the calibrations is higher than that of the baseline level for  $N_1$ . This increase in  $N_1$  would have the effect of raising the overall pressure ratio across the two compressors for the same airflow. Further analysis indicates that, for the same  $N_2$ , a larger airflow is obtained from the calibrations than from the baseline data. The net effect of this is to reduce the pressure ratio across the two compressors. It may be that the increase in  $N_1$  has the more predominant influence on the compressor system in the  $N_2$  range under discussion and would thus be consistent with the results shown in the figure. In any case, agreement of the calibration data with the estimated data is reasonable.

The associated high pressure compressor discharge temperature characteristics are shown in Figure 13. The data from the calibrations generalize very well on a single curve as evidenced by negligible data scatter. This is implicit that the corrected parameter concept accurately models the performance of the high pressure compressor discharge temperature. A high degree of correlation with the baseline data taken from Reference 6 is also shown in the figure.

#### BURNER PERFORMANCE

The burner static pressure ratio characteristics are shown in Figure 14. Although no data were available from Reference 6 for comparison, these characteristics are assumed to be reasonable. This assumption is based on the fact that the engine performance characteristics of the components

located upstream and downstream of the burner cans (with the exception of  $T_{t_7}/\theta_{t_2}$  discussed later in this section) are in order.

#### TURBINE EXHAUST CHARACTERISTICS

Figure 15 shows the turbine exhaust pressure ratio characteristics as a function of  $F_n/\delta_{t_2}$ . The turbine exhaust pressure ratio is well behaved as expected since  $F_n/\delta_{t_2}$  should, for all practical purposes, be an explicit function of  $P_{t_7}/P_{t_2}$ . The generalization of the calibration data onto a single curve confirms this fact. At high thrust levels no noticeable difference is seen between the calibration and baseline data. In the low to moderate thrust range the calibration data indicate a slightly higher  $P_{t_7}/P_{t_2}$  than do the baseline performance levels. However, the magnitude of the deviation is not considered serious.

The corresponding turbine exhaust gas temperature characteristics are shown in Figure 16. The  $T_{t_7}/\theta_{t_2}$  data, as obtained from the basic engine calibrations, are slightly higher than the baseline levels in the low to moderate thrust range. This trend is consistent with the trends found in the airflow data in this thrust range, i.e., a reduced amount of airflow must be at a higher  $T_{t_7}$  to obtain the same thrust output. The  $T_{t_7}/\theta_{t_2}$  data obtained at the higher thrust levels is questionable, as evidenced by the increase in slope of the curve. The Standard Day Military Thrust ( $F_n/\delta_{t_2} = 9,300 \text{ lb} = 41,366 \text{ nt}$ ) turbine exit temperature limit for operation of 30 min is 1660 R (Reference 6) and is shown on the figure. This limit is only 20 R above the level given by the calibration data. This margin is unrealistically too small. Also, since airflow and  $T_{t_7}$  determine thrust, it becomes obvious that the  $T_{t_7}$  data are inconsistent with the airflow data in the high thrust range. The airflow data discussed earlier in this section were found to be in good agreement with the baseline levels in the high thrust range. Because the  $T_{t_7}$  data in this thrust range were questionable, an estimate of the turbine exhaust temperature was computed for the

final engine calibration throughout the entire thrust range and is shown on the figure for comparison. This estimate, based on balancing the system's energy, was computed from the uncorrected data using the following relationships and assumptions:

$$T_{t_7} = f(h_7) \quad (1)$$

where  $h_7 = (h_2 w_a + n_b LHV w_f) / (w_a + w_f)$   
 $h_2 = f(T_{t_2})$   
 $n_b$  = burner efficiency (assumed to be 1.0)  
LHV = lower heating value of JP-5 fuel = 18,300 Btu/lb  
(40,344 Btu/kg)  
 $h_2$  and  $h_7$  = specific enthalpies (obtained from Keenan and Kaye gas tables given in Reference 8)

It should be mentioned that this method of computing  $T_{t_7}$  is in concurrence with the methods used by Pratt and Whitney Aircraft. Figure 16 shows that the computed values of  $T_{t_7} / T_{t_2}$  in the moderate thrust range agree very well with the calibration data. The increase in the computed data at the very low thrust level is due to the decrease in burner efficiency occurring at this condition which is not accounted for in the above relationships. At the very high thrust levels, the computer data agree quite well with the baseline data from Reference 6. The previously mentioned change in slope of the curve is not seen in the computed data as is seen in the calibration data. The computed values of  $T_{t_7} / T_{t_2}$  are more representative of the turbine exhaust characteristics in the high thrust range than those values indicated by the calibrations. In reference to the Standard Day Military Thrust level, the computed level of  $T_{t_7}$  is 1605 R. This temperature is well within limits in comparison to the 1660 R temperature limit of the engine at this thrust condition.

## BLEED FLOW CALIBRATION RESULTS

The J52-P-8A engine performance characteristics while operating under the influence of high bleed flow extraction rates as obtained during the bleed flow calibration are presented in Figures 17-27. The associated bleed flow quality results are presented in Figures 28-31. The results are given in most of the figures as a function of bleed flow extraction rate ( $W_b/W_a$ ) for constant values of PLA. As noted in the figures, the curves are defined by Military Thrust or a percentage of NRT. These values of thrust output correspond to the thrust of the engine with no bleed flow extraction. The bleed flow extraction rate is defined as the ratio in percentage of the corrected bleed flow ( $W_b \sqrt{\theta_{t_2}} / \delta_{t_2}$ ) of the actual corrected  $W_a$  occurring at that value of bleed flow, and not the corrected  $W_a$  associated with no bleed flow extraction. Table 3 presents the associated PLA and inlet conditions for the data.

The procedure employed in obtaining the data was first to install both of the large 3.10 in. (7.874 cm) diameter measuring nozzles downstream of the compressor bleed manifold. Bleed flow calibration data were then generated at bleed flow conditions where the measuring nozzle pressure ratio could adequately be maintained above three by using either one or both of these nozzles in combination. The data taken in this manner are shown as the circles in the figures and, for the most part, represent the higher bleed flow conditions. It should be mentioned that the maximum bleed flow at a given PLA is limited slightly by manifold system pressure losses and not bleed port choking. (This subject is discussed in more detail in the Appendix.) To obtain the performance characteristics at the lower bleed flow conditions, it was necessary to shut down the engine and substitute the small 1.875 in. (4.673 cm) diameter measuring nozzle for a larger one to obtain measuring nozzle pressure ratio above three. This operational aspect introduced some difficulty in matching the engine operating conditions with the zero bleed flow data previously taken due to a slight amount of "play" in the power lever and possibly different inlet conditions. For these reasons, check points were taken to reference the subsequent data.

taken with bleed flow. These check points are presented in the engine calibration curves given in Figures 8-16 as the semicircled data. The deviations of the check point data from the previously taken zero bleed flow data, denoted by the triangular symbols, are relatively small. The associated inlet conditions for the check point data are given in Table 3. These check point data were used in conjunction with the zero bleed flow calibration data to adjust the data taken with bleed flow to the appropriate performance level. This was accomplished by including the increment in the performance parameter between the two sets of zero bleed flow calibration data in the data taken with bleed flow when using the smaller diameter measuring nozzle alone or in combination with the larger diameter nozzle. These adjusted data are denoted by triangular symbols in Figures 17-31.

#### ROTOR SPEED PERFORMANCE

Figure 17 shows the corrected  $N_1$  performance;  $N_1$  is linearly dependent on  $W_b/W_a$  throughout the entire thrust range. The slope of the curves indicate that the  $N_1$  penalty is about 60 rpm per percent of bleed flow extraction. In reference to the  $N_1$  penalty associated with  $W_b$ , it can be determined by an examination of the airflow data that the  $N_1$  penalty is about 165 rpm/lb (75 rpm/kg) and 452 rpm/lb (205 rpm/kg) for the Military and 20.3 percent NRT conditions, respectively. This is an expected result as an equivalent amount of  $W_b$  being extracted at the high thrust condition represents a smaller portion of the working fluid passing through the engine in comparison to the lower thrust conditions and thus results in a reduced  $N_1$  penalty associated with  $W_b$  for the high thrust conditions.

The corrected  $N_2$  performance is shown in Figure 18. As in the case of  $N_1$ ,  $N_2$  is linearly dependent on  $W_b/W_a$ . The  $N_2$  penalty associated with  $W_b/W_a$  is roughly 23 rpm per percent of bleed flow extraction throughout most of the thrust conditions. At the very low thrust condition, this penalty increases to about 28 rpm per percent; for values of  $W_b/W_a$  less than 10 percent at Military Thrust, the penalty decreases to about 12 rpm per percent. This type of behavior is induced by the changing of the droop slope value incorporated into the speed governing system.

## AIRFLOW AND FUEL FLOW PERFORMANCE

The corrected airflow performance is given in Figure 19. This parameter decreases linearly with  $W_b/W_a$  except at the condition of high thrust and low bleed flow. In this region of operation the penalty in airflow due to  $W_b/W_a$  is less severe mainly because the sensitivity of airflow with  $N_1$  and  $N_2$  is reduced. The maximum value of  $W_b/W_a = 16.84$  percent obtained during the bleed flow calibration occurred at the Military Thrust condition where the corresponding maximum  $W_b \sqrt{\theta_{t_2}} / \delta_{t_2} = 22.01$  lb/sec (9.98 kg/sec). As stated in the Introduction, the J52-P-8A is currently limited at this thrust condition to  $W_b/W_a = 2.5$  percent or roughly 15 percent of the amount obtained during the investigation. At NRT the maximum  $W_b/W_a = 16.77$  percent as shown in the figure and represents about a 240-percent increase over the  $W_b/W_a = 5.0$  percent current limitation.

The corrected fuel flow performance is given in Figure 20. At high thrust levels the fuel flow rate decreases slightly with  $W_b/W_a$ . The slope becomes shallower in the moderate thrust range and slightly positive in the low thrust range. This behavior is predominantly governed by  $N_2$ ,  $P_{s_b}$ , and the droop slope. One item of interest is that the specific fuel consumption (sfc) increases significantly with  $W_b/W_a$ . This is due to the thrust decreasing noticeably, while the fuel flow is only slightly affected. At the very low thrust condition and  $W_b/W_a = 0$  percent, the sfc = 0.836; whereas, at the maximum  $W_b/W_a = 15.44$  percent, the sfc = 1.415. This difference corresponds to a 69-percent increase in sfc at the low thrust condition. At the Military Thrust condition the sfc = 0.777 and 0.964 for  $W_b/W_a = 0$  percent and 16.84 percent, respectively. At this thrust condition the sfc thus increases by 24 percent due to maximum  $W_b/W_a$ .

## HIGH PRESSURE COMPRESSOR DISCHARGE CHARACTERISTICS

The high pressure compressor discharge pressure ratio characteristics are given in Figure 21. These data also indicate a linear relationship with  $W_b/W_a$ . The penalty in performance due to  $W_b/W_a$  increases with increased thrust. At the Military Thrust condition and maximum  $W_b/W_a$ , the pressure

ratio drops by 20-percent to 11.05 from the value of 13.8 at  $W_b/W_a = 0$  percent. At the very low thrust condition the pressure ratio decreases from a value of 5.05 at  $W_b/W_a = 0$  percent to 3.80 at maximum  $W_b/W_a$ . This corresponds to a 25-percent decrease in performance for the low thrust setting.

The corresponding high pressure compressor discharge temperature characteristics are shown in Figure 22. These data again exhibit a linear dependence on  $W_b/W_a$  with the sensitivity increasing with thrust setting. At the low thrust condition,  $T_{t_4}/\theta_{t_2}$  drops from 873 R at  $W_b/W_a = 0$  percent to 802 R at the maximum  $W_b/W_a = 15.44$  percent. At the Military Thrust condition,  $T_{t_4}/\theta_{t_2}$  drops from 1220 R at  $W_b/W_a = 0$  percent to 1120 R at maximum  $W_b/W_a = 16.84$  percent.

#### BURNER PERFORMANCE

Figure 23 presents the burner static pressure ratio characteristics. Here again a linear dependence on  $W_b/W_a$  is seen throughout the thrust range. The burner pressure decreases by 20 percent at the Military Thrust condition due to maximum bleed flow, as evidenced by  $P_{s_b}/P_{t_2} = 13.25$  and 10.65 for  $W_b/W_a = 0$  percent and maximum  $W_b/W_a$ , respectively. At the low thrust condition,  $P_{s_b}/P_{t_2} = 4.82$  and 3.62 for  $W_b/W_a = 0$  percent and maximum  $W_b/W_a$ , respectively. This corresponds to a 33-percent decrease in burner static pressure.

#### TURBINE EXHAUST CHARACTERISTICS

The turbine exhaust pressure ratio characteristics are shown in Figure 24. At NRT and Military Thrust the curves appear to be linear with  $W_b/W_a$ . At the Military Thrust condition the  $P_{t_7}/P_{t_2}$  drops by 18 percent from 2.79 at  $W_b/W_a = 0$  percent to 2.29 at maximum  $W_b/W_a$ . At NRT the corresponding drop in  $P_{t_7}/P_{t_2}$  due to maximum  $W_b/W_a$  is computed to be 22 percent. The decrease in the performance penalty at Military Thrust is due to the increase in the droop slope of the speed governing system. In the moderate thrust range the curves show a tendency to become less sensitive to  $W_b/W_a$ .

at large  $W_b/W_a$ , and at the low thrust condition the variation in  $P_{t_7}/P_{t_2}$  becomes linear again throughout the  $W_b/W_a$  range.

The turbine exhaust temperature characteristics are shown in Figure 25. At low thrust settings,  $T_{t_7}/\theta_{t_2}$  increases with  $W_b/W_a$ . This trend is predominantly governed by the increase in fuel-to-air ratio induced by  $W_b/W_a$  at these low thrust settings. In this figure the  $T_{t_7}/\theta_{t_2}$  characteristics have been computed at the NRT and Military Thrust conditions. The data taken during the bleed flow calibration are shown in the figure for these two thrust settings but are questionable. This aspect was discussed in the Basic J52-P-8A Engine Calibration Results section. The computed characteristics are more representative of the actual temperatures occurring at the turbine exit station. The computed performance levels were calculated by using the previously mentioned energy balance equation modified to account for bleed flow being taken from the engine:

$$h_7 = \frac{h_2 W_a + n_b LHV W_f - h_4 W_b}{W_a - W_b + W_f} \quad (2)$$

The assumptions used are identical to those defined previously and the introduction of  $h_4$  (obtained from  $T_{t_4}$ ) accounts for the energy being withdrawn by bleed flow extraction. Again this method of computing  $T_{t_7}$  is in concurrence with the method used by Pratt and Whitney Aircraft. These computed results indicate that the rate of increase of  $T_{t_7}/\theta_{t_2}$  at these higher thrust settings is less severe than at lower thrust levels. This is due to the fuel-to-air ratio being relatively insensitive to  $W_b/W_a$  at the higher thrust levels.

#### THRUST PERFORMANCE

Figure 26 shows the variation in thrust performance with  $W_b/W_a$ . At the Military Thrust condition, the thrust decreases from 9,700 lb (43,150 nt) at  $W_b/W_a = 0$  percent to 7,140 lb (31,759 nt) at maximum  $W_b/W_a$ . The

associated maximum  $W_b \sqrt{\theta} / \delta t_2$  = 22.01 lb/sec (9.98 kg/sec). For an inlet temperature of 38 F, this value corresponds to  $W_b / \delta t_2$  = 22.45 lb/sec (10.19 kg/sec). The associated thrust loss is 2,560 lb (11,391 nt), and the associated thrust penalty due to  $W_b / W_a$  is computed to be 114 lb sec/lb (1,117 nt sec/kg). By the same methodology, the thrust penalty at the NRT condition increases to 135 lb sec/lb (1,320 nt sec/kg); at the very low thrust setting, the penalty decreases to 76 lb sec/lb (744 nt sec/kg). The thrust penalty being larger at NRT than at Military Thrust is primarily due to the reduced level of droop slope at the NRT condition. The significant reduction in the penalty at the very low thrust setting is due to the large increase in  $T_{t_7}$  with  $W_b / W_a$  as shown in Figure 25.

Figure 27 is a summary of the most important performance quantities; namely, thrust and bleed flow. This figure is generated by crossplotting the net thrust found in Figure 26 against the bleed flow rate as computed from the airflow data given in Figure 17. The solid lines in the figure correspond to a specific PLA and zero bleed flow thrust setting and the dashed lines represent lines of constant  $W_b / W_a$ . Also the standard bleed flow extraction rate limits are shown for comparison. The bleed flow rates available from the engine are far greater than the standard bleed flow extraction rates allow. The maximum value of  $W_b \sqrt{\theta} / \delta t_2$  = 22.01 lb/sec (9.98 kg/sec) obtained can be seen for the Military thrust setting with the associated thrust loss of 2,560 lb (11,391 nt). This was discussed in the previous paragraph. Also mentioned above were the thrust penalties associated with  $W_b \sqrt{\theta} / \delta t_2$ . These penalties are the slopes of the solid lines in

Figure 27.

#### BLEED FLOW QUALITY

The quality of the bleed flow is described in Figures 28-31 which present the bleed port total and static pressures and temperatures. A detailed discussion of bleed flow quality measurement technique is given in the Appendix. The data presented in these figures dictate the design of the compressor bleed manifold to be used on the Flight Demonstrator aircraft

and identify critical areas of the aircraft requiring insulation and/or temperature limitations imposed upon the high lift system. It should be mentioned that the data shown in Figures 28 and 31 represent an area-weighted average of the measurements taken during the bleed flow calibration. This was done to reduce the influence of the fuel heater port (because its area is substantially smaller than the other bleed ports) when measurements deviated from those taken at the other bleed ports.

Figure 28 presents the bleed port total pressure ratio. As can be seen,  $P_{t_{bl}}/P_{t_2}$  reduces from 13.1 at  $W_b/W_a = 0$  percent to 8.9 at maximum  $W_b/W_a$  for the Military Thrust condition. This corresponds to a 32-percent decrease in pressure for this thrust condition. The pressure drop through the bleed ports is found with the aid of Figure 21, which presents the high pressure compressor discharge pressure. At Military Thrust with  $W_b/W_a = 0$  percent, the associated  $P_{t_4}/P_{t_2} = 13.8$  while  $P_{t_{bl}}/P_{t_2} = 13.1$ . This corresponds to a 5-percent loss in pressure external to the bleed ports. At the maximum  $W_b/W_a$  for this thrust condition,  $P_{t_4}/P_{t_2} = 11.05$  while  $P_{t_{bl}}/P_{t_2} = 8.9$ . This corresponds to a 20-percent loss in pressure as the flow passes through the ports. The pressure levels shown in Figure 28 represent adequate levels (Reference 5) for the bleed flow system to be used on the Flight Demonstrator.

Figures 29-30 present the individual bleed port total pressure ratios ( $P_{t_{bl}}/P_{t_2}$ ) and total-to-static pressure ratios ( $P_{t_{bl}}/P_{s_{bl}}$ ) for the military thrust and 20.3-percent NRT conditions, respectively. For reference, the bleed port identification number can be found in Figure A.1 in the Appendix. The  $P_{t_{bl}}/P_{t_2}$  data show a slightly nonsymmetric pressure distribution about the engine at the higher  $W_b/W_a$  values. The fuel heater port (Bleed Port 2) data show this port has a reduced pressure in comparison to the other ports. Also, the  $P_{t_{bl}}/P_{s_{bl}}$  data are lower for this particular port, as evidenced in the figures. These data indicate that the internal geometry of the high pressure compressor discharge area induces a larger pressure drop in the

vicinity of the fuel heater port and that the flow from the fuel heater port is at a lower indicated velocity in comparison to the other bleed ports.

The bleed port temperature is given in Figure 31. The data taken at low  $W_b/W_a$  are questionable because the bleed port temperature should be very near the temperature of the flow at the high pressure compressor discharge area. For this reason, the  $T_{t_4}/\theta_{t_2}$  values as extracted from Figure 22 are plotted on the vertical axis for  $W_b/W_a = 0$  percent. A comparison of the  $T_{t_{bl}}/\theta_{t_2}$  data at the higher  $W_b/W_a$  with the corresponding  $T_{t_4}/\theta_{t_2}$  data shows excellent agreement and confirms, to some degree, that the bleed port temperature measurements at low  $W_b/W_a$  are questionable. These data indicate that the compressor bleed manifold installed on the Flight Demonstrator must be capable of withstanding temperatures on the order of 1200 R at the Military Thrust condition.

#### TURBINE INLET AND EXHAUST TEMPERATURE LIMITATIONS

This section examines the influence of bleed flow extraction on the turbine inlet ( $T_{t_5}$ ) and exhaust temperatures in reference to their respective limits. If either of these limits are exceeded, either the thrust or bleed flow must then be restricted to appropriate levels to avoid engine overheating. For normal operation,  $T_{t_5}$  can essentially be correlated to  $T_{t_7}$ , and any limits imposed upon  $T_{t_5}$  can be set by imposing a limit on  $T_{t_7}$ . However, the possibility exists that the correlation between  $T_{t_5}$  and  $T_{t_7}$  may not be valid at excessive bleed flow rates. If this were the case, it is conceivable that the  $T_{t_5}$  limit could be exceeded while the  $T_{t_7}$  is within its required limits.

Figures 32-33 show the variation in  $T_{t_7}/\theta_{t_2}$  and  $T_{t_5}/\theta_{t_2}$ , respectively, as a function of  $F_n/\delta_{t_2}$  for constant values of  $W_b/W_a$  and PLA. Figure 32 is generated by crossplotting the data given in Figures 25-26 at the higher

thrust levels. Note that the computed levels of  $T_{t_7} / \theta_{t_2}$  for NRT and Military Thrust shown in Figure 25 were used due to the discrepancy in the  $T_{t_7} / \theta_{t_2}$  data obtained from the basic engine and bleed flow calibrations.

The  $T_{t_5} / \theta_{t_2}$  data shown in Figure 33 are computed values since  $T_{t_5}$  was not measured during this investigation because of the difficulties associated with measurement of this parameter. These computed data were calculated from the following equation, obtained by balancing the compressor and turbine work:

$$T_{t_5} = f(h_5) \quad (3)$$

where 
$$h_5 = \frac{(h_4 - h_2) W_a + h_7 (W_a - W_b + W_f) - h_4 W_{t_{ca}}}{W_a + W_f - W_{t_{ca}}}$$

and

$$W_{t_{ca}} = 0.0195 W_a - 0.0033 W_b$$

The term  $W_{t_{ca}}$  represents the turbine cooling air which is drawn from the high pressure compressor discharge area and deposited into the turbine section. The uncorrected bleed flow calibration data were used in this equation for computing the values of  $T_{t_5}$ . This method of computing  $T_{t_5}$  is in agreement with the method used by Pratt and Whitney Aircraft.

As previously mentioned in Basic J52-P-8A Engine Calibration Results, the  $T_{t_7}$  at Standard Day Military Thrust is limited to 1660 R for operation of 30 min. The following chart presents a listing of some turbine exit temperatures that are either limits or measures of performance, that is, the data shown in this chart that are not specifically noted as limits represent the maximum  $T_{t_7}$  values expected for the very deficient engine.

STATIC TURBINE EXIT TEMPERATURES  
(Standard day, sea level conditions)

Thrust Rating	Turbine Exit Temperature
NRT and below (continuous operation)	1100 F (1560 R)
Military (30 min operation)	1180 F (1640 R)
Military (30 min operation)	1200 F (1660 R) - limit
Military (8 min operation)	1250 F (1710 R) - limit

Unfortunately, information relevant to the  $T_{t_5}$  limitations are not specifically defined; thus, the corresponding  $T_{t_5}$  limits were computed from the above equation under the assumption that the  $T_{t_5}$  limits are reached at the corresponding  $T_{t_7}$  limits for zero bleed flow operation. This assumption should provide a somewhat conservative estimate for the  $T_{t_5}$  limits. The same approach was taken in computing the maximum expected values of  $T_{t_5}$ . The values of  $W_a$ ,  $W_f$ , and  $T_{t_4}$  required in the above equation were taken from Reference 6 and used with the appropriate value of  $T_{t_7}$  to arrive at  $T_{t_5}$ . The results of the computations are shown in the following chart:

STATIC TURBINE INLET TEMPERATURES (COMPUTED)  
(Standard day, sea level conditions)

Thrust Rating	Turbine Inlet Temperature
NRT and below (continuous operation)	1685 F (2145 R)
Military (30 min operation)	1803 F (2263 R)
Military (30 min operation)	1823 F (2283 R) - limit
Military (8 min operation)	1873 F (2333 R) - limit

The  $T_{t_7}$  and  $T_{t_5}$  limits are shown in Figures 32 and 33 with the estimated performance at standard day conditions denoted by the dotted dashed lines. The maximum expected temperatures shown in these figures provide a

qualitative assessment of the engine temperatures associated with bleed flow in comparison to the temperatures associated with a highly deficient operational engine with no bleed flow. The engine can be operated at all thrust levels up to NRT and at all bleed flow rates without exceeding the maximum expected temperatures. At Military Thrust the  $T_{t_7}$  and  $T_{t_5}$  limits for 30 min operation are reached at  $W_b/W_a = 16.0$  percent and 14.5 percent, as shown in Figures 32-33, respectively. The computed  $T_{t_5}$  limits may be conservative. Thus it is possible that  $W_b/W_a = 16.0$  percent is permissible for 30 min operation at Military Thrust. If maximum  $W_b/W_a$  at Military Thrust for 30 min is desired, the thrust should be downtrimmed by 180 lb (800 nt) or 90 lb (400 nt) as dictated by the  $T_{t_5}$  and  $T_{t_7}$  limits, respectively: however, maximum  $W_b/W_a$  at Military Thrust is obtainable if the operational time is restricted to 8 min. The proposed Flight Demonstrator ducting system is limited to  $W_b/W_a = 10$  percent, which should present no overheating problems during normal operations; however, loss of an engine will induce  $W_b/W_a$  in excess of 10 percent if no corrective action is taken to limit the bleed flow. Operation under these conditions should be carefully examined, since engine temperature limits may be approached or exceeded.

#### FUEL CONTROL SYSTEM PERFORMANCE AND OPERATION

The fuel controller installed on the J52-P-8A engine is a JFC 25-3 hydromechanical fuel control operated by a single power lever. The power lever controls thrust in the range from Idle to Military Thrust and activates fuel flow cutoff below the Idle position. The fuel flow is regulated as a function of high pressure compressor-turbine unit speed, burner pressure, power level position, and inlet temperature. By monitoring these parameters, the fuel controller governs engine starting, steady state selected high pressure compressor-turbine unit speed, maximum burner pressure, and engine acceleration and deceleration transient characteristics.

Figure 34 shows the performance and operating characteristics of the fuel controller. The figure presents the ratio of  $W_f$  to  $P_{S_b}$  as a function of  $N_2$  for various values of  $W_b/W_a$ . These data were generated from the uncorrected data taken during the bleed flow calibration. The dashed lines represent the steady state operating conditions; as shown in the figure, the operating line shifts upward with increased  $W_b/W_a$ . This upward shift of the operating line is indicative of a deterioration in engine efficiency. Also shown is the steady state operating line of a typical production line J52-P-8B engine. These particular data were supplied through the courtesy of Pratt and Whitney Aircraft. Valid comparisons of these data with those obtained during the investigation can be made since the difference between the J52-P-8A and the J52-P-8B engines is that the J52-P-8B engine incorporates the use of smokeless burner cans. However, these cans do not affect the engine operating line performance. This operating line is somewhat lower than the corresponding one for no bleed flow extraction as determined from the investigation indicating that there is some slight deficiency in the performance of the engine used for this investigation.

The dependence of the steady state operating line performance on  $W_b/W_a$  is attributable to the operation of the fuel control and speed governing systems. If the engine is being operated at a steady state condition and  $W_b/W_a$  is changed, the engine experiences a change in burner pressure and rotor speed such that the rotor speed has a linear dependence on the change in the ratio of fuel flow to burner pressure. Thus, a new steady state operating condition is determined. The linear dependence described above is the speed governor droop slope ( $D_S$ ) and is mathematically defined as:

$$D_S = d(W_f/P_{S_b})/dN_2 = -0.02 \text{ in.}^2/\text{hr rpm} (-3.58 \times 10^{-5} \text{ cm}^2/\text{sec rpm})$$

The numerical value stated is the design value of  $D_S$ .

The solid lines connecting the bleed flow calibration data shown in Figure 34 represent the specific thrust levels investigated during the calibration and correspond to a specific power lever position. The associated

nominal PLA and thrust setting shown in the figure are extracted from Table 3. The slopes of these lines are the actual values of the speed governer droop slope. The speed governer droop slope line is shown for the Military Thrust condition and is in good agreement with the slope indicated by the calibration data. The solid line at the top of the figure, supplied by Pratt and Whitney Aircraft, is the engine accelerating schedule. This line and the droop slope define the manner in which fuel flow is metered to accomplish engine acceleration. This aspect of performance is discussed in the Engine Acceleration Performance section.

Figure 35 presents the variation in  $D_S$  as a function of PLA for the zero and maximum bleed flow extraction rate conditions. These data, derived from Figure 34, indicate that  $D_S$  deviates substantially from its design value. The maximum deviation is approximately 20 percent and occurs at about 80 percent NRT ( $PLA \approx 73$  deg). The upper and lower tolerance limits for  $D_S$  are shown for comparison and are within limits. No change in  $D_S$  occurs due to  $W_b/W_a$  at thrust levels less than NRT; but at higher thrust levels,  $D_S$  decreases slightly at the maximum  $W_b/W_a$ . This trend is due to the steady state operating line at these conditions approaching the engine acceleration schedule. The decrease in  $D_S$  at these conditions tends to increase the  $N_2$  drop associated with  $W_b/W_a$ . This, in turn, results in a larger thrust penalty associated with high  $W_b/W_a$  in comparison to lower values.

#### ENGINE ACCELERATION PERFORMANCE

Upon completion of the bleed flow calibration, a brief investigation was undertaken of the J52-P-8A engine acceleration performance when operating at high bleed flow rates. This information was gathered to aid in assessing the capability of the engine to perform a waveoff maneuver during the low speed power approach phase of operation. The baseline acceleration performance throughout the thrust range was obtained for comparison from Pratt and Whitney Aircraft.

Results of the engine accelerating performance are shown in Figure 36. This figure presents the time required to accelerate from a given thrust level to 95 percent Military Thrust. The specific conditions investigated were the acceleration times from idle with no bleed flow and maximum bleed flow and from 40 percent NRT with maximum bleed flow. These three data points are shown in the figure. Each data point represents the numerical average of three successive engine acceleration runs. In the case of the maximum bleed flow acceleration runs, the thrust levels shown represent the thrust based on the standard day Military Thrust and NRT levels with maximum bleed flow. These values are obtainable from Figures 32 or 33 where the standard day NRT and Military Thrust levels are  $F_n/\delta_{t_2} = 5,396 \text{ lb}$  (24,000 nt) and 6,632 lb (29,500 nt), respectively, at the maximum bleed flow condition. The baseline acceleration performance from Idle to the required level is 6.3 sec. The datum point, denoted by a square symbol, is the corresponding acceleration time from 40 percent NRT as supplied by Pratt and Whitney Aircraft. The acceleration time of 6.3 sec from Idle is in agreement with the information supplied by the engine manufacturer. The data taken at maximum  $W_b/W_a$  show a drastic increase to 16.7 sec in the acceleration time at the Idle condition. At the 40-percent NRT condition the acceleration time is 2.6 sec, which is only slightly longer than the corresponding case with no bleed flow.

These results can be explained by understanding the manner in which engine acceleration is accomplished. In the previous section dealing with the fuel control system performance, the steady state operating line performance and droop slope were discussed. The results were shown in Figure 34 along with the engine acceleration schedule. Engine acceleration is accomplished by the use of the acceleration schedule and the droop slope. When the engine is at a steady state condition and the power lever commands a higher  $N_2$ , the fuel controller immediately increases the fuel flow rate to the level dictated by the acceleration schedule. The fuel controller then maintains operation along the acceleration schedule to the point where the droop slope of the commanded  $N_2$  intersects the schedule. The fuel flow is then metered to follow the droop slope down to the new steady state

operating point. The droop slope is followed to avoid engine overspeed and high temperature overshoots. The difference between the acceleration schedule and the steady state operating point represents the fuel available for acceleration. As the operating line raises with increased bleed flow, less fuel flow is available for acceleration resulting in longer acceleration times. This can be clearly seen in Figure 34 for the 40-percent NRT condition; however, at this condition and maximum  $W_b/W_a$  there is still an adequate margin between the steady state operating point and the acceleration schedule. This aspect results in the slightly longer acceleration time required for this condition shown in Figure 36. At the Idle condition, the margin is greatly reduced and results in the significantly increased acceleration time for the maximum bleed flow condition. Operation at the maximum  $W_b/W_a$  and low thrust levels is not anticipated for the Flight Demonstrator; thus the increased acceleration time at these conditions is reduced to an academic problem. One reasonable solution is to raise the Idle  $N_2$  to such a level that an adequate margin exists between the steady state operating point and the acceleration schedule.

#### ENDURANCE EVALUATION

A 50-hr endurance evaluation of the J52-P-8A engine was undertaken after completion of the bleed flow calibration. This endurance evaluation was designed to qualify the engine operating under the influence of high bleed flow extraction rates for the proposed 50-hr flight evaluation of the Flight Demonstrator. The entire endurance evaluation was done at maximum bleed flow conditions which were about 15 percent at the low thrust settings increasing to about 17 percent at the high thrust levels. The engines in the Flight Demonstrator will be limited to a maximum bleed flow extraction rate of about 10 percent; the engines will be operated at this limit for only a relatively small portion of the 50-hr flight evaluation. Based on these facts, the endurance evaluation represents a very conservative qualification basis for the engine as a candidate for flight evaluation.

The endurance evaluation, approved by Pratt and Whitney Aircraft, was composed of a series of 25 cycles, each of 2-hr duration. Each cycle

consisted of a set of various transient and steady state thrust conditions designed to simulate the operation of the J52-P-8A engine during the 50-hr flight evaluation program. The cycle used for the evaluation is listed below with the representative flight conditions simulated.

**ENDURANCE CYCLE, MAX  $W_b/W_a$**

<u>Power Setting</u>	<u>Time (min)</u>	<u>Simulated Flight Conditions</u>
Military Thrust	5	Warmup and Takeoff
NRT	10	Climb
1-Sec Snap Deceleration to 40-percent NRT	5 x (6)	Cruise
1-Sec Snap Acceleration to Military Thrust	cycle 6 times	Cruise
95-percent NRT	15	Cruise
45-percent NRT	15	Descend and Land
20-percent NRT	10	
<u>Idle</u>	<u>5</u>	Shutdown
Total Time	120 min = 2 hr	

A total of 92.95 hr of successful operation were accumulated by the engine during the basic engine calibrations, the bleed flow calibration, and the engine acceleration and endurance evaluations. This total includes 19.3 hr of operation at Military Thrust and 39 engine starts. This information, coupled with the results of the hot section inspections, confirms to a high degree of confidence that the J52-P-8A engine is capable of being operated at bleed flow extraction rates in excess of the standard limits for at least 50 hr with no expected seriously damaging effects to the engine.

## HOT SECTION INSPECTION RESULTS

This section presents the results of the three hot section inspections performed on the engine. These inspections require an engine teardown of the major engine components for visual and measurable engine wear. A bore-scope was used in determining engine wear of certain components not easily accessible.

Three hot section inspections were made on the J52-P-8A engine used in this investigation. The first inspection occurred prior to the initial installation of the engine into the test cell to document the condition of the engine. The second inspection occurred 22 hr into the 50 hr endurance evaluation; the last inspection occurred after final engine removal from the test cell. The inspections taken in this manner give an indication of progressive engine wear; however, it is difficult to isolate the effects of engine wear due to excessive bleed flow from the normal engine wear that must occur. The hot section inspection results are presented below and are compared to the serviceability limits in the Intermediate Maintenance Instructions, NAVAIR 92B-10DAA-6-1. (The items in parenthesis, e.g., (5-122), in the inspection reports refer to appropriate sections in this instruction.) Photographs of the hot section were taken to document the condition of the engine.

Several bleed flow collectors failed near the beginning of the endurance evaluation; however, damage was not deemed critical as only a small amount of leakage was noted, and the evaluation was continued. These bleed flow collectors were repaired at the time of the second hot section inspection.

### FIRST INSPECTION REPORT

The first inspection occurred on 6 December 1976. Engine operating time since last overhaul was 110 hr. Although the following discrepancies were observed, the engine was within service limits.

1. Inlet (reference paragraph 5-122). The first stage compressor blades had many blends on the leading edge. One blade had a 1/4- by 1/8- by 1/32-in. dent on the leading edge approximately 3 in. from the tip that was not blended. The compressor inlet was dirty gray from airborne contamination.

2. Compressor Sixth Stage (reference paragraph 5-124). A borescope inspection via instrumentation ports at 2 and 10 o'clock revealed many blends on the sixth stage leading edge. No unblended damage was noted.

3. Compressor Twelfth Stage Blades (reference paragraph 5-125). Numerous leading edge and trailing edge blends were noted. There was no unblended damage.

4. Compressor Twelfth Stage Exit Guide Vanes (reference paragraph 5-136C). At the 7 o'clock position, 0.075-in. nicks were observed on the trailing edge of two vanes. At 3 to 5 o'clock there were several 0.100-in. diameter discolorations. Possible scaling was noted on all vanes.

5. Combustion Liner (reference paragraph 5-136). Discrepancies were noted as follows:

a. Can 4 - Two mold erosion spots immediately downstream of ignitor port, each approximately 1/2-in. diameter.

b. Can 6 - Axial crack on inner surface of fuel nozzle guide.

c. Can 7 - Two small burned areas, each less than 5/8-in. diameter, one on inner part of dome and one directly aft on the first segment.

d. Can 8 - Possible small crack on downstream edge of dome on internal surface.

e. Can 9 - Score on internal surface of dome.

6. Combustion Chamber Pins (reference paragraph 5-132). Wear on support pin mating areas was within the 0.015 in. allowable.

7. Combustion Chamber Inner Outlet Duct (reference paragraph 5-138). A possible 1-in. long radial crack was noted in the weld area. A 3-in. crack is allowable. Moderate light gray splatter was observed in transition duct.

8. Turbine Inlet Guide Vanes (reference paragraph 5-141). Coloration was noted throughout area. No cracks, chipping, or bulging were found.

9. Fuel Nozzles. No cracks were found in nozzle outer heat shield. Nozzles were carbon stained but no buildup was present.

10. Fuel Control. As a result of previous testing, the main fuel control was tagged out as insensitive to PLA movements between 15 and 25 deg.\*

#### SECOND INSPECTION REPORT

The second inspection occurred 6 January 1977. Engine operating time since last overhaul was 168.81 hr. Although the following discrepancies were noted, the engine was within service limits with the exception of item 8:

1. Inlet (reference paragraph 5-122). Same observation as the first inspection.
2. Compressor Sixth Stage (reference paragraph 5-124). Same observation as the first inspection.
3. Compressor Twelfth Stage Blades (reference paragraph 5-125). Same observation as the first inspection.
4. Compressor Twelfth Stage Exit Guide Vanes (reference paragraph 5-136C). Same observation as the first inspection.
5. Combustion Liners (reference paragraph 5-136). Discrepancies were noted as follows:
  - a. Can 1 - Carbon discoloration around smoke shoes. Rub indication on mating surfaces of crossover tubes and fuel nozzle guides. Light blue/gray coloration on inside area of can.
  - b. Can 2 - Carbon discoloration and slight carbon buildup on and around smoke shoes. Rub indication on mating surfaces of crossover tubes and fuel nozzle guides. Light blue/gray coloration on inside area of can.
  - c. Can 3 - Slight carbon buildup around smoke shoes. Light blue/gray coloration on inside area of can. Rub indication on mating surfaces of crossover tubes and fuel nozzle guides.
  - d. Can 4 - Mild 1/8- by 1/2- by 3/4-in. carbon buildup on dome immediately downstream of ignitor. First- and second-segment carbon and heat discoloration immediately downstream of smoke shoes. Previously reported erosion covered by carbon discoloration. Burn area (1/8 by 1/2 in.) on

---

\*The source of this information could not be defined or substantiated as the main fuel control appeared sensitive to PLA movements in this range during the subsequent investigation.

skirt inside surface immediately downstream of crossover tube opposite ignitor. Rub indication on mating surfaces of crossover tubes and fuel nozzle guides. Light blue/gray coloration on inside area of can.

e. Can 5 - Mild carbon buildup around smoke shoes. Rub indication on mating surfaces of crossover tubes and fuel nozzle guides. Light blue/gray coloration on inside area of can.

f. Can 6 - Axial crack on inner surface of fuel nozzle guide (same observation as the first inspection). Rub indication on mating surfaces of crossover tubes and fuel nozzle guides. Light blue/gray coloration on inside area of can.

g. Can 7 - Carbon discoloration around smoke shoes. Slight carbon buildup downstream of ignitor in dome and discoloration on first and second segment. Light blue/gray coloration on inside area of can. Rub indication on mating surfaces of crossover tubes and fuel nozzle guides. Previously reported burned areas covered with carbon discoloration.

h. Can 8 - Carbon stain around smoke shoes. Rub indication on mating surfaces of crossover tubes and fuel nozzle guides. Light blue/gray coloration on inside area of can. Previously reported crack not visible.

i. Can 9 - Slight carbon buildup around smoke shoes. Score on inner surface of dome (same observation as the first inspection). Rub indication on mating surfaces of crossover tubes and fuel nozzle guides. Light blue/gray coloration on inside area of can.

6. Combustion Chamber Pins (reference paragraph 5-137). Wear on support pin mating areas was within the 0.015 in. allowable.

7. Combustion Chamber Inner Outlet Duct (reference paragraph 5-139). Same observation as the first inspection.

8. Turbine Inlet Guide Vanes (reference paragraph 5-144). These vanes had a light red/brown coloration turning to light blue/gray at the outboard lands. No cracks or bulging were noted. Three 1/8-in. diameter chips and one 1/16-in. diameter chips were found on the leading edge of a vane at 6:30 o'clock. This is in excess of service limits (not more than three chips, each with 1/16 in. diameter). The initiation of erosion on the leading edges of several vanes was noted. Erosion on one vane, estimated to be out of service limits, covered an area 1/8 in. wide by 5/8 in. long on the leading edge of the vane at 11 o'clock.

9. Fuel Nozzles. No cracks were found on the nozzle outer heat shield. The nozzles were carbon stained and heat discolored. No carbon blockage was present in the primary jets.

During removal of the failed twelfth stage bleed flex joints, several pieces of the failed stainless steel bellows section fell into the engine bleed manifold. Several pieces were removed during inspection by vacuuming. One piece (approximately the size of a dime), located in the 11 o'clock bleed strut and lodged behind the number 4 bearing oil supply tube, could not be extracted. Since it was determined that the metal could not work its way into the internal cavities of the engine, the investigation was continued with the belief that the metal piece would stay in position or blow out the bleed manifold; if the piece did work its way into the gas path, it would probably pass through the turbine section without major damage.

#### THIRD INSPECTION REPORT

The third inspection occurred 1 February 1977. Engine operating time since last overhaul was 202.95 hr. Although the following discrepancies were noted, the engine hot section was within service limits with the exception of items 6 and 8.

1. Inlet (reference paragraph 5-122). Same observation as the first inspection.

2. Compressor Sixth Stage (reference paragraph 5-124). A borescope inspection was conducted through the 10-o'clock port while rotating high pressure compressor. Two blades each had a leading edge nick of less than 0.030 in. This damage is within limits.

3. Compressor Twelfth Stage Blades (reference paragraph 5-125). Same observation as the first inspection.

4. Compressor Twelfth Stage Exit Guide Vanes (reference paragraph 5-136C). Same observation as the first inspection. Tan coloration from airborne contamination was evident throughout the compressor discharge area.

5. Combustor Liners (reference paragraph 5-136). Discrepancies were noted as follows:

Can 1 - Same observation as the second inspection.  
Can 2 - Same observation as the second inspection.  
Can 3 - Same observation as the second inspection.  
Can 4 - Same observation as the second inspection.  
Can 5 - Same observation as the second inspection.  
Can 6 - Same observation as the second inspection plus slight carbon buildup around smoke shoes.

Can 7 - Carbon discoloration and slight buildup around smoke shoes.  
Same observation as the second inspection on remaining items.

Can 8 - Same observation as the second inspection.  
Can 9 - Same observation as the second inspection.

6. Combustion Chamber Pins (reference paragraph 5-137). Eight of the nine combustion chamber pins were replaced due to excessive wear. Five of the nine combustion chamber mount pin retaining lugs (diffuser case, inner) had internal diameter wear in excess of the 0.015 in. allowable.

7. Combustion Chamber Inner Outlet Duct (reference paragraph 5-139). Same observation as the first inspection. Light blue/gray coloration was found throughout the area.

8. Turbine Inlet Guide Vanes (reference paragraph 5-141). Same observation as the second inspection. The chipping and erosion did not progress measurably.

9. Fuel Nozzles. Same observation as the second inspection.

The foreign object reported (Second Inspection Report) lodged behind the oil supply tube in the diffuser case strut at the 11-o'clock position was gone, and, presumably, had blown out through the bleed pipe.

These results show that only engine wear of a minor nature occurred as the investigation progressed. Most, and possibly all, of the engine wear found by these inspections can be classified as normal and therefore is not attributable to high bleed flow extraction. The most predominant engine wear that may be associated with high bleed flow extraction is the erosion and chipping of the turbine inlet guide vanes. This particular engine wear could possibly be induced by approaching the turbine inlet temperature limit. Note that all engine wear is classified as minor;

whether some engine wear may have been caused by excessive bleed flow appears to be a question of an academic nature.

#### CONCLUSIONS

1. The basic engine calibration results reveal that the engine performed at an acceptable level, thus confirming the validity of the bleed flow calibration results.
2. Bleed flow extraction rates of 16 to 17 percent are obtainable throughout most of the thrust range. A maximum corrected bleed flow value of 22.01 lb/sec (9.98 kg/sec) was obtained at the Military Thrust setting during the investigation. These values of bleed flow extraction rate represent sufficient levels to provide the Flight Demonstrator with an adequate STOL demonstration potential (References 4-5).
3. Thrust penalties associated with bleed flow extraction are approximately 135 lb sec/lb (1320 nt sec/kg) at the moderate and Normal Rated Thrust-levels. The penalty decreases for the low and Military Thrust levels. The penalties should allow sufficient thrust levels for power approach in the low speed regime obtainable by the Flight Demonstrator (Reference 5).
4. Bleed flow pressures are adequate to power the CCW system on the Flight Demonstrator. The associated temperatures obviously will require insulation of critical areas of the manifold and ducting system used on the Flight Demonstrator (Reference 5).
5. Maximum bleed flow at Military Thrust is permissible only for a period of 8 min or less. Operation up to 30 min at Military Thrust and maximum bleed flow is permissible if the thrust is downtrimmed by a small amount. Downtrimming of the thrust is not required if the maximum bleed flow rate were limited to 15 to 16 percent. These restrictions arise due to turbine inlet and exit temperature limitations. For the Flight Demonstrator, these limitations can evolve only in the event of an engine failure, as normal operation is restricted to a maximum bleed flow extraction rate of 10 percent.
6. A preliminary investigation of engine acceleration performance operating at maximum bleed flow indicates that engine spinup time should

be sufficient to provide the Flight Demonstrator with an adequate level of waveoff maneuver capability.

7. The 50-hr endurance evaluation (being quite conservative in scope) and the hot section inspection results indicate that the J52-P-8A engine is capable of being operated at bleed flow rates in excess of the standard limits. These results serve as a conservative qualification basis for the proposed 50-hr flight evaluation of the Flight Demonstrator.

## REFERENCES

1. Englar, R.J., "Subsonic Two-Dimensional Wind Tunnel Investigations of the High Lift Capability of a Circulation Control Wing," NSRDC Report ASED-274, AD-A-024-346 (May 1975).
2. Englar, R.J., "Subsonic Wind Tunnel Investigation of the High Lift Capability of a Circulation Control Wing on a 1/5-Scale T-2C Aircraft Model," NSRDC Report ASED-299, AD-781-856 (May 1973).
3. Lacey, D.W. and R.A. Hemmerly, "A Preliminary Investigation of the Low Speed Performance and Handling Qualities of a T-2C Aircraft Modified with a Circulation Control Flap System," NSRDC Report ASED 318, AD-B-008-365 (Mar 1974).
4. Englar, R.J. et al., "Development of the Circulation Control Wing to Provide STOL Potential for High Performance Aircraft," AIAA Paper 77-578 presented at the AIAA/NASA Ames V/STOL Conference, Palo Alto, California (6-8 Jun 1977).
5. "Feasibility Study of an A-6A Aircraft Modified with a Circulation Control Wing (CCW)," Grumman Aerospace Corporation Report PDR-651F-3, Contract No. N00019-76-C-0243 (Jul 1976).
6. "Specification No. N-1844-C, Model J52-P-8A and -8B Engines," Pratt & Whitney Aircraft (Aug 1974).
7. Trout, A.M. et al., "Internal Performance of Several Divergent Shroud Ejector Nozzles with High Divergence Angles," NACA RM E57F13 (Oct 1957).
8. Van Wylen, G.J. and R.E. Sonntag, "Fundamentals of Classical Thermodynamics," Second Edition John Wiley and Sons, Inc., New York (Aug 1968), pp. 634.

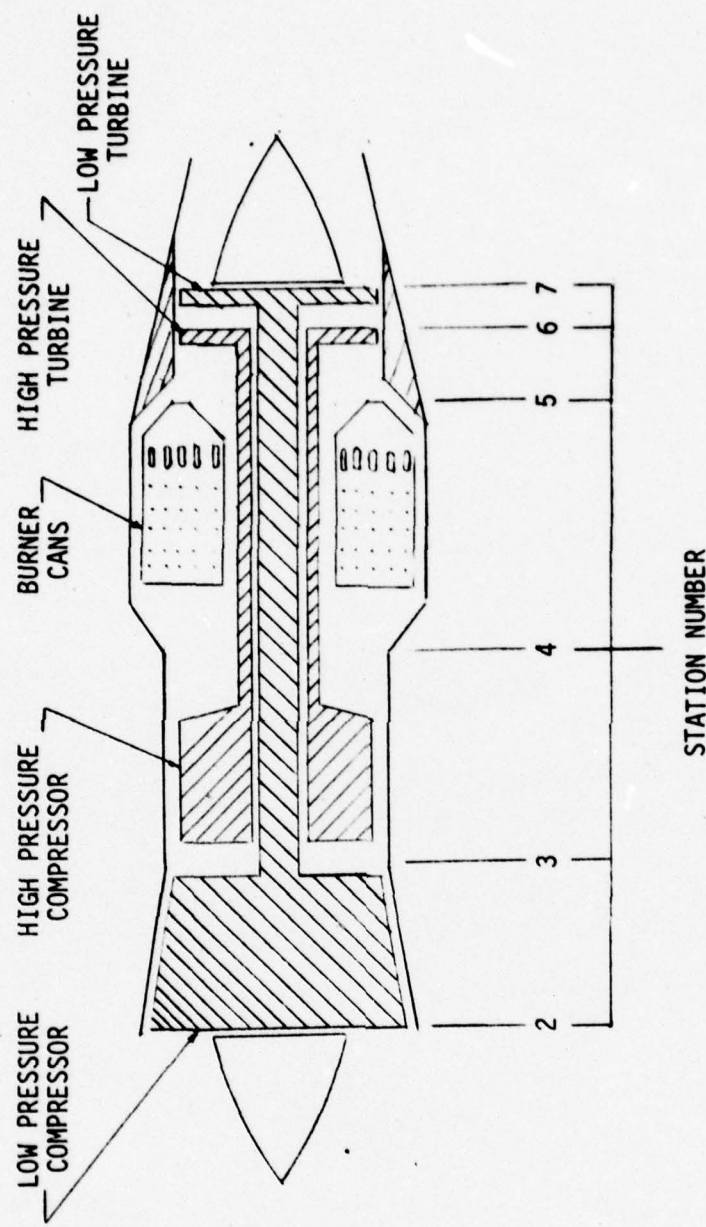


Figure 1 - Schematic of J52-P-8A Engine and Station Notation

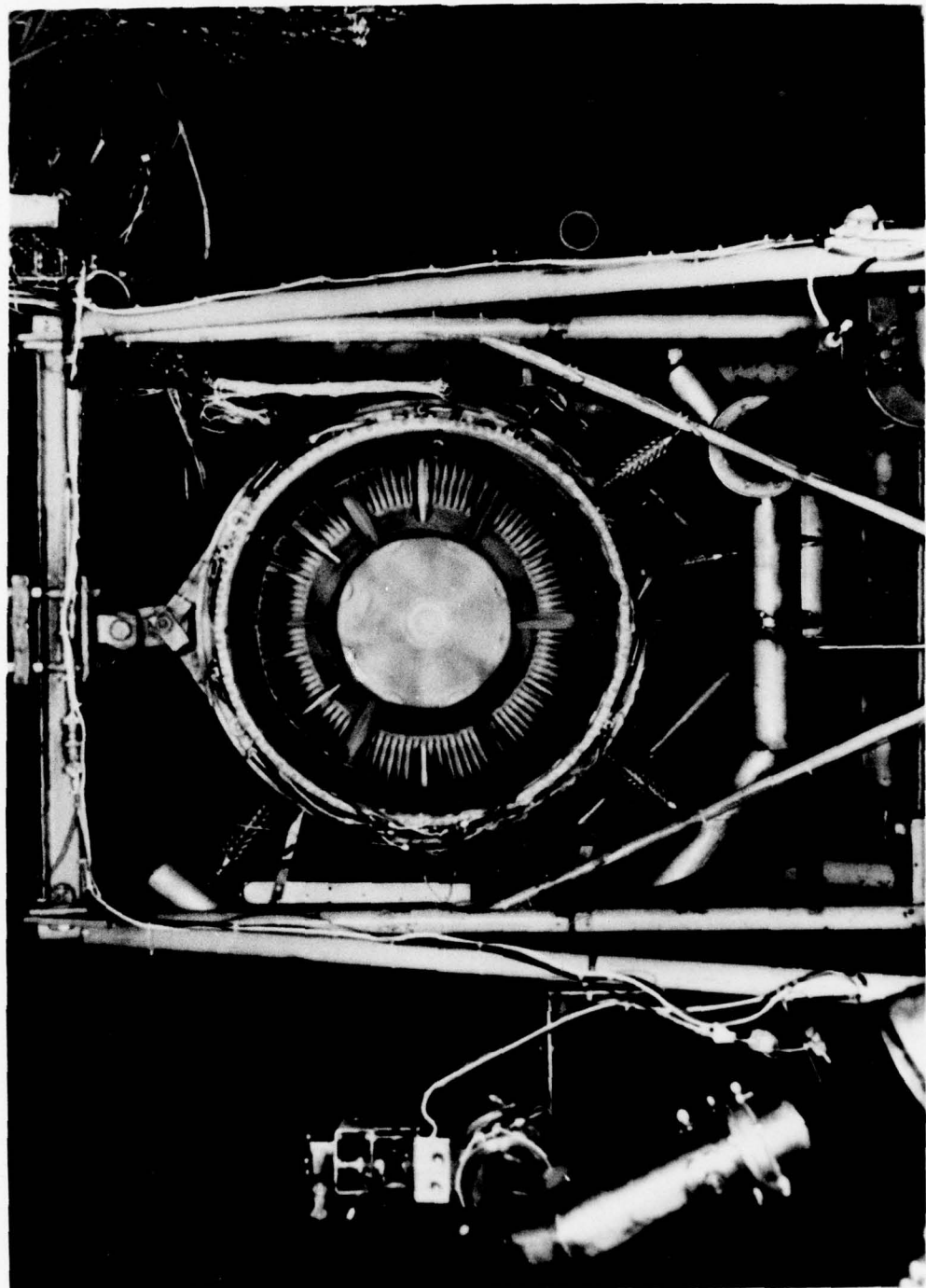


Figure 2 - Rear View of Engine Showing Turbine Blades

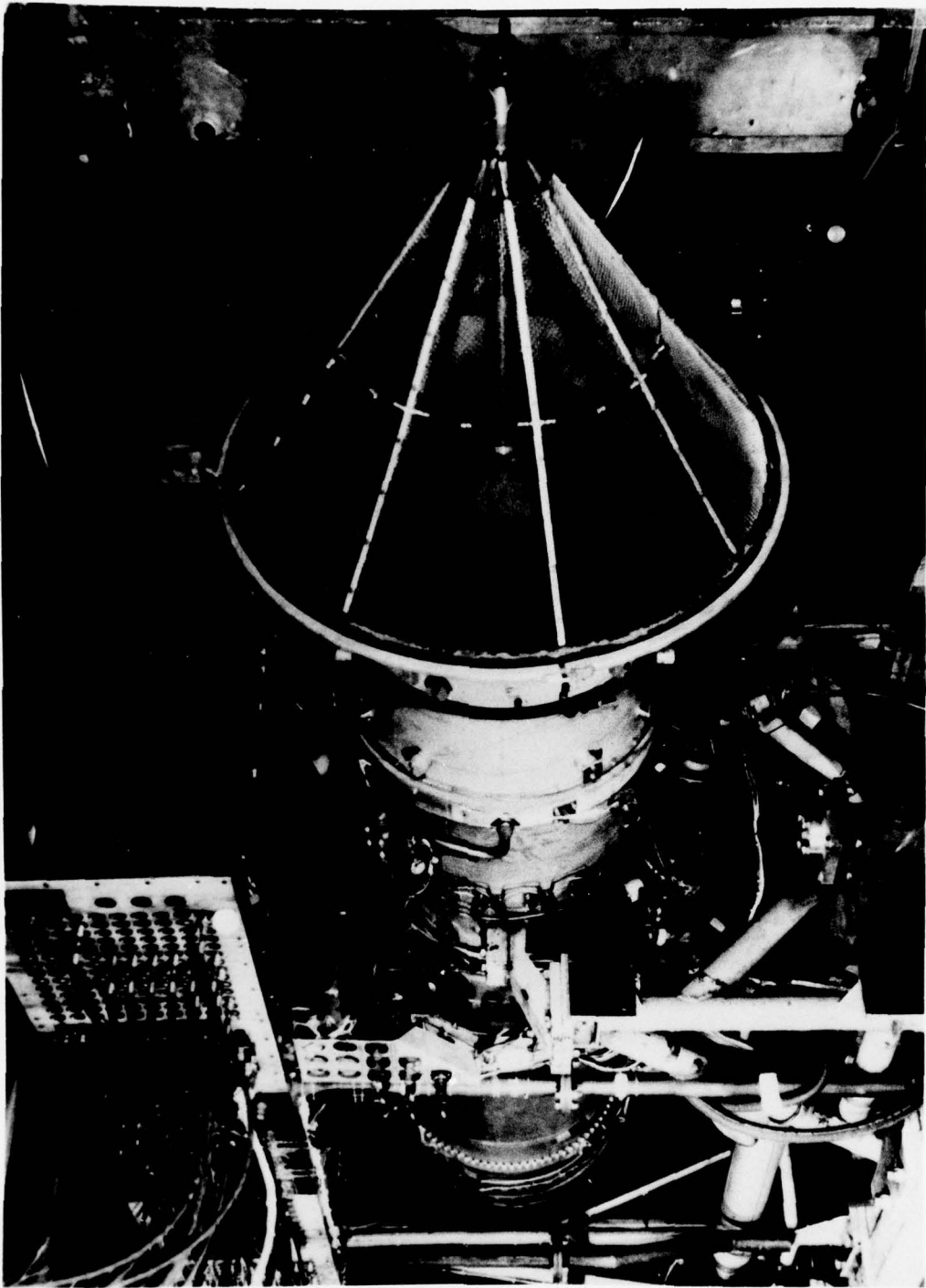


Figure 3 - Front-Left Side View of Engine Showing  
Bellmouth Inlet

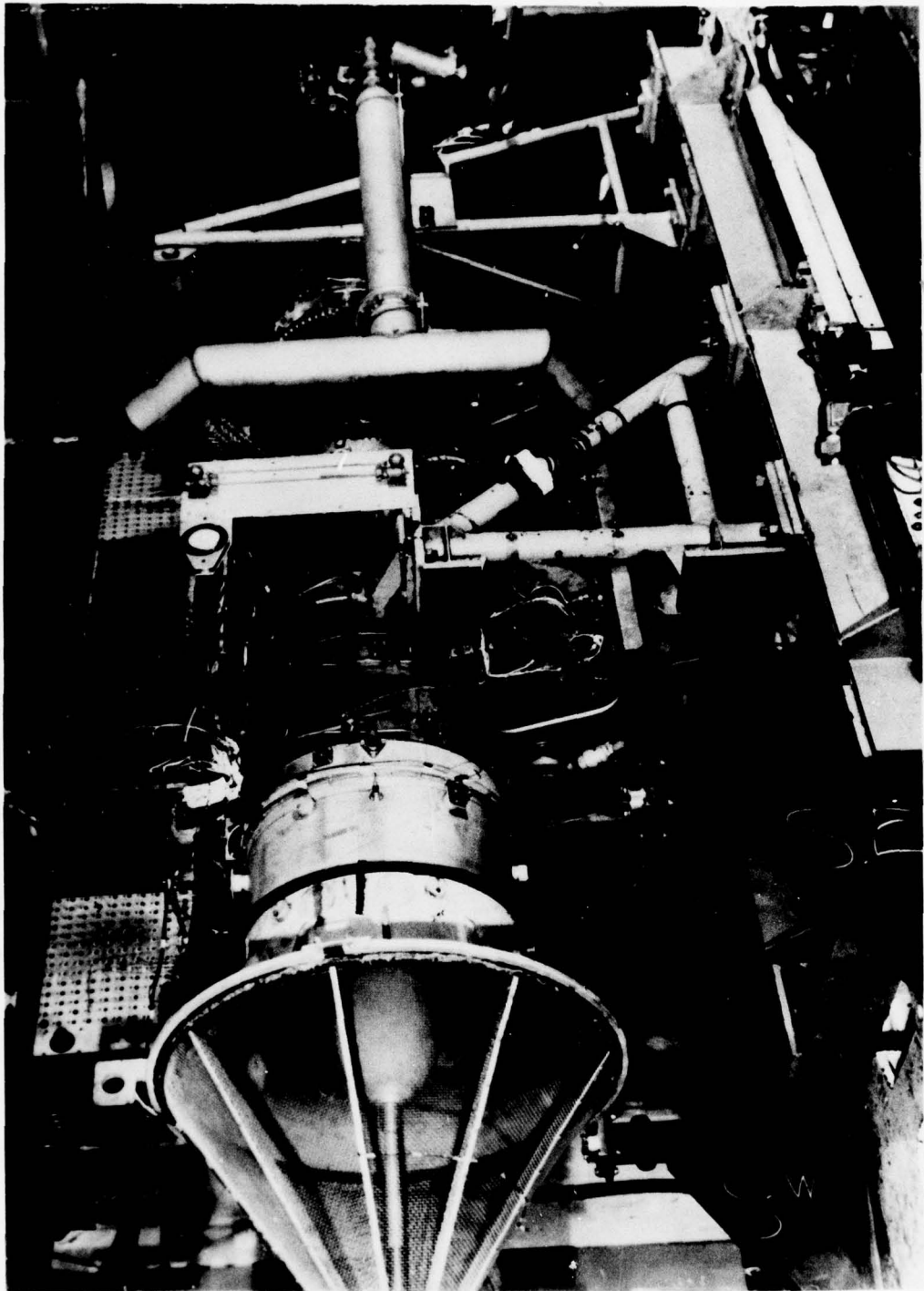


Figure 4 - Front-Right Side View of Engine Showing  
General Layout of Bleed Manifold System

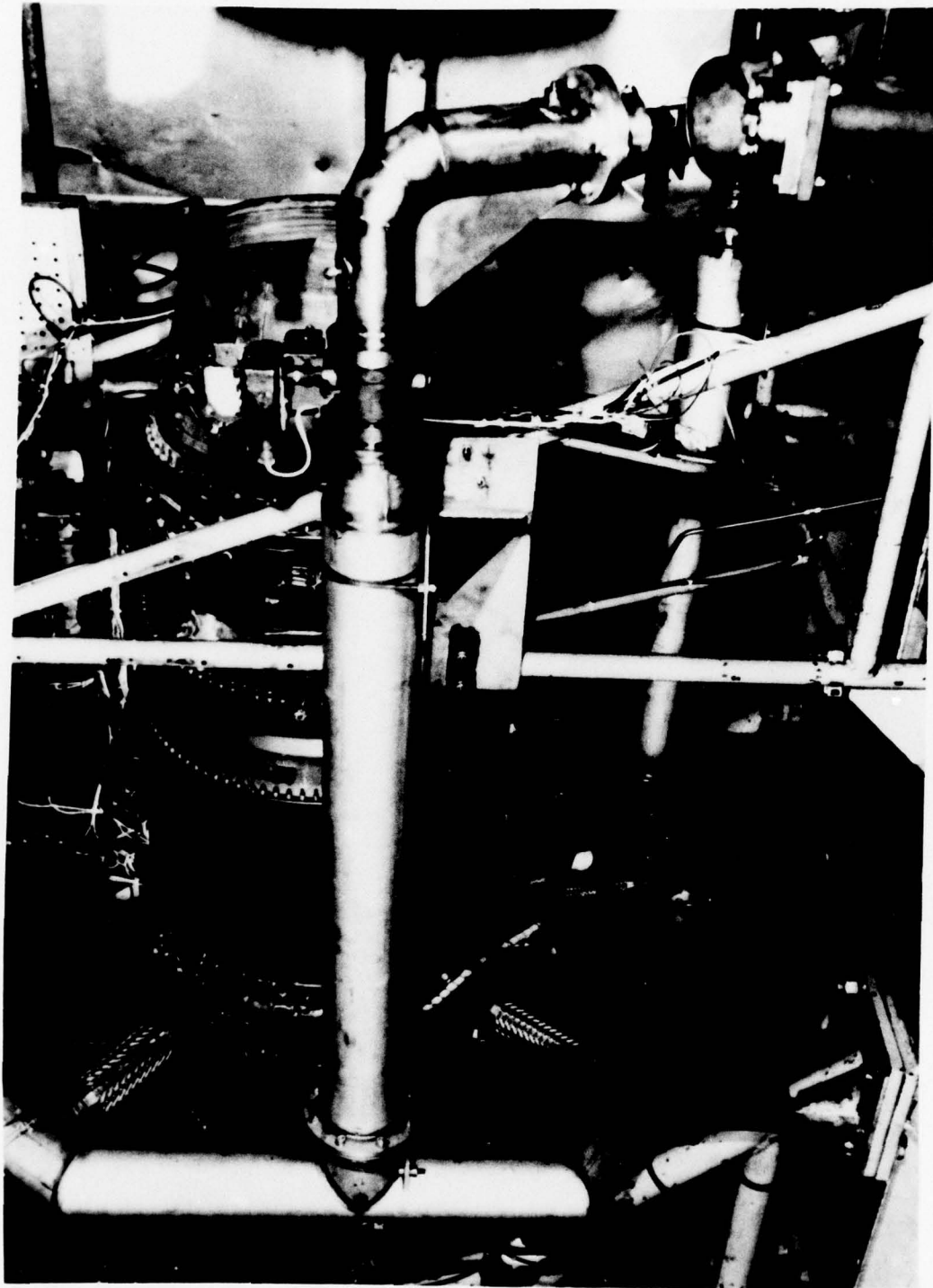


Figure 5 - Closeup View of Bleed Manifold System  
Showing Reducer Pipe, Butterfly Valve  
and Measuring Nozzle

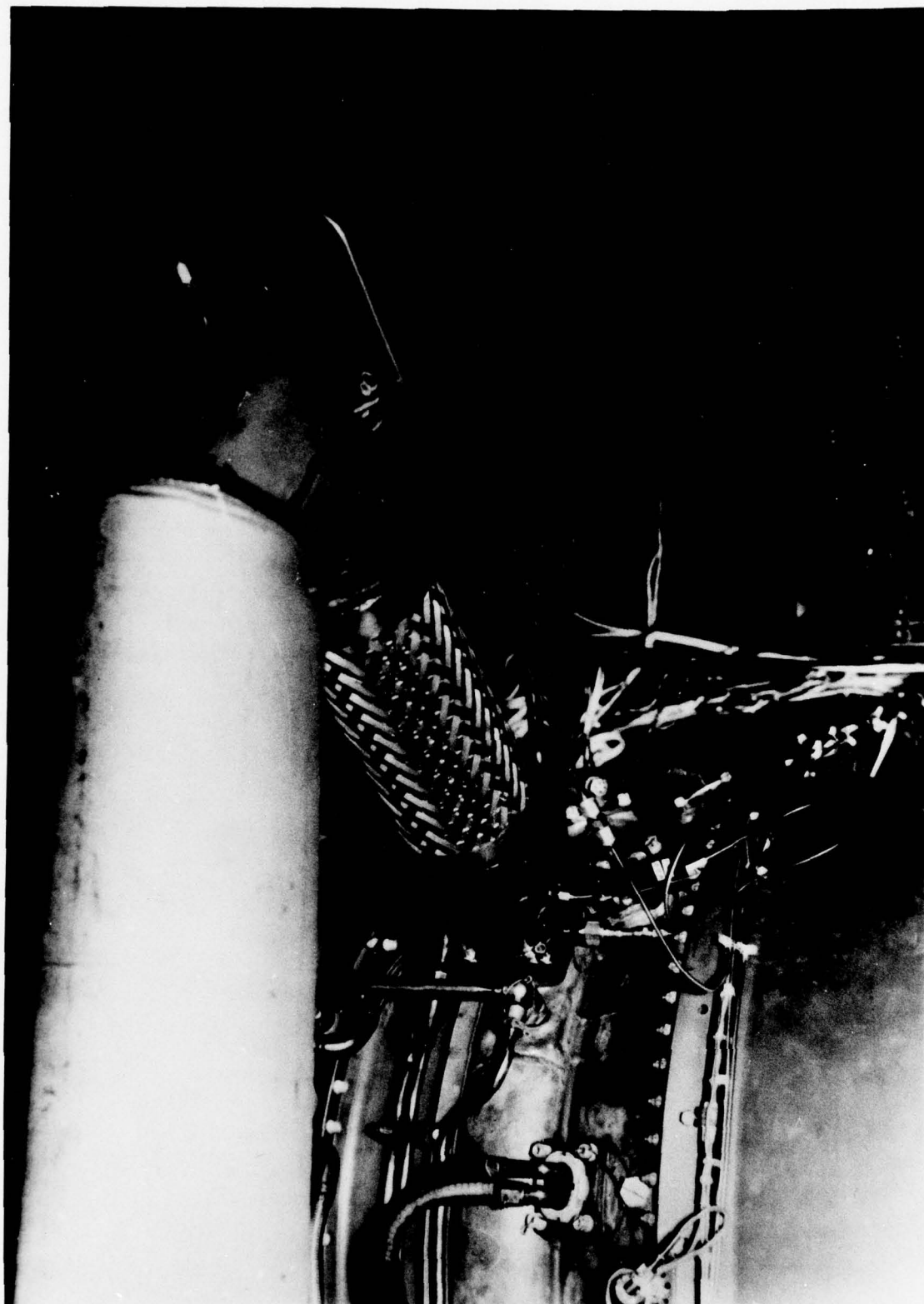


Figure 6 - Closeup View of Static Tap Installed on Bleed Manifold

Nozzles were carbon stained but no buildup was present.

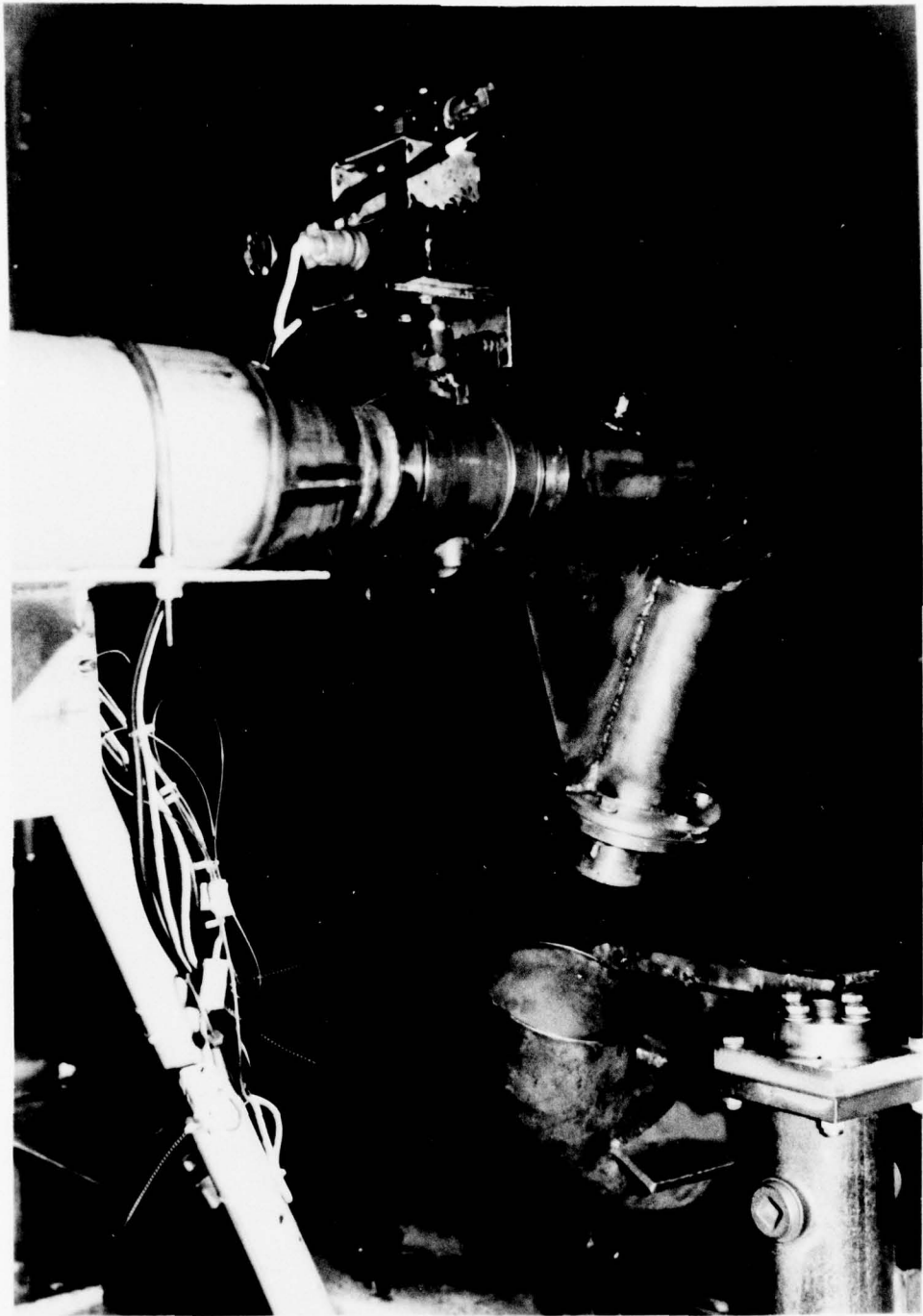


Figure 7 - Closeup View of Butterfly Valve, Measuring  
Nozzle and Collector Pipe

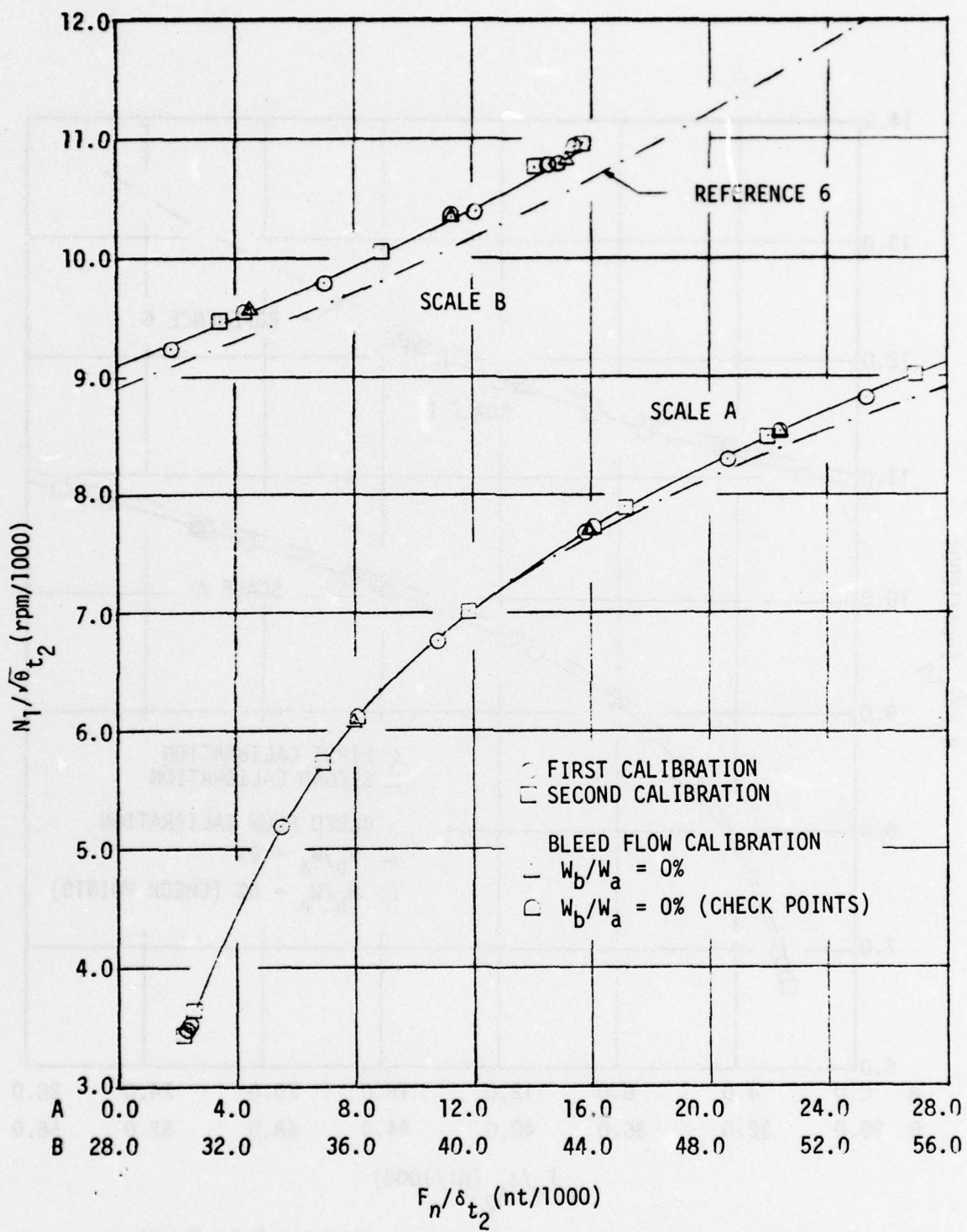


Figure 8 - Low Pressure Compressor-Turbine Unit Speed as a Function of Net Thrust

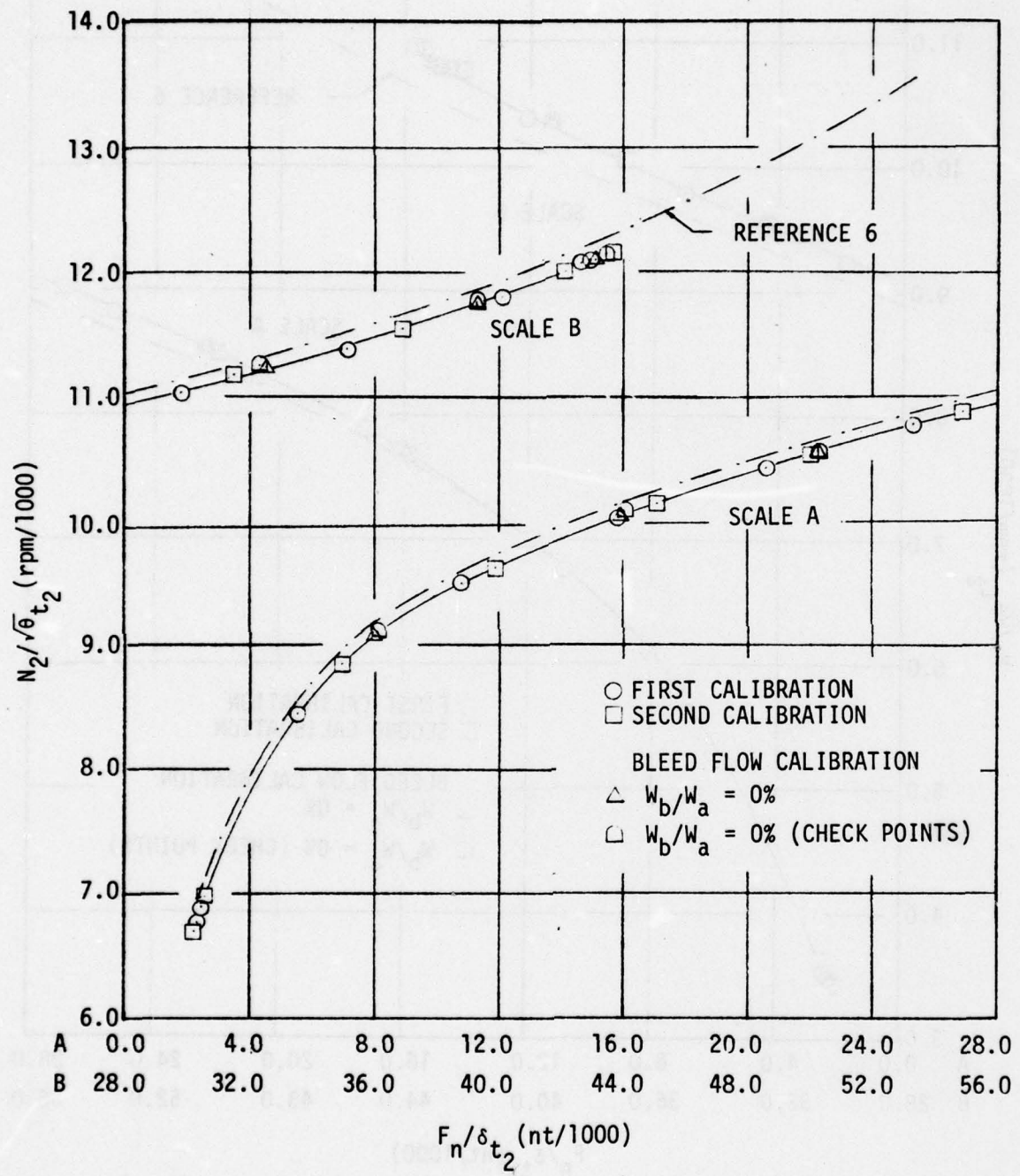


Figure 9 - High Pressure Compressor-Turbine Unit Speed as a Function of Net Thrust

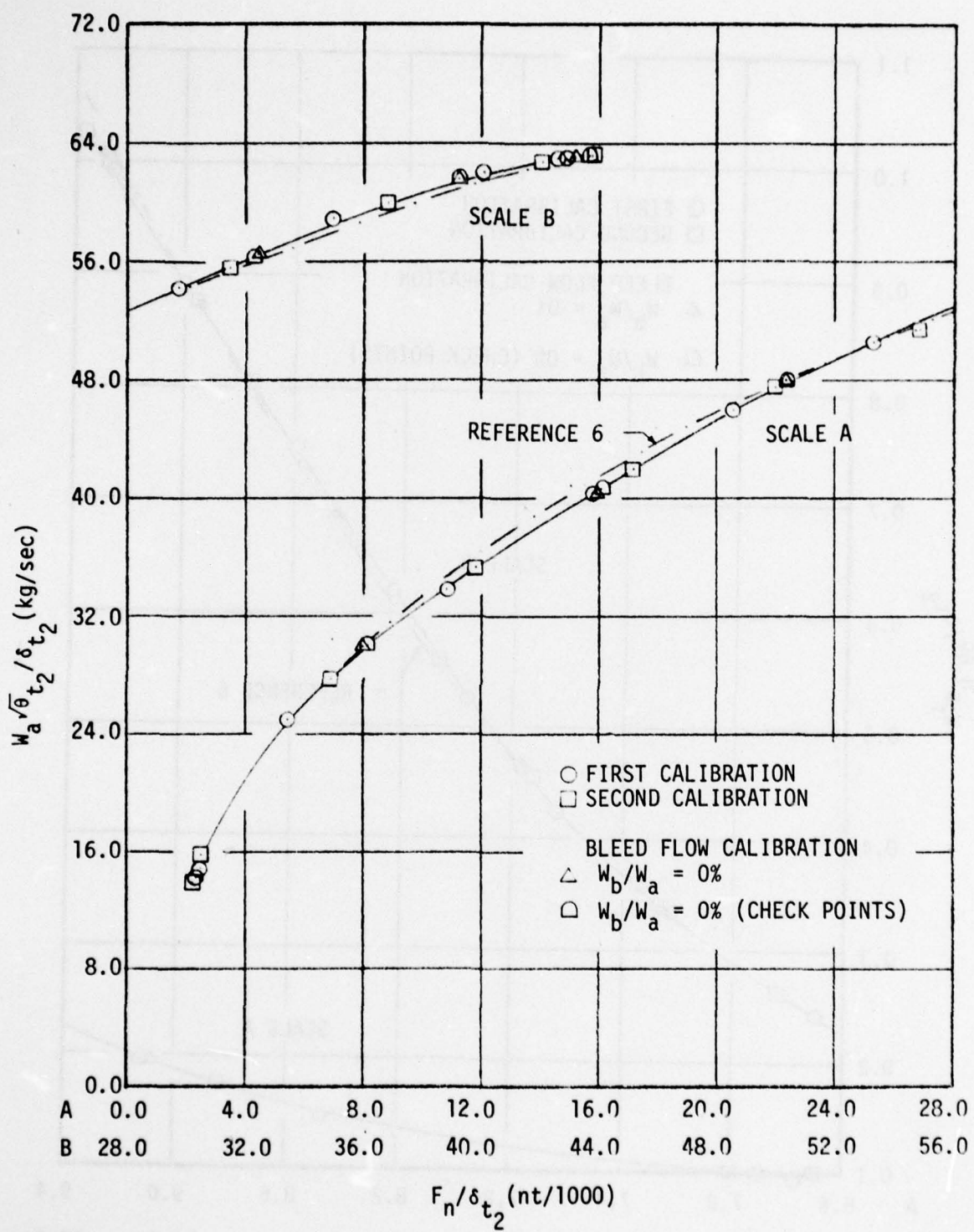


Figure 10 - Engine Airflow as a Function of Net Thrust

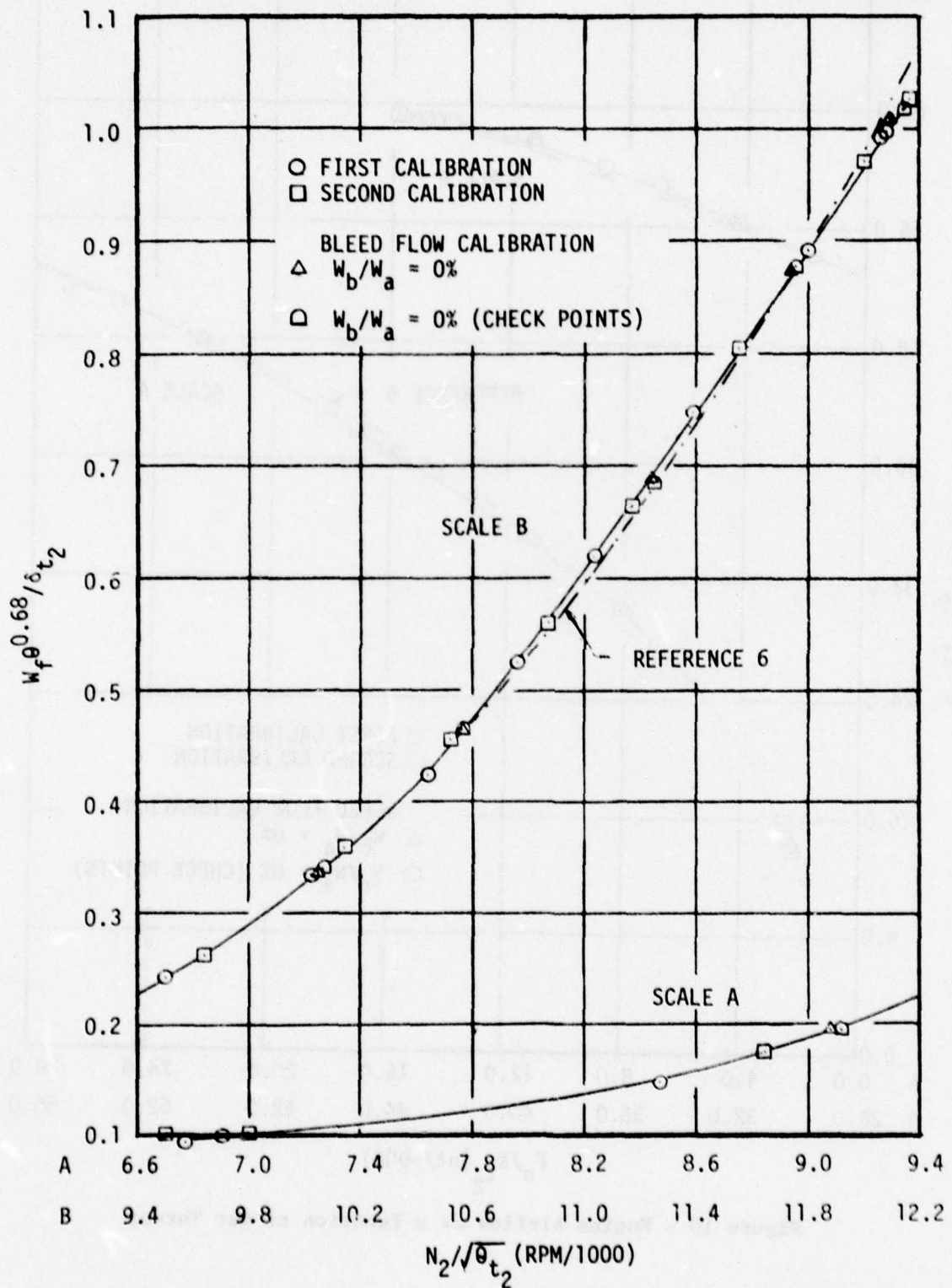


Figure 11 - Fuel Flow Rate as a Function of High Pressure  
 Compressor-Turbine Unit Speed

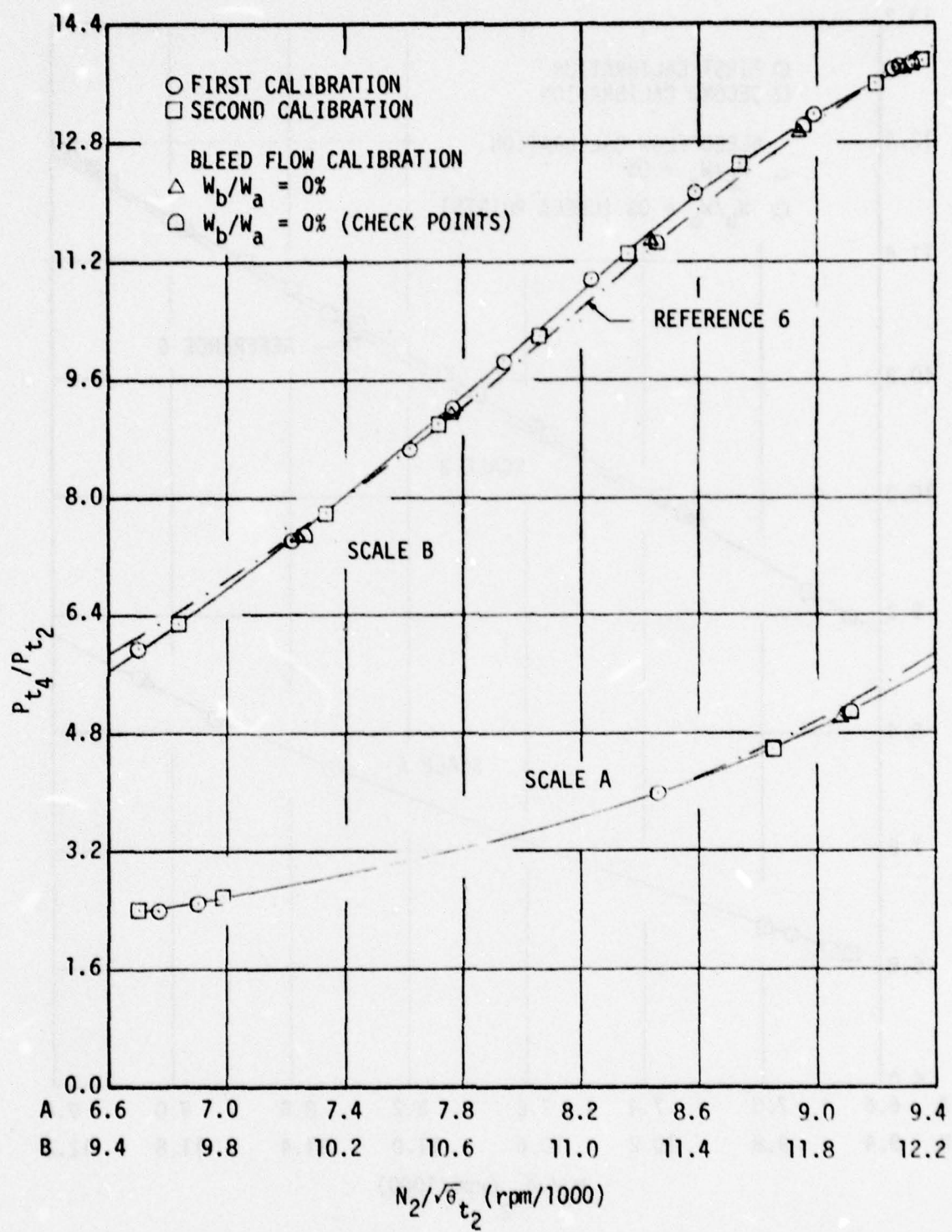


Figure 12 - High Pressure Compressor Discharge Pressure Ratio as a Function of High Pressure Compressor-Turbine Unit Speed

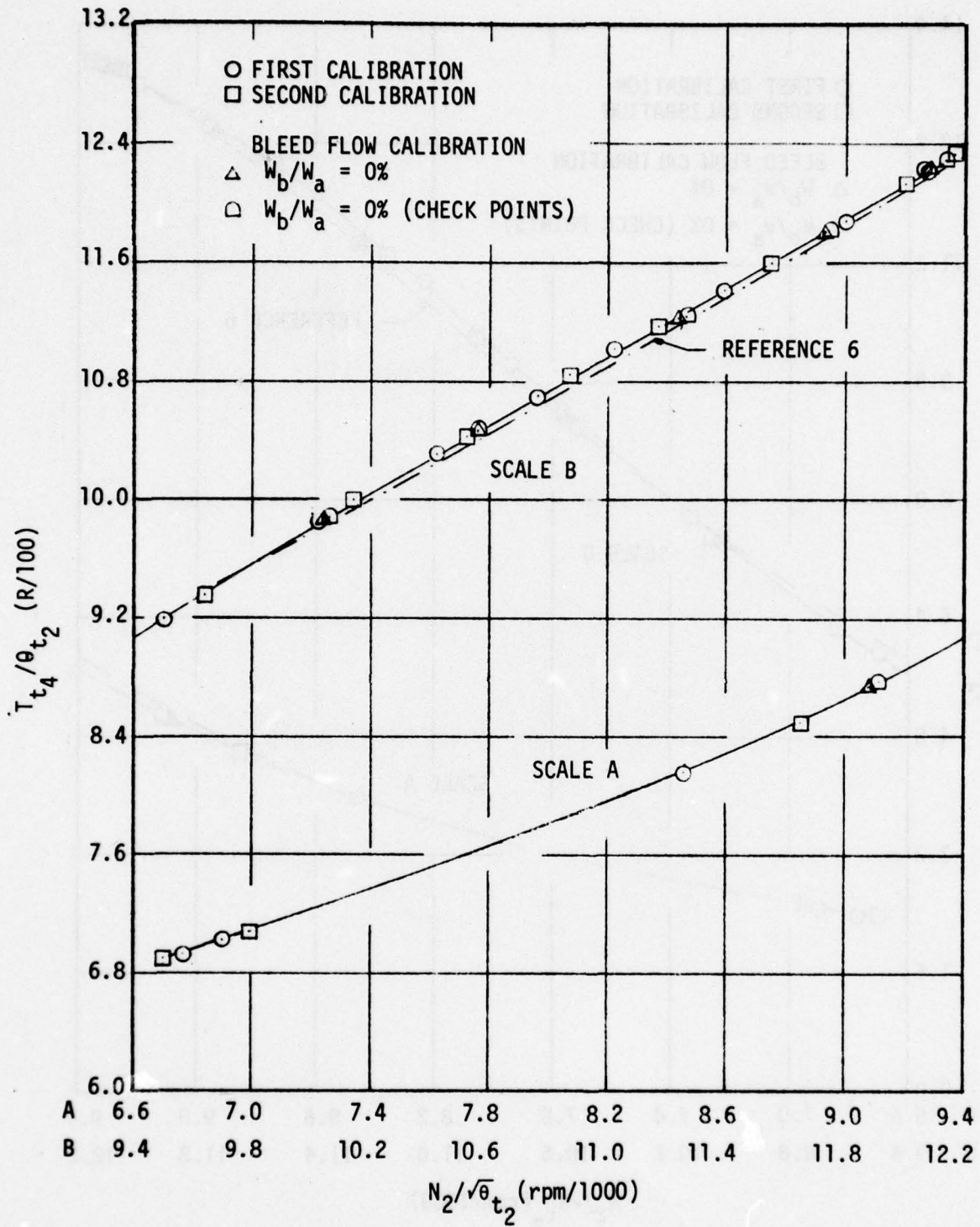


Figure 13 - High Pressure Compressor Discharge Temperature as a Function of High Pressure Compressor-Turbine Unit Speed

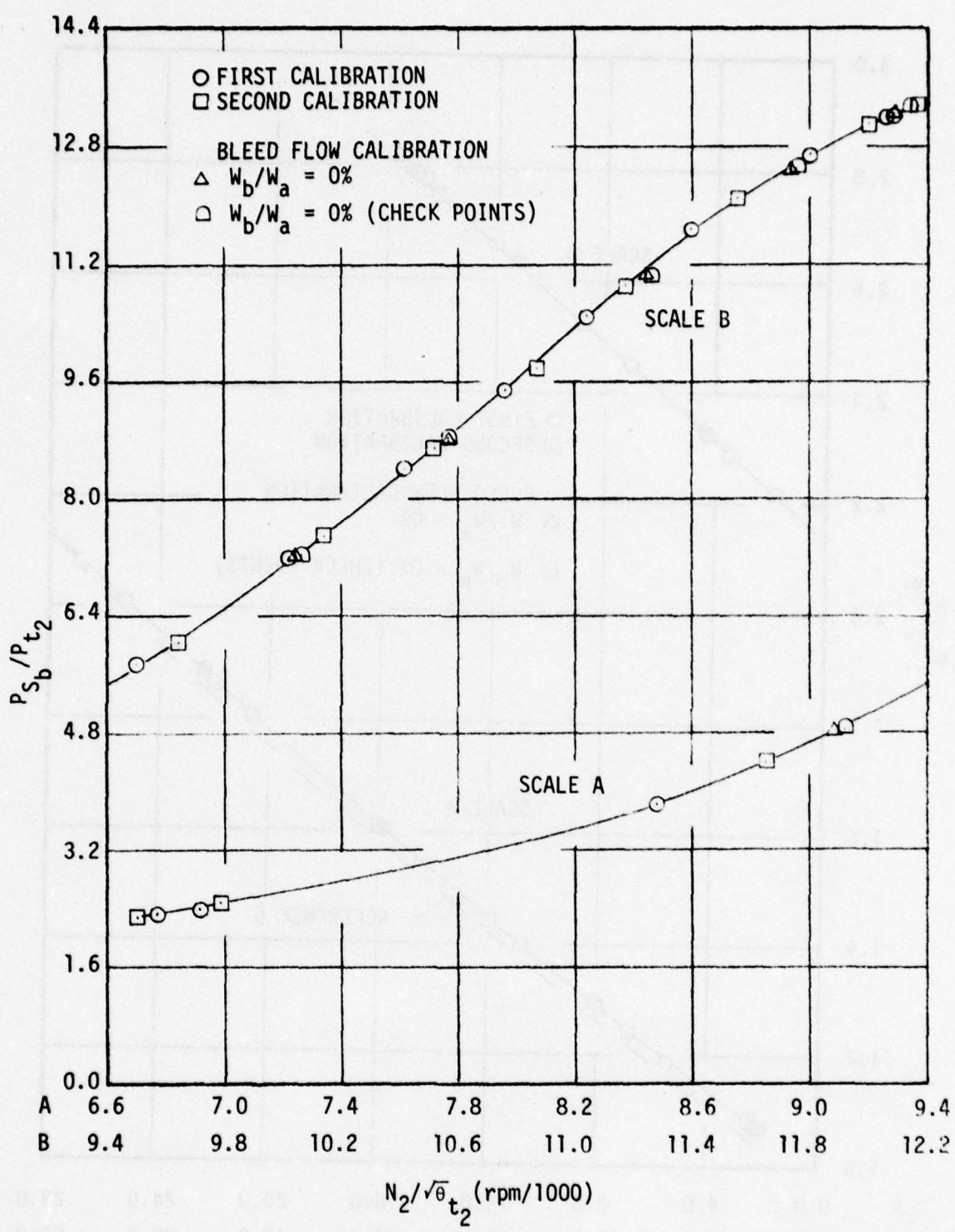


Figure 14 - Burner Static Pressure Ratio as a Function of High Pressure Compressor-Turbine Unit Speed

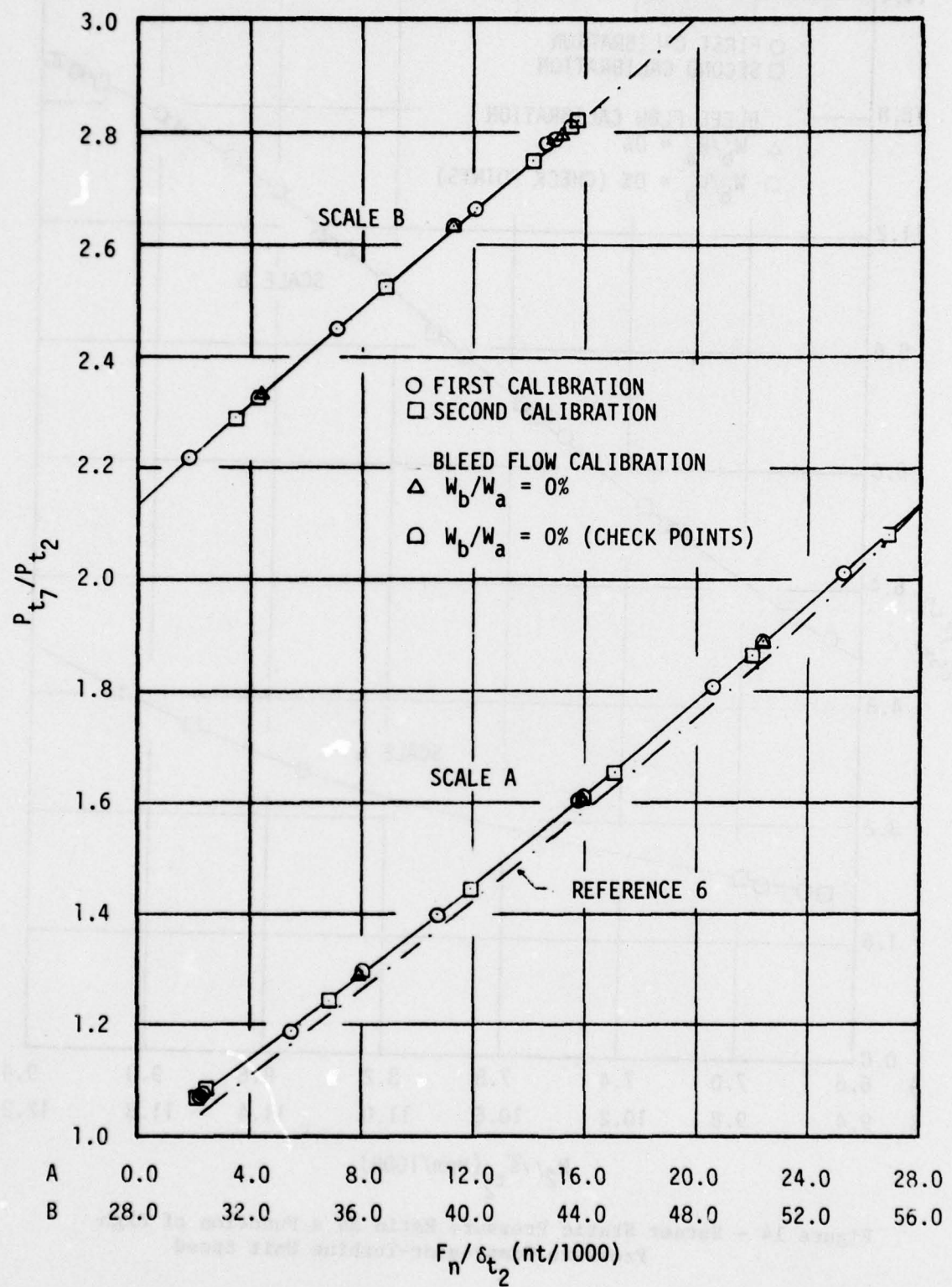
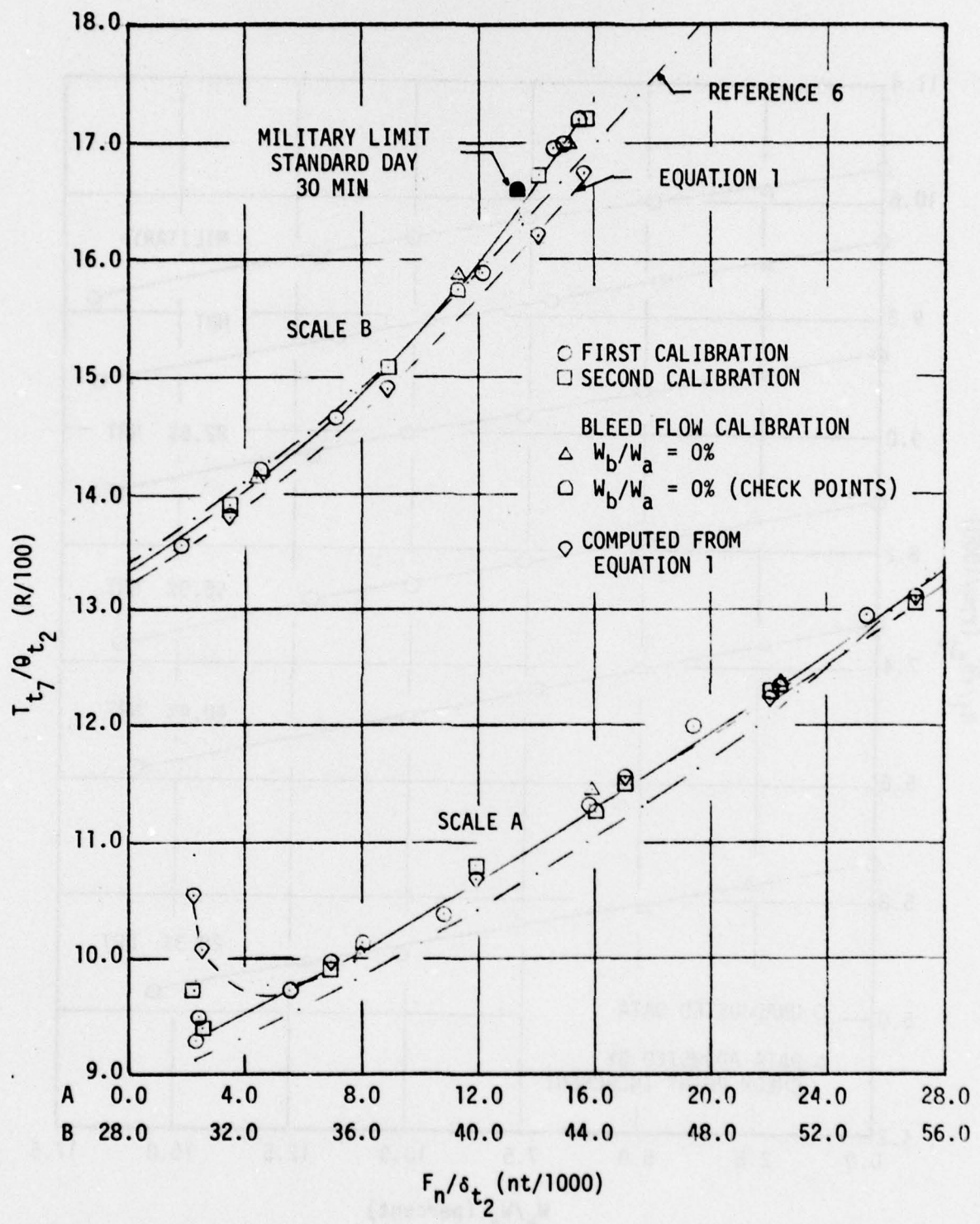


Figure 15 - Turbine Exit Pressure Ratio as a Function of Net Thrust



**Figure 16 - Turbine Exit Temperature as a Function of Net Thrust**

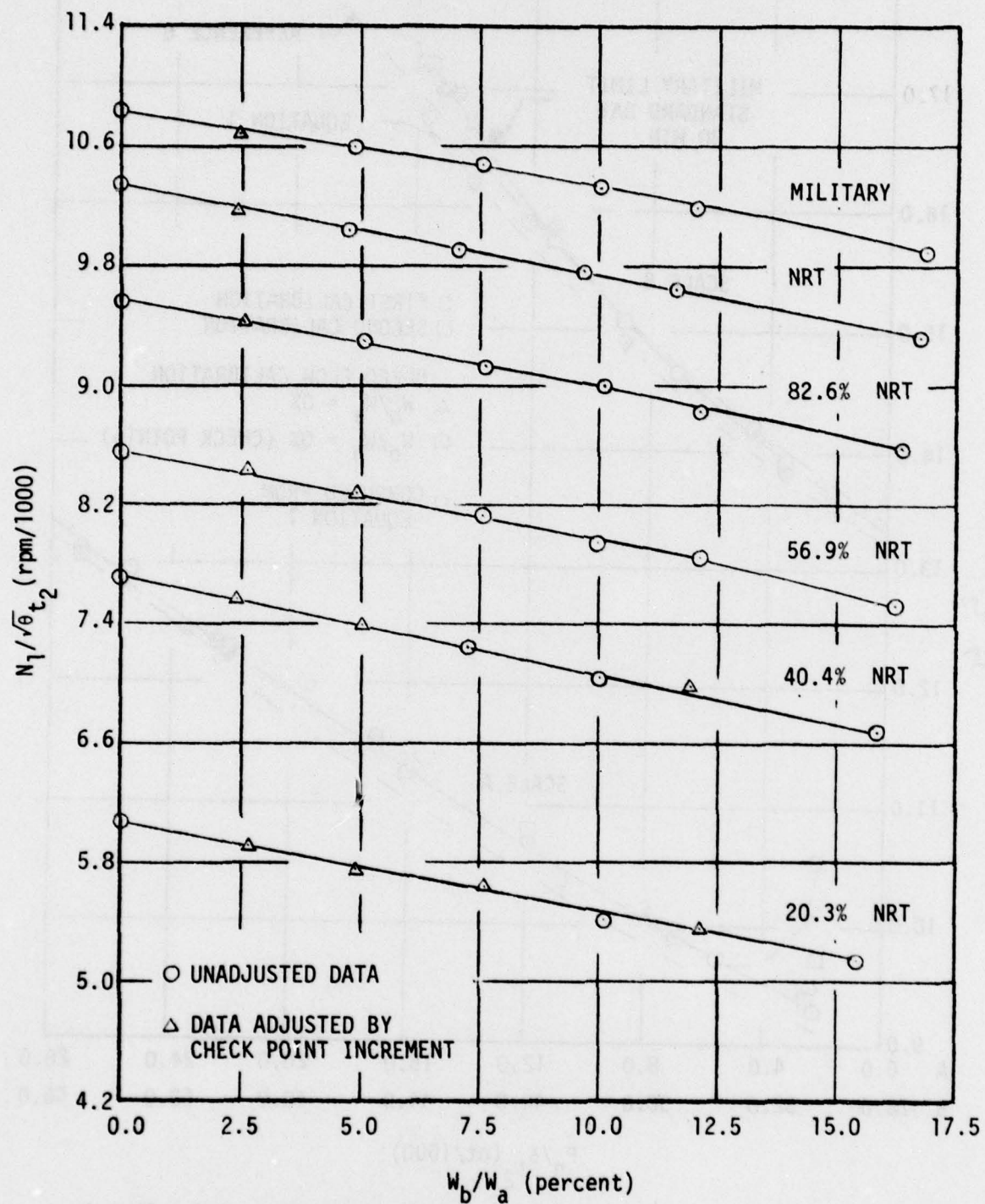


Figure 17 - Low Pressure Compressor-Turbine Unit Speed as a Function of Bleed Flow Extraction Rate

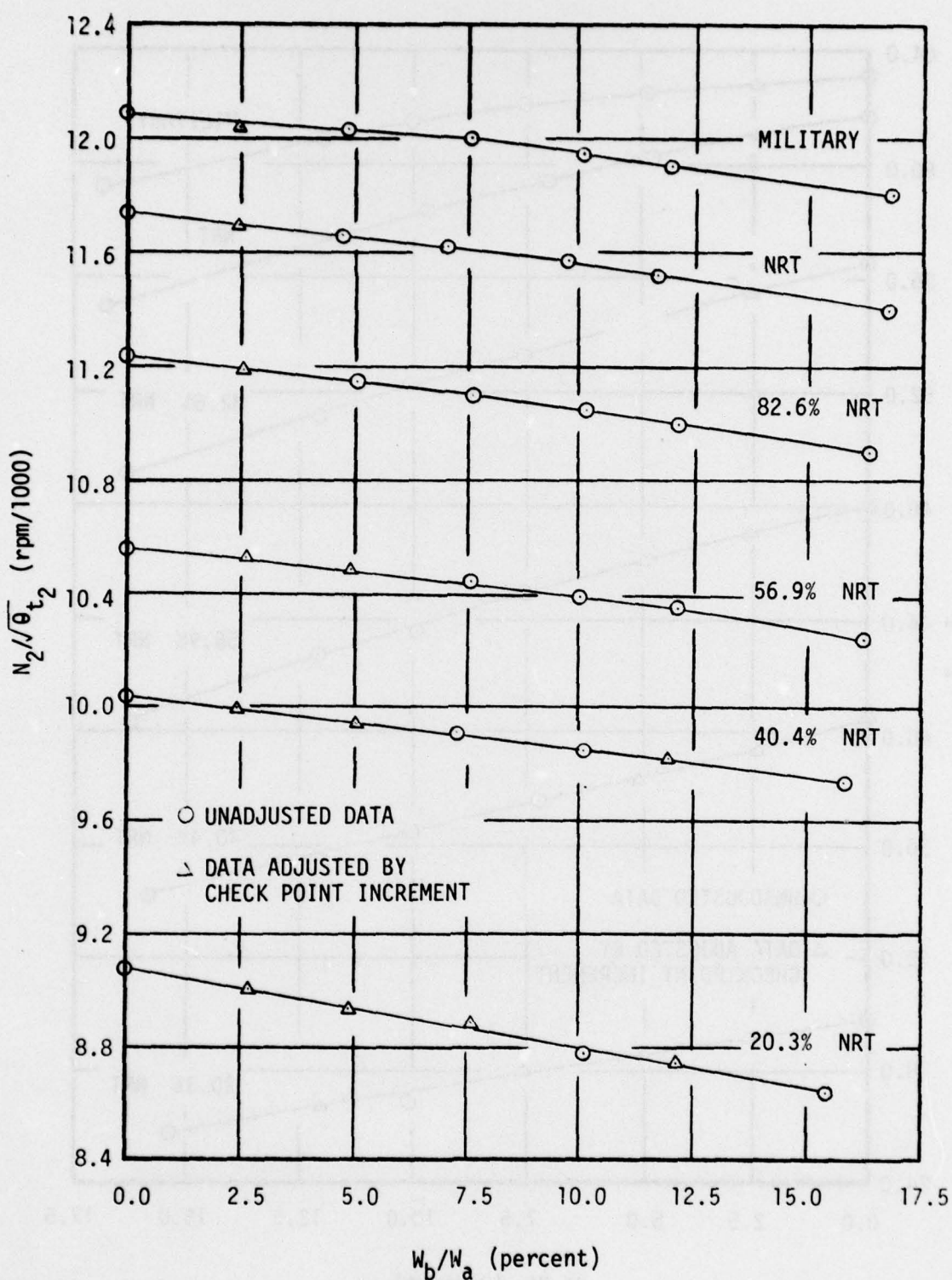


Figure 18 - High Pressure Compressor-Turbine Unit Speed as a Function of Bleed Flow Extraction Rate

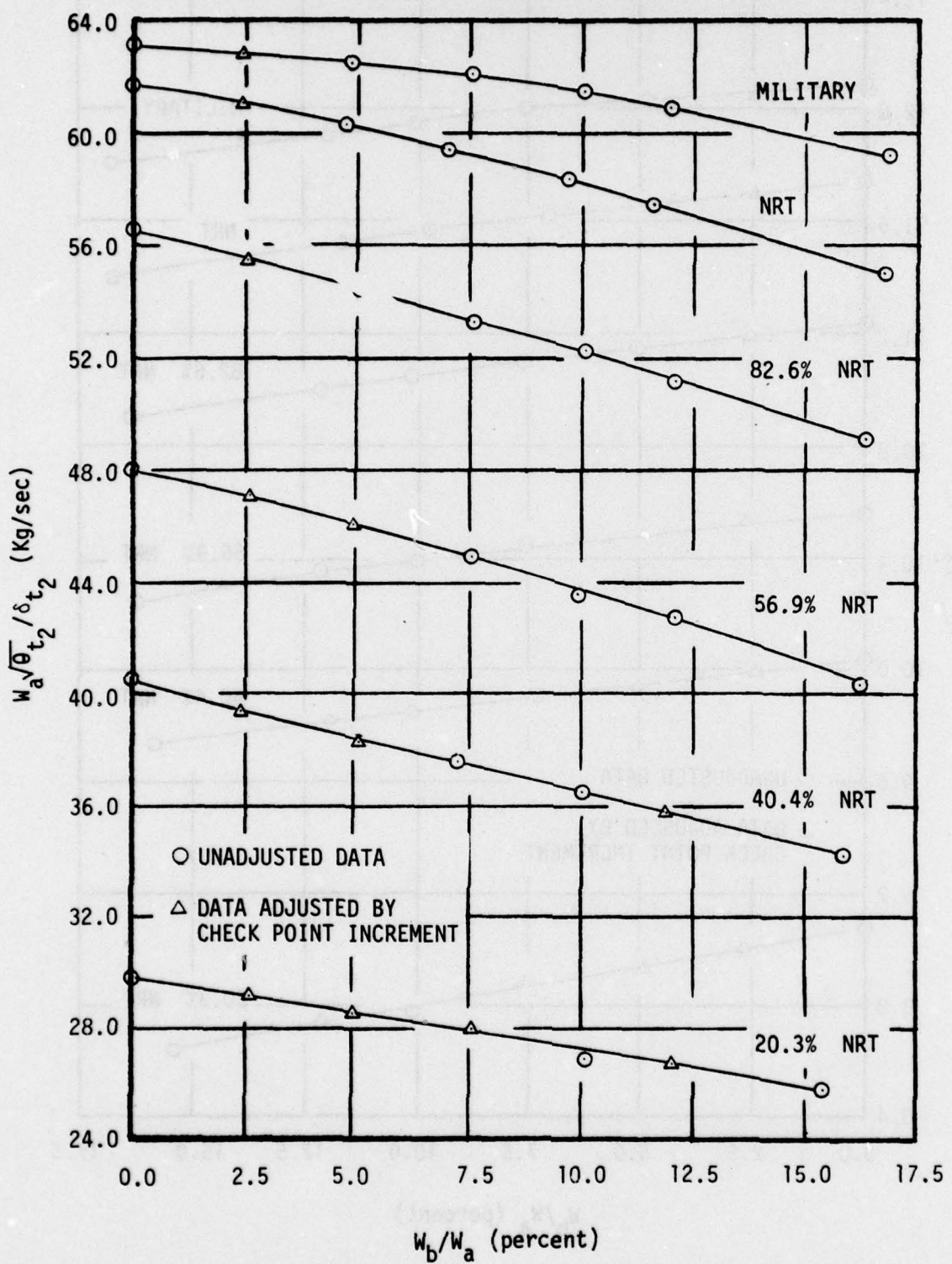


Figure 19 - Engine Airflow as a Function of Bleed Flow Extraction Rate

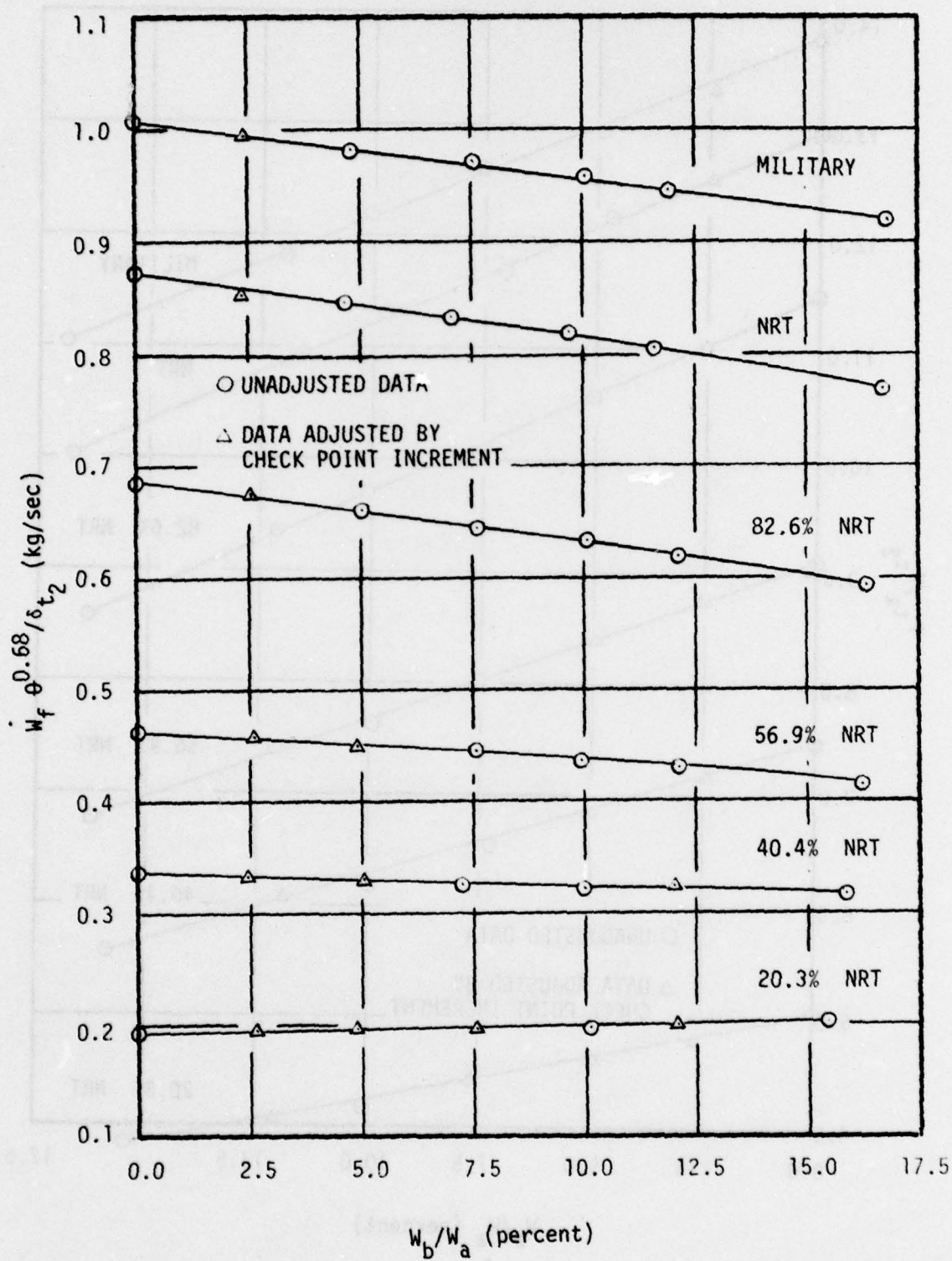


Figure 20 - Fuel Flow Rate as a Function of Bleed Flow Extraction Rate

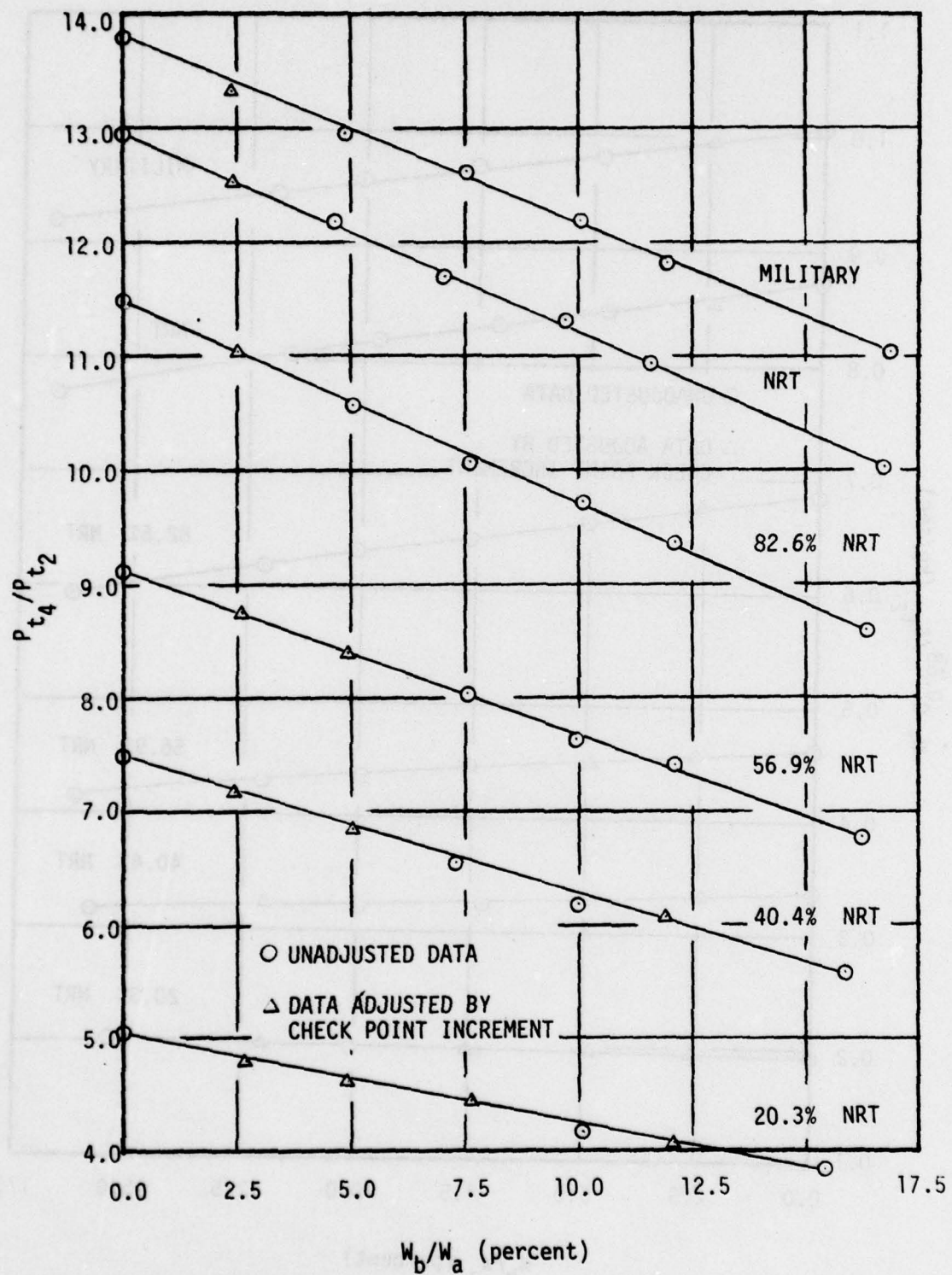


Figure 21 - High Pressure Compressor Discharge Pressure Ratio as a Function of Bleed Flow Extraction Rate

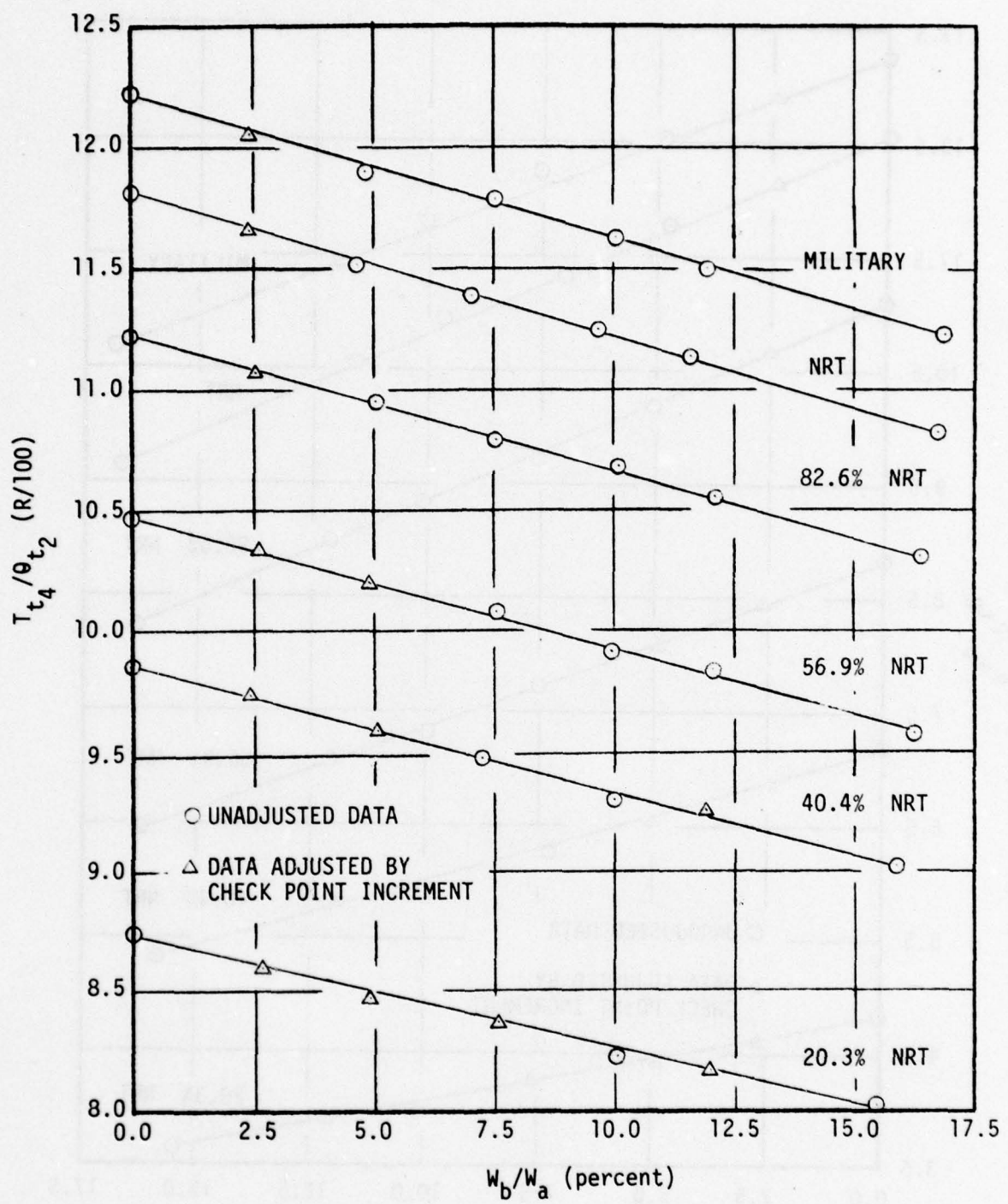


Figure 22 - High Pressure Compressor Discharge Temperature as a Function of Bleed Flow Extraction Rate

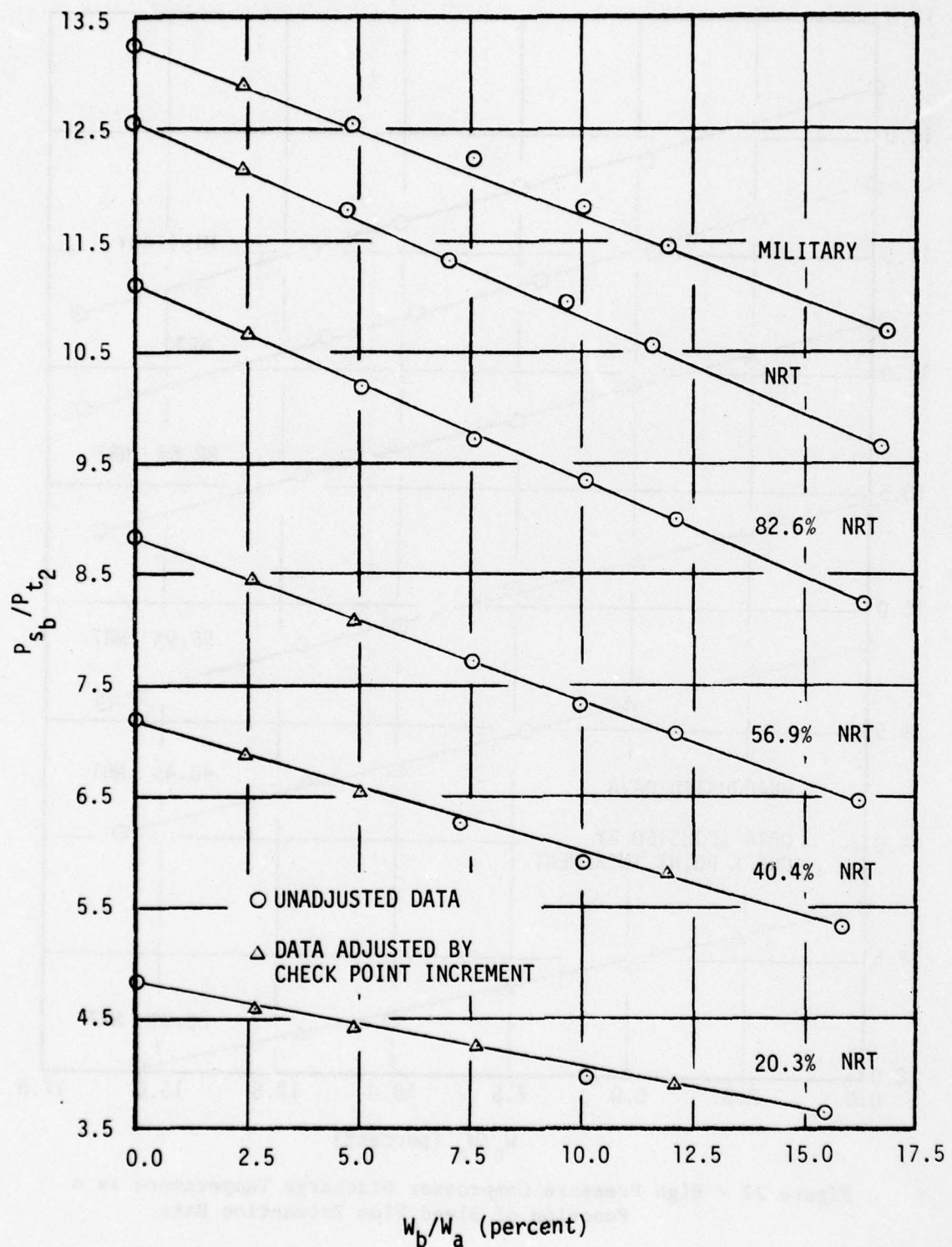


Figure 23 - Burner Static Pressure Ratio as a Function of Bleed Flow Extraction Rate

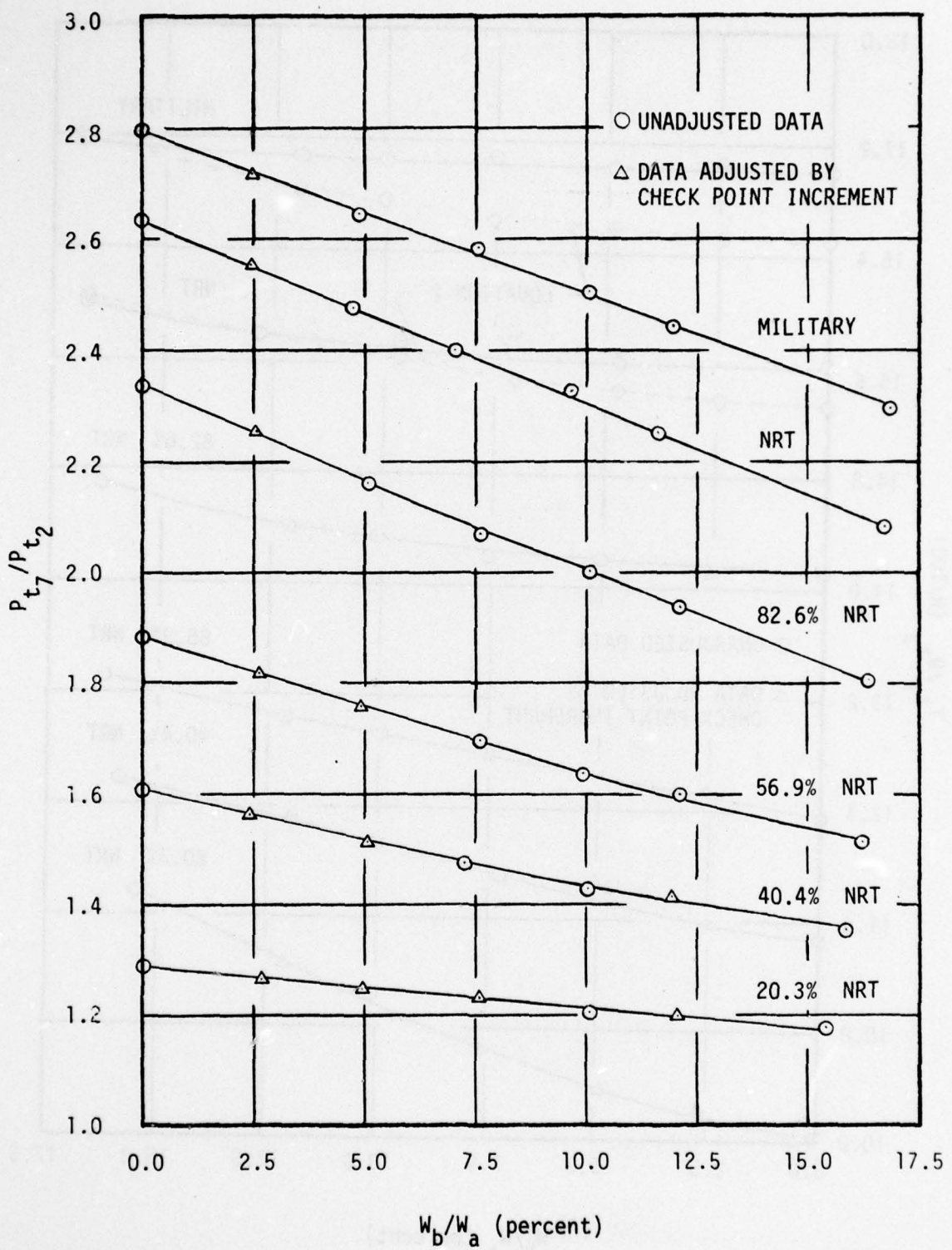


Figure 24 - Turbine Exit Pressure Ratio as a Function of Bleed Flow Extraction Rate

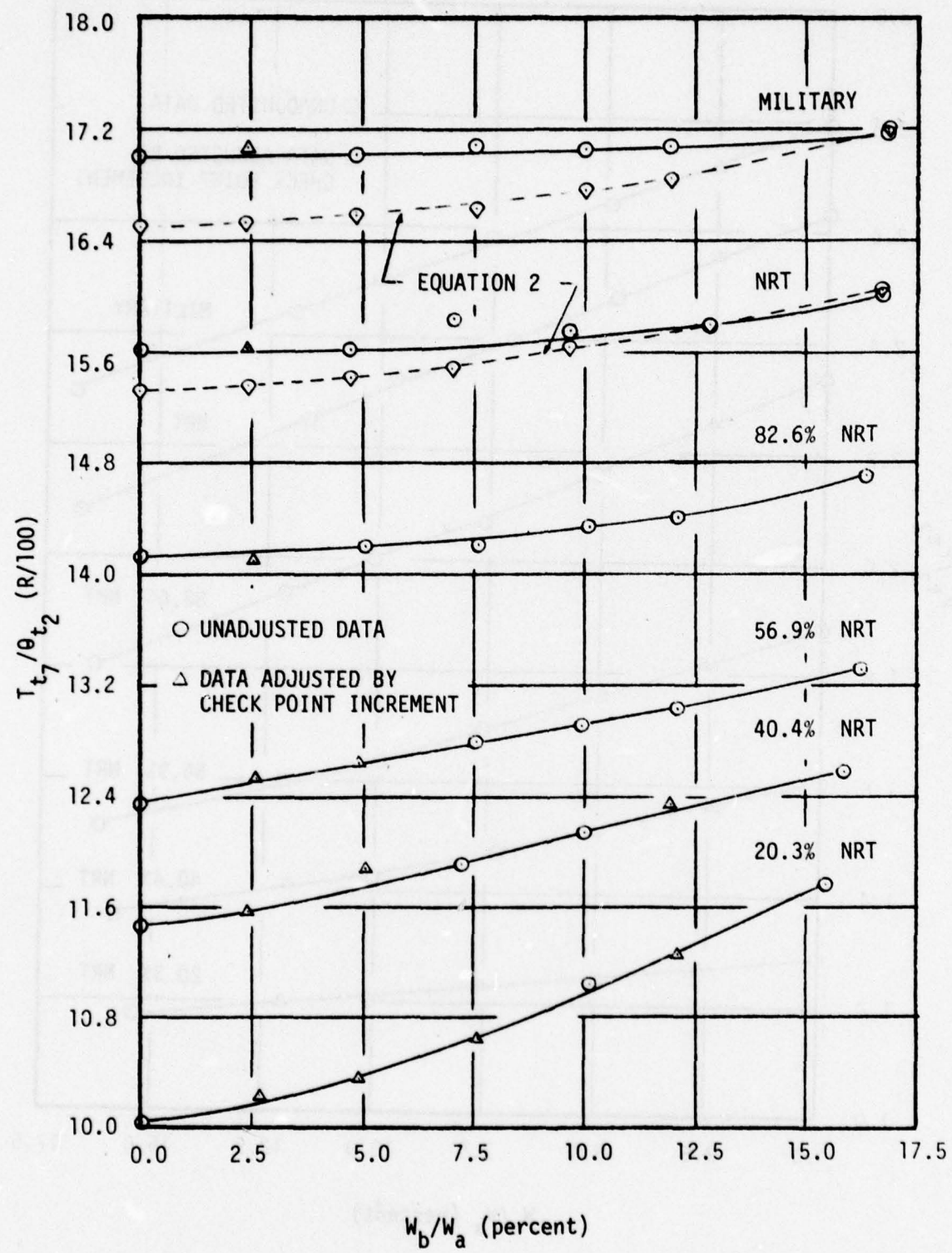


Figure 25 - Turbine Exit Temperature as a Function of Bleed Flow Extraction Rate

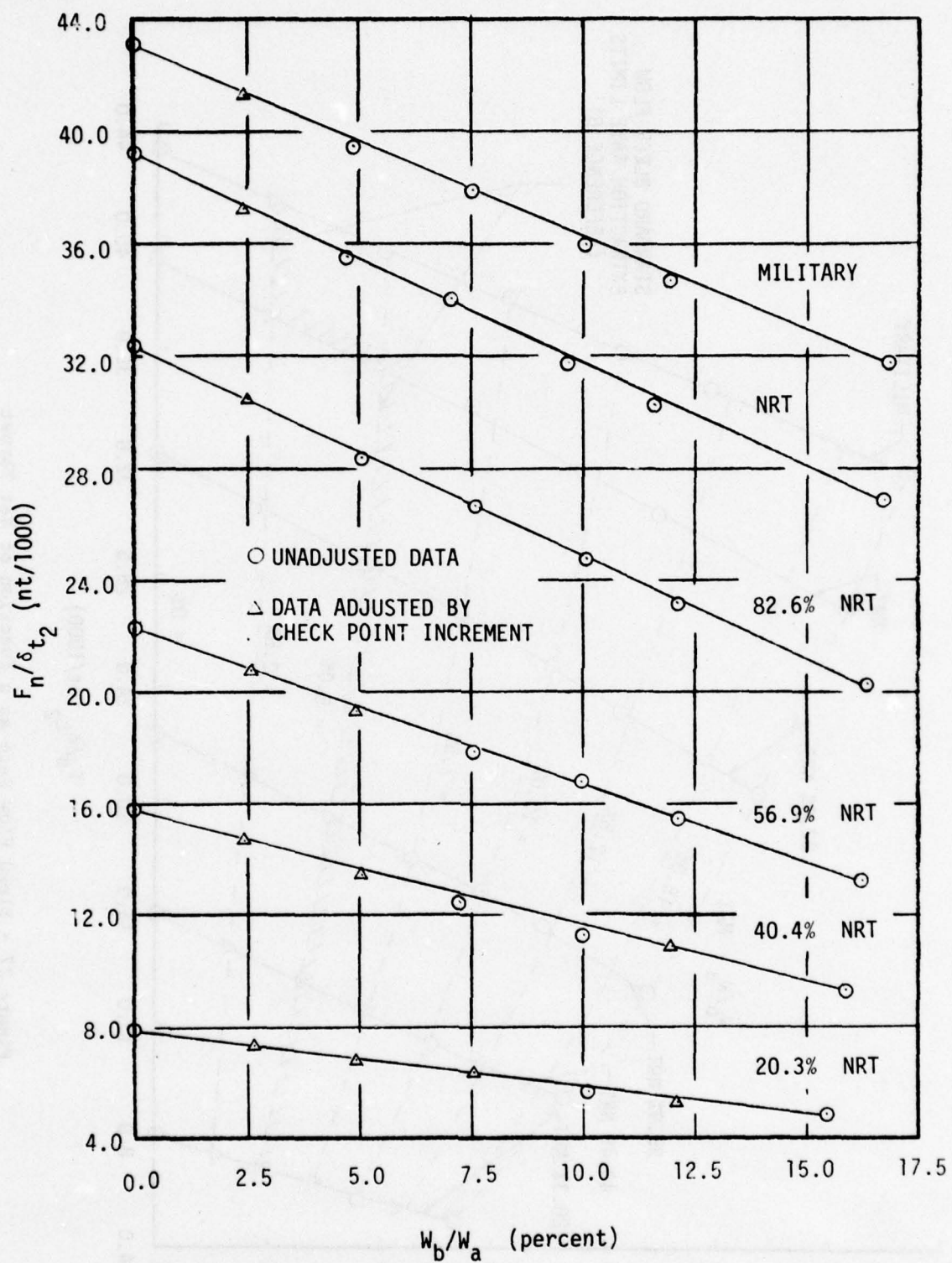


Figure 26 - Net Thrust as a Function of Bleed Flow Extraction Rate

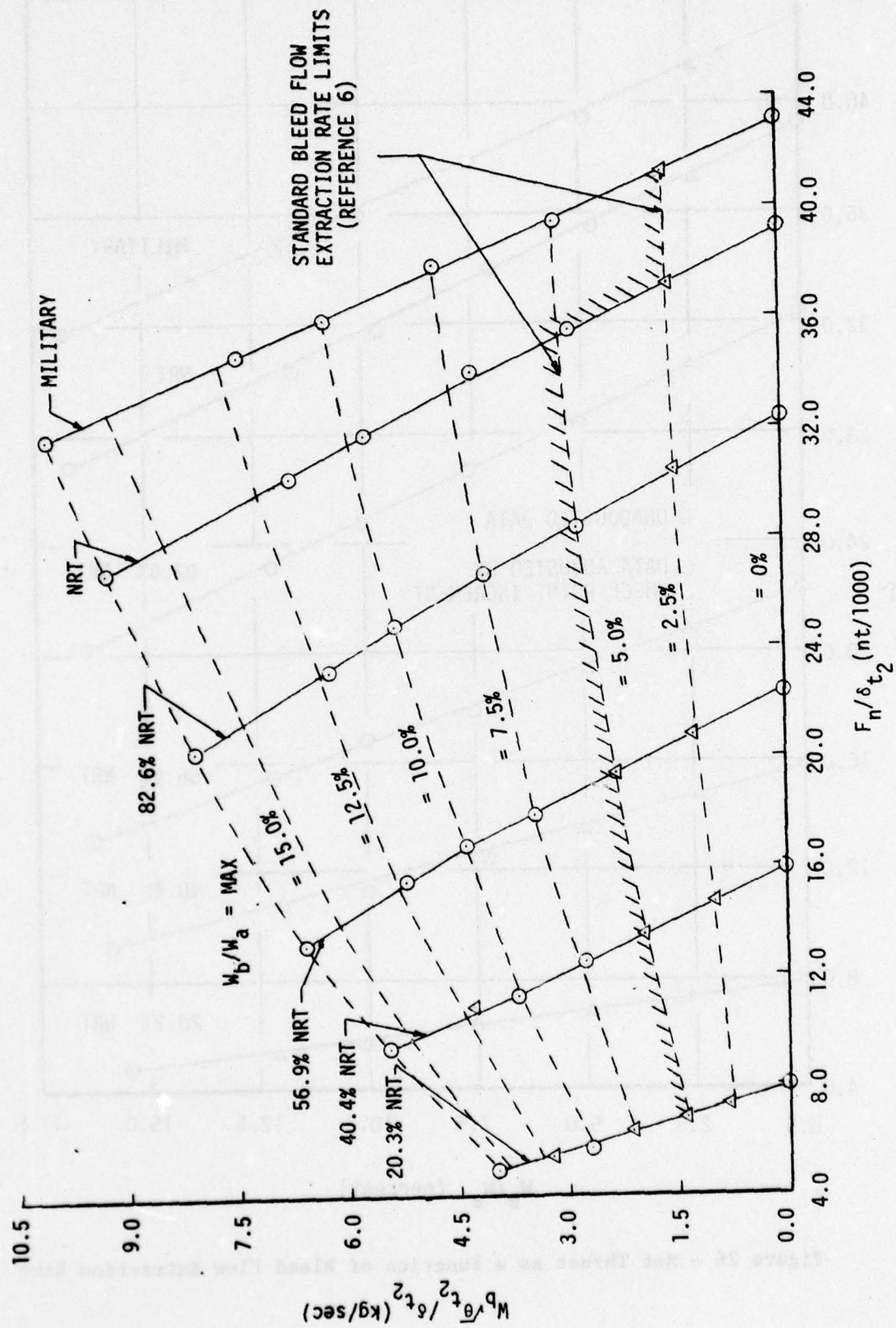


Figure 27 - Bleed Flow Rate as a Function of Net Thrust

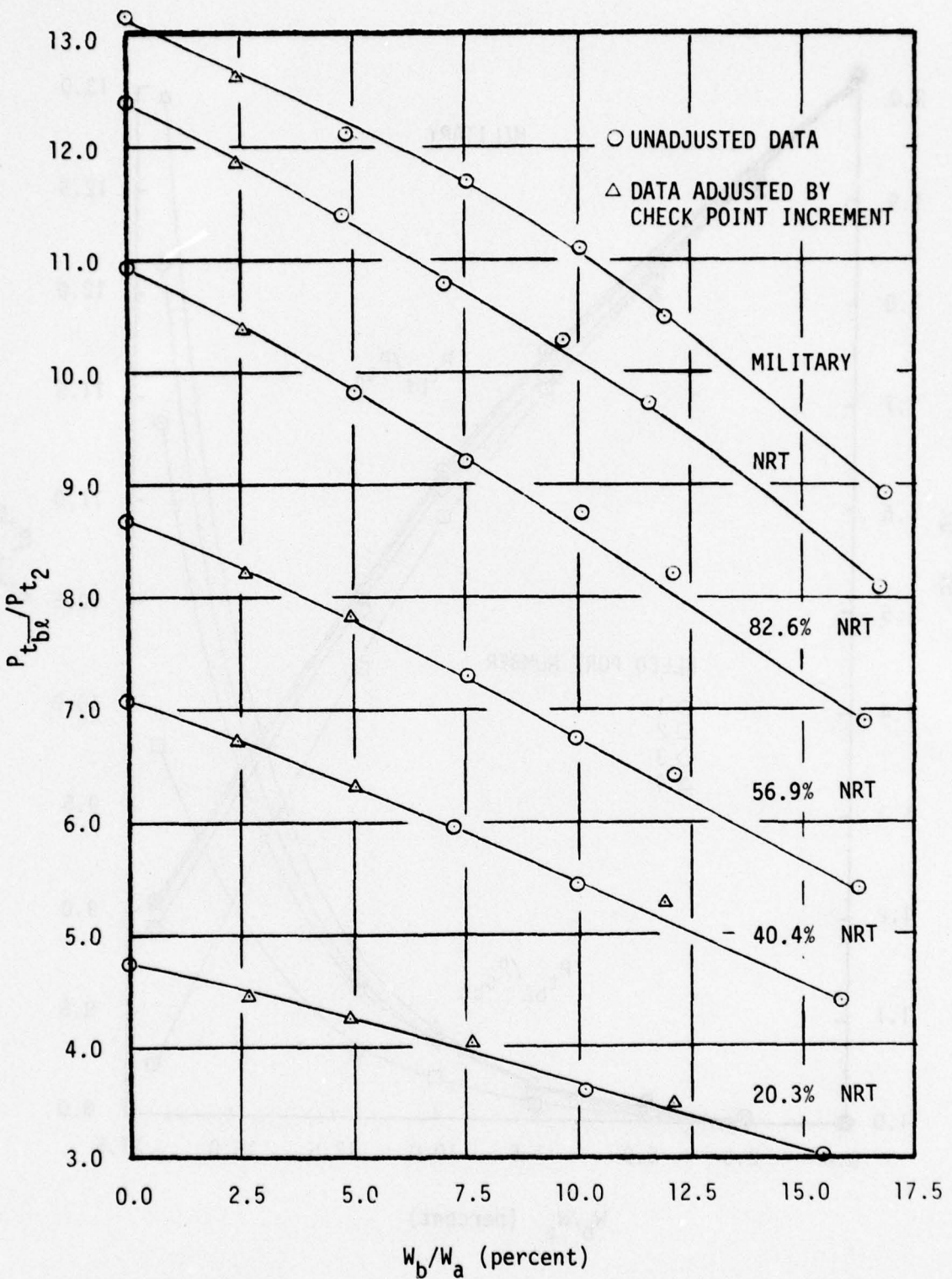


Figure 28 - Average Bleed Port Total Pressure Ratio as a Function of Bleed Flow Extraction Rate

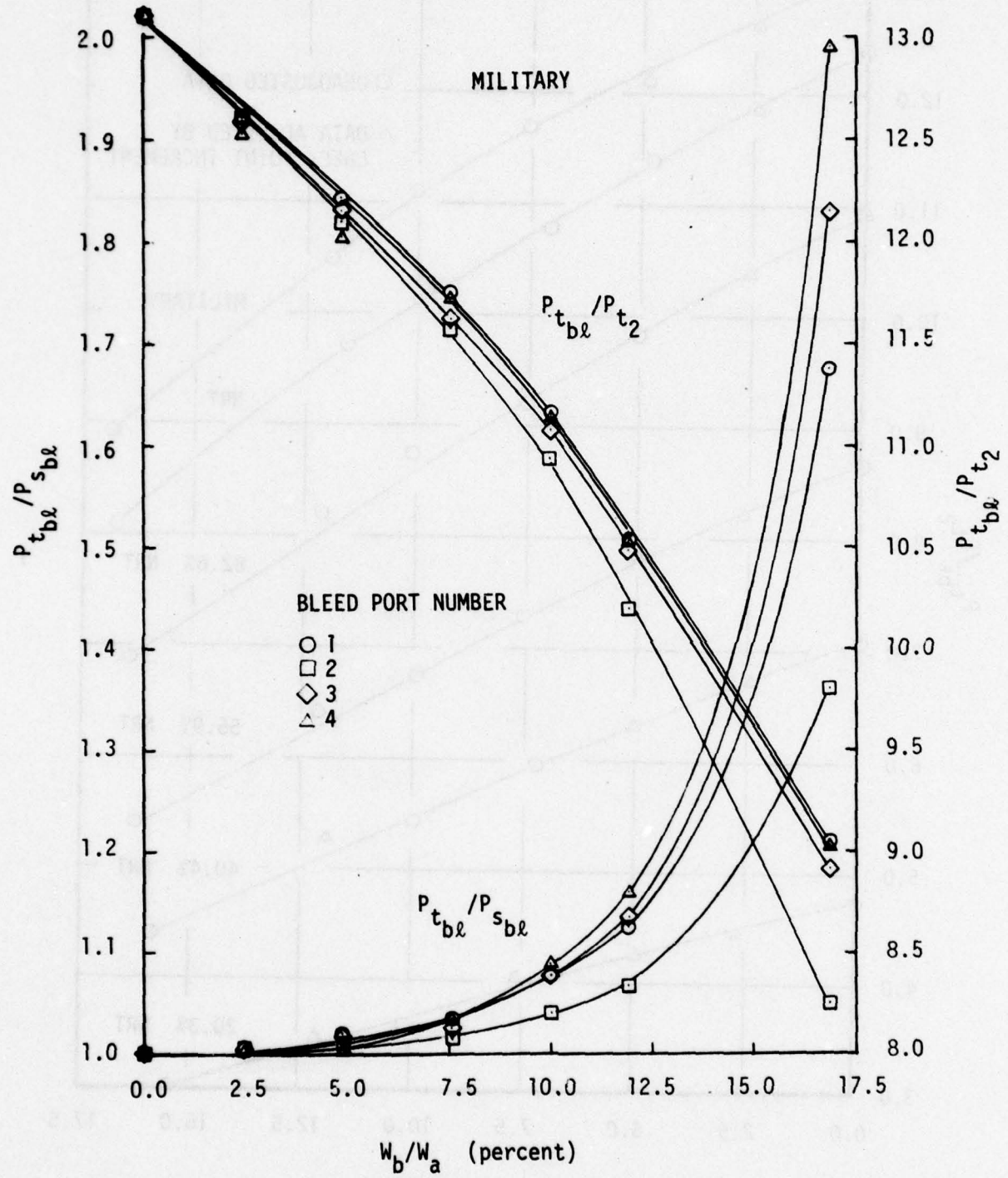


Figure 29 - Individual Bleed Port Total Pressure Ratio and Total to Static Pressure Ratio as a Function of Bleed Flow Extraction Rate at Military Thrust

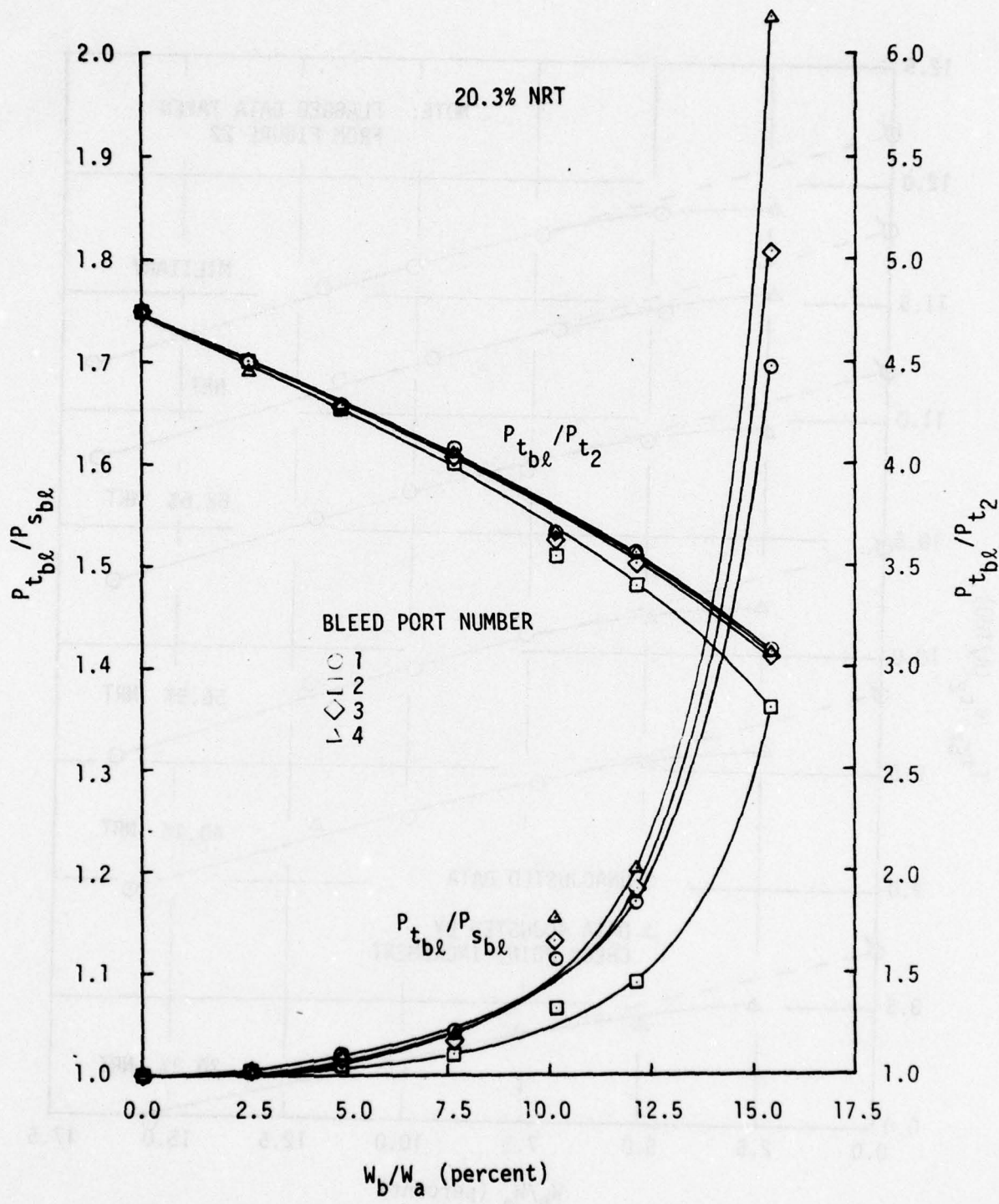


Figure 30 - Individual Bleed Port Total Pressure Ratio and Total to Static Pressure Ratio as a Function of Bleed Flow extraction Rate at 20.3-percent NRT

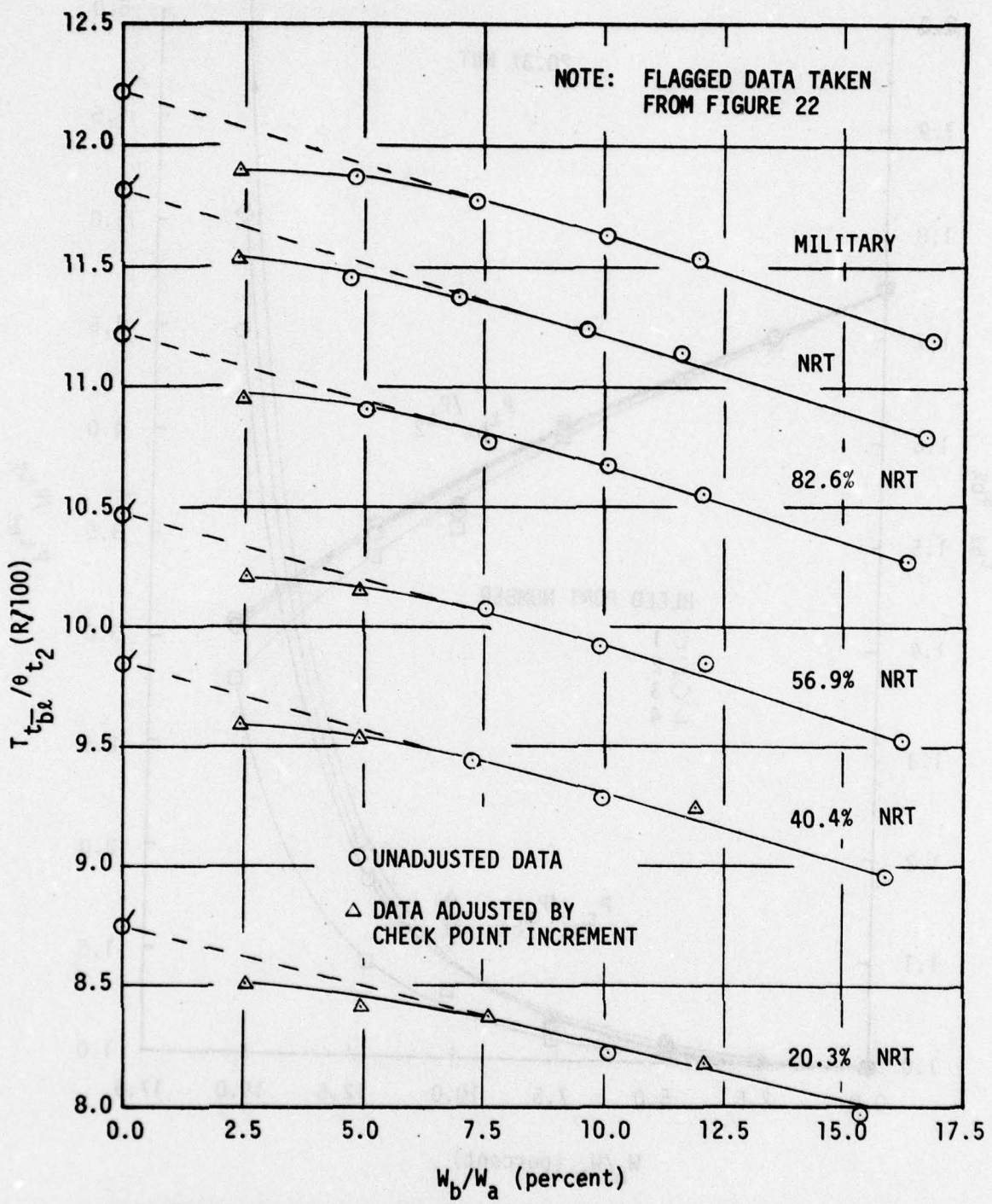


Figure 31 - Average Bleed Port Temperature as a Function of Bleed Flow Extraction Rate

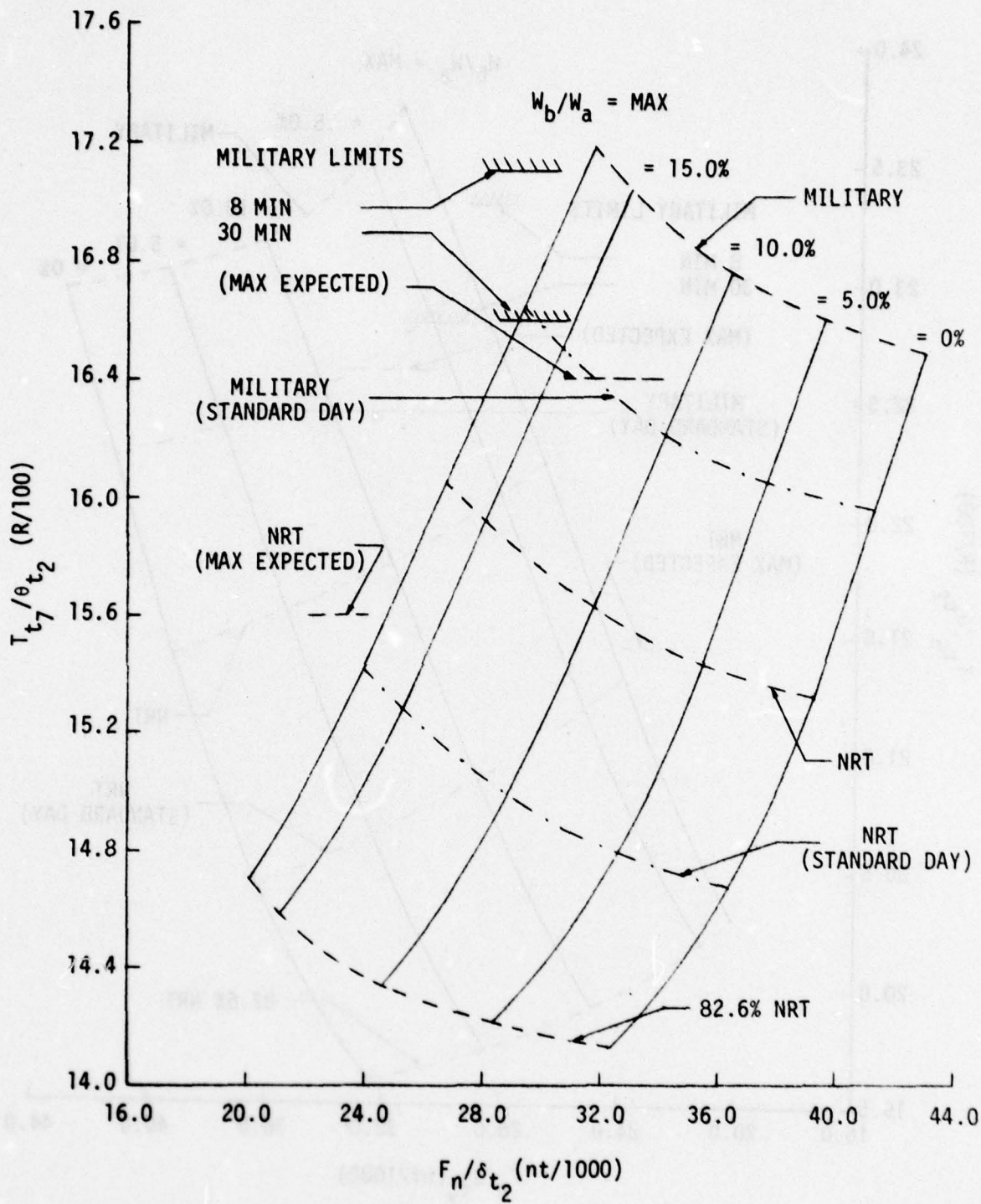


Figure 32 - Turbine Exit Temperature as a Function of Net Thrust  
for Various Values of Bleed Flow Extraction Rate

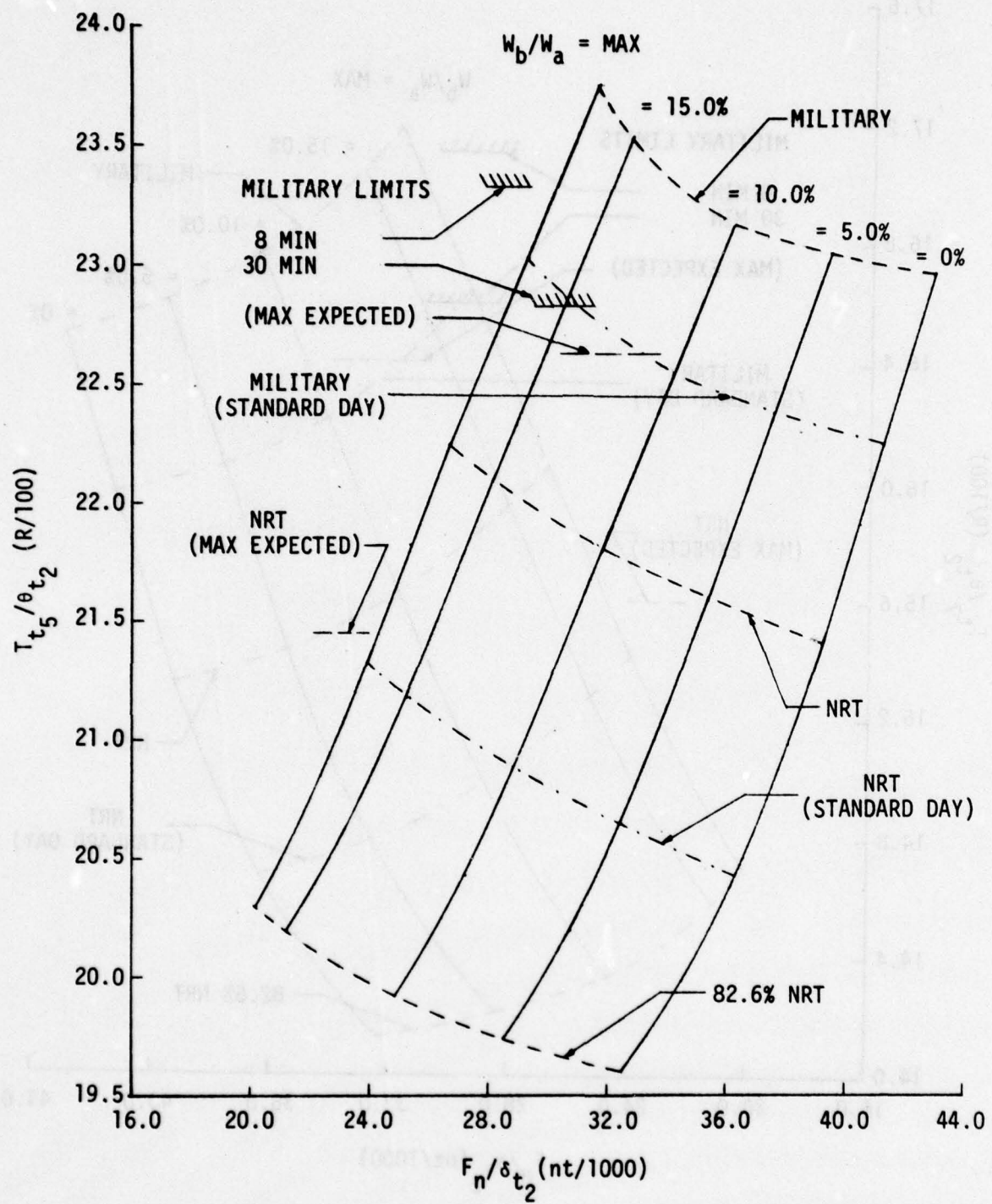


Figure 33 - Turbine Inlet Temperature as a Function of Net Thrust  
for Various Values of Bleed Flow Extraction Rate

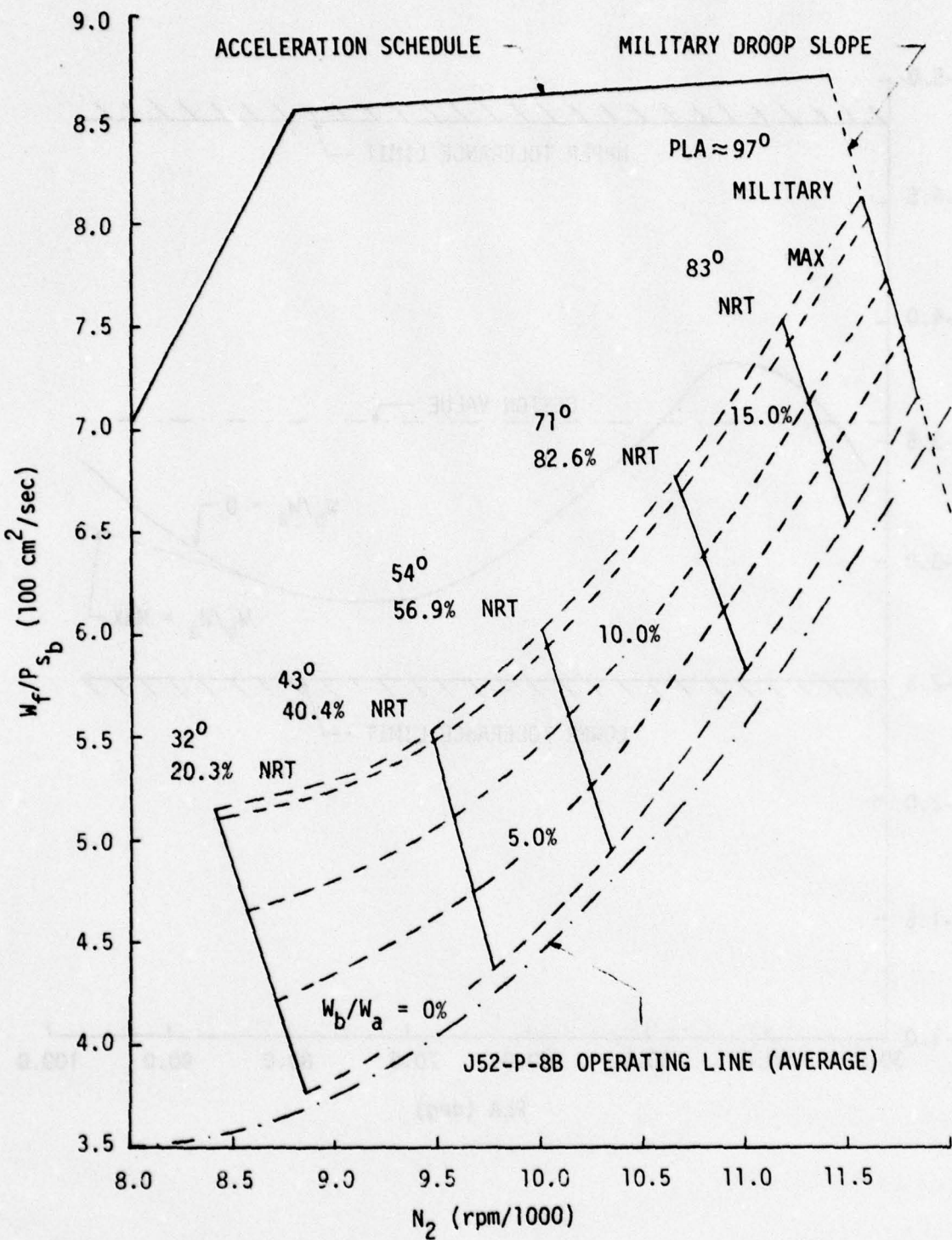


Figure 34 - Steady State Operating Line Performance as a Function of Bleed Flow Extraction Rate

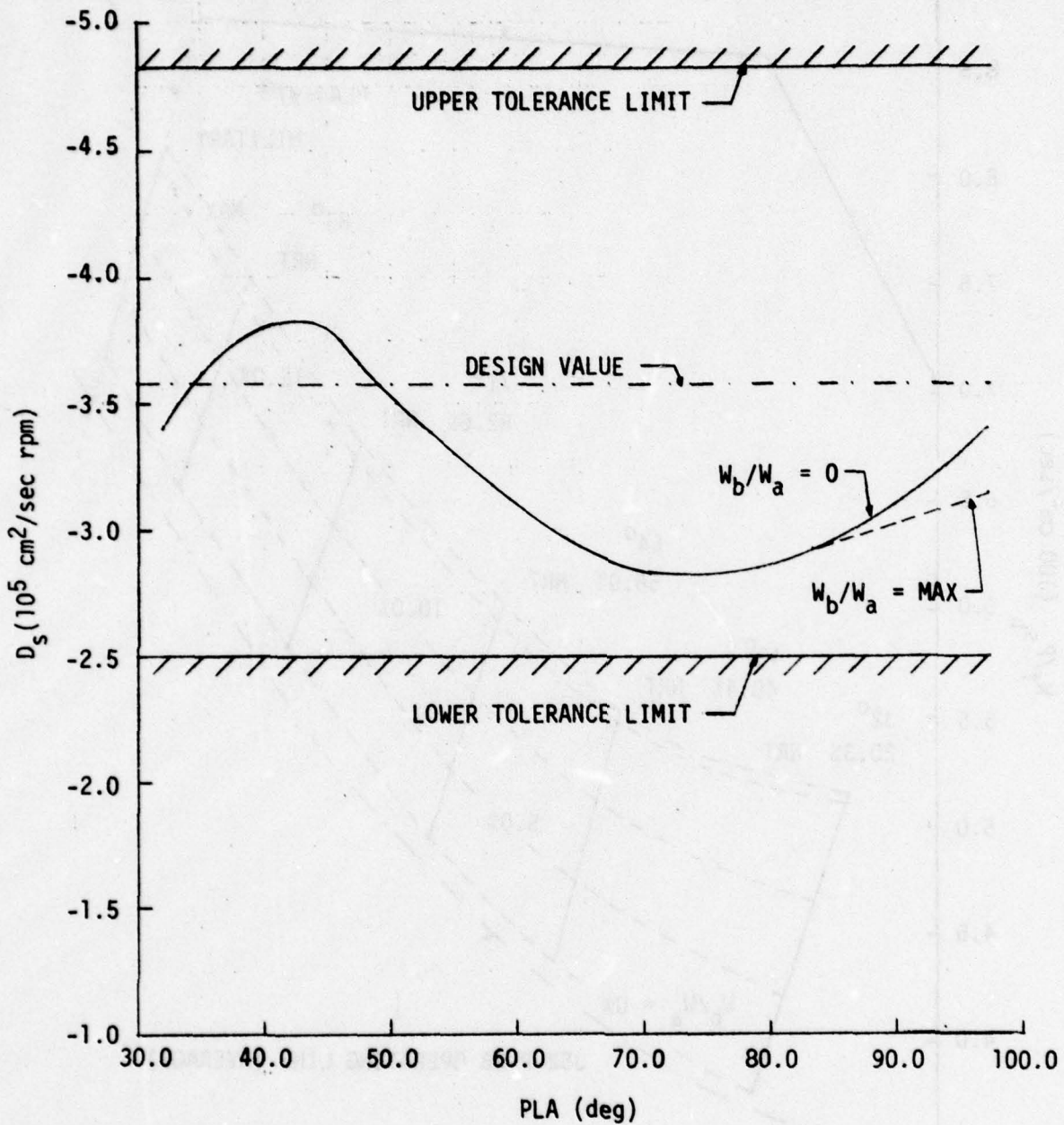


Figure 35 - Speed Governor Droop Slope Performance

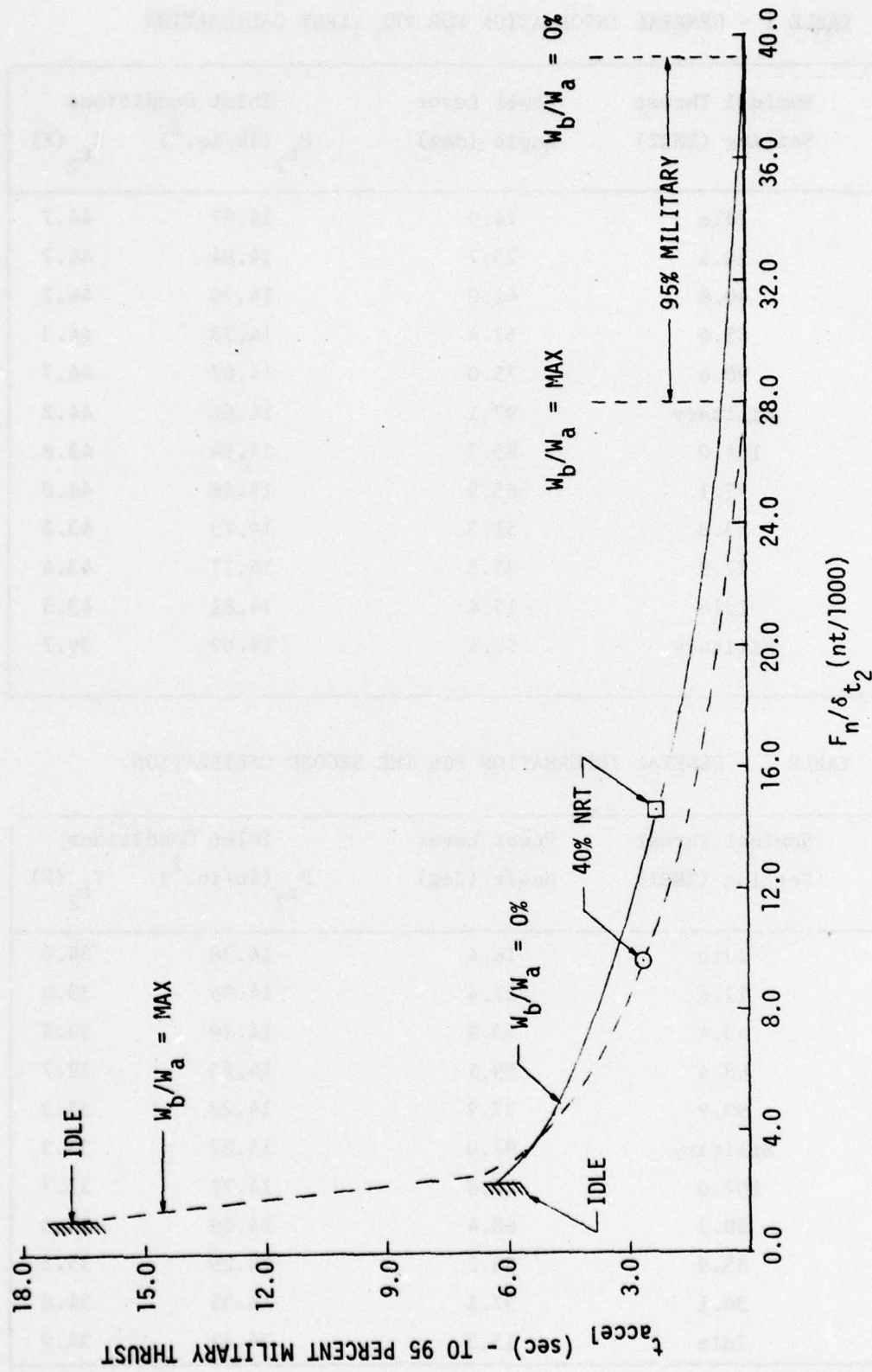


Figure 36 - J52-P-8A Engine Acceleration Performance with Zero and Maximum Bleed Flow

TABLE 1 - GENERAL INFORMATION FOR THE FIRST CALIBRATION

Point Number	Nominal Thrust Setting (%NRT)	Power Lever Angle (deg)	Inlet Conditions	
			$P_{t_2}$ (lb/in. <sup>2</sup> )	$T_{t_2}$ (F)
6	Idle	14.9	14.87	44.7
7	14.1	25.7	14.84	44.7
8	40.8	42.0	14.70	44.2
9	65.6	57.4	14.73	44.3
10	90.6	75.0	14.67	44.7
11	Military	97.1	14.62	44.2
12	104.0	85.2	14.64	43.8
13	77.1	65.9	14.68	44.0
14	53.3	51.3	14.73	43.2
15	27.9	35.5	14.77	43.4
16	Idle	15.4	14.81	43.5
17	Military	97.1	14.62	39.7

TABLE 2 - GENERAL INFORMATION FOR THE SECOND CALIBRATION

Point Number	Nominal Thrust Setting (%NRT)	Power Lever Angle (deg)	Inlet Conditions	
			$P_{t_2}$ (lb/in. <sup>2</sup> )	$T_{t_2}$ (F)
165	Idle	16.4	14.38	34.6
166	17.6	27.4	14.35	33.8
167	43.4	43.9	14.29	33.8
168	68.4	59.1	14.25	32.7
170	93.9	77.7	14.22	33.3
171	Military	97.0	14.22	33.3
172	107.0	88.3	14.22	33.7
173	80.3	68.4	14.29	35.3
174	55.9	53.2	14.29	35.3
175	30.1	37.1	14.35	34.8
176	Idle	15.3	14.41	34.9

TABLE 3 - GENERAL INFORMATION FOR THE BLEED FLOW CALIBRATION

Nominal Bleed Flow Rate (%)	Nominal Thrust Setting (%NRT)	Point Number	Power Lever Angle (deg)	$P_{t_2}$ (lb/in. <sup>2</sup> )	Inlet Conditions $T_{t_2}$ (F)
0.0	20	53	30.5	14.71	32.5
	40	59	41.9	14.64	31.5
	60	140	54.2	14.35	35.9
	80	130	70.5	14.29	36.9
	100	104	83.2	14.28	38.1
Military		115	96.9	14.22	38.5
0.0 (check pts)	20	143	32.0	14.45	34.9
	40	151	43.2	14.42	37.0
	60	155	54.2	14.39	37.3
	80	160	70.0	14.36	36.5
	100	158	83.2	14.33	36.6
Military		163	97.3	14.33	36.6
2.5	20	146	32.0	14.45	35.4
	40	152	43.2	14.42	36.9
	60	157	54.1	14.41	36.9
	80	161	70.0	14.36	36.7
	100	159	83.2	14.35	36.8
Military		162	97.4	14.33	37.2

TABLE 3 (Continued)

Nominal Bleed Flow Rate (%)	Nominal Thrust Setting (%NRT)	Point Number	Power Lever Angle (deg)	Inlet Conditions	
				$P_{t_2}$	$T_{t_2} (F)$
5.0	20	148	31.9	14.46	37.5
	40	153	43.3	14.43	36.4
	60	156	54.2	14.41	37.4
	80	135	70.5	14.32	36.0
	100	112	83.2	14.25	38.0
	Military		96.9	14.22	38.3
	20	149	31.9	14.46	37.2
	40	64	41.9	14.65	31.3
	60	139	54.2	14.38	35.7
	80	134	70.5	14.32	36.3
7.5	100	111	83.3	14.26	37.5
	Military		96.6	14.23	37.6
	20	55	30.5	14.71	32.0
	40	68	41.9	14.67	31.4
	60	138	54.2	14.38	35.7
	80	133	70.5	14.32	36.5
	100	109	83.3	14.28	38.0
	Military		96.5	14.22	37.7
	20	55	30.5	14.71	32.0
	40	68	41.9	14.67	31.4

TABLE 3 (Continued)

Nominal Bleed Flow Rate (%)	Nominal Thrust Setting (%NRT)	Point Number	Power Lever Angle (deg)	$P_{t_2}$ (lb/in. <sup>2</sup> )	Inlet Conditions $T_{t_2}$ (F)
12.0	20	147	32.0	14.46	36.5
	40	154	43.3	14.45	37.3
	60	137	54.2	14.38	35.6
	80	132	70.5	14.32	36.7
	100	108	83.2	14.29	38.1
Military		124	97.1	14.25	38.1
Maximum	20	56	30.5	14.73	31.7
	40	69	41.9	14.67	30.4
	60	136	54.2	14.38	36.0
	80	131	70.5	14.33	36.6
	100	106	83.2	14.30	38.5
Military		125	96.9	14.25	38.1

## APPENDIX

### EXPERIMENTAL APPARATUS, INSTRUMENTATION, AND TECHNIQUE

#### COMPRESSOR BLEED MANIFOLD SYSTEM

The J52-P-8A engine has four bleed ports from which bleed flow can be extracted. These ports are located radially about the high pressure compressor discharge area. Three of these ports have diameters of 2.25 in. (5.715 cm), and the remaining port (fuel heater port) has a smaller diameter of 1.25 in. (3.175 cm). To measure the bleed flow quality and quantity, it was necessary to manufacture a manifold system to collect the individual bleed flows from each port and deliver them to the measuring nozzles. This manifold system can be seen in the various photographs of the engine (Figures 2-6). The system consists of four individual bleed flow collectors, the main body of the compressor bleed manifold, and two supply lines with each accommodating a reducer pipe, a butterfly valve, and a 90-deg elbow downstream of the butterfly valve. Figure A.1 shows a schematic of the main body of the manifold and the bleed flow collectors. Also shown in the figure is the identification used for the bleed flow collectors and supply lines. The individual bleed flow collectors delivered the outputs of each bleed port to the main body of the compressor bleed manifold for common stagnation. These bleed flow collectors also provided for thermal expansion of the compressor bleed manifold and reduced vibration levels by the use of corrugated flexible metal tubing. The main body of the manifold delivered the stagnated flow to the pipe reducers through the supply lines. The butterfly valve (Figure 7) located in each of these reducers provided for manifold backpressure regulation and thus controlled the quantity of bleed flow to the measuring nozzles. The 90-deg elbows were used to direct the bleed flows exiting from each measuring nozzle perpendicular to the engine thrust axis so no force of the bleed flow would be measured by the thrust stand.

#### BLEED FLOW QUALITY MEASUREMENT AT THE BLEED PORTS

A knowledge of the total temperature and pressure as well as the static pressure at the bleed ports is required to completely describe the

bleed flow quality. Due to the manner in which the bleed flow enters the bleed port area, it was suspected that local flow separation and/or a distortion of the flow distribution across the bleed port could possibly arise, particularly at the high bleed flow conditions. The following paragraphs discuss the design of the components of the compressor bleed manifold near the bleed ports and the rationale behind the design. The validity of the results of the bleed flow quality measurements is also discussed.

The structural arrangement of the compressor bleed manifold hardware located at the face of the bleed ports consisted of a mounting plate and an expansion duct which delivered the bleed flow to the corrugated flexible metal tubing. These features are shown in the various photographs of the engine, and specific details of this arrangement for one of the large bleed ports are shown in Figure A.2. A static tap was located in the mounting plate 0.25 in. (0.64 cm) from the bleed port face. Total pressure was measured by a Kiel total pressure probe located in this same plane with an immersion depth of one-third of the local diameter. The total temperature was measured by a chromel alumel temperature probe located further downstream in the expansion duct, as noted on these figures, also with an immersion depth of one-third of the local diameter. Measurement of the total temperature conditions at this location is representative of those existing at the bleed port face; however, some concern over the accuracy of the pressure measurements was given due to the possibilities of flow angularity, local flow separation, and distortion of the flow distribution in the measuring station plane. The design of the mounting plate and the location of the pressure instrumentation devices were influenced by a need to minimize the possibility of either inducing or compounding a flow separation problem at the bleed port face. The expansion duct was designed to decrease the velocity of the bleed flow and deliver it to the flexible pipe without inducing separation and a subsequent loss in pressure as would occur in an abrupt expansion joint. The ratio of the flexible pipe cross-section area to the bleed port area for the smaller bleed port was designed to be the same as the area ratio associated with the larger bleed ports. This was done to make the static pressure in the smaller bleed port as close as possible to the static pressure present in the larger bleed ports. In

essence, this can be viewed as an attempt to minimize the effect of a non-uniform backpressure distribution on the engine.

A Kiel total pressure probe was used to measure the bleed port total pressure due to its capability of accepting flow angularity up to 40-deg; but no guarantee on accuracy could be provided if the flow distribution became significantly distorted, which was a possibility at the higher bleed flow rates. To insure the validity of these particular measurements, another measurement of total pressure was taken. This measurement was accomplished by positioning four static taps on the outside wall of the compressor bleed manifold. These taps were located to coincide with the axial centerline of each bleed port and should thus provide a realistic value of the bleed port total pressure even if a highly distorted pressure distribution existed at the bleed port measuring station. One of these taps is shown in Figure 6. Results of the bleed flow calibration indicate that these taps measured total pressures only slightly lower than the values obtained by the Kiel probes at the bleed port measuring station. This is encouraging as some minimal pressure drop can be expected due to the pressure losses through the flexible pipe and its junction with the compressor bleed manifold pipe. The fact that a high level of correlation exists between these two measurements confirms that the total pressure information obtained by the Kiel probes is valid. It also confirms, to some degree, that a local separation problem at the bleed port measuring station, if present, was not so severe as to produce a significant distortion of the flow distribution.

Flow impingement on the bleed port static taps induced by flow angularity and/or separation in the locality of the taps could invalidate the static pressure measurements during the bleed flow calibration. To assess the validity of these measurements, Figure A.3 is presented. This figure is derived from the data taken during the bleed flow calibration and presents the ratio of the actual bleed flow ( $W_b$ ) to the one-dimensional isentropic bleed flow ( $W_{b_i}$ ) as a function of the corresponding isentropic Mach number ( $M_i$ ). These values are obtained by applying the subsonic one-dimensional isentropic flow equations to the information gathered at the bleed ports as follows:

$$W_{b_1} = A_{b_1} P_{t_{b_1}} \sqrt{\frac{2g\gamma}{(\gamma-1)RT_{b_1}}} \left[ \left( \frac{P_{s_{b_1}}}{P_{t_{b_1}}} \right)^{2/\gamma} - \left( \frac{P_{s_{b_1}}}{P_{t_{b_1}}} \right)^{\gamma+1/\gamma} \right]$$

$$M_1 = \sqrt{\frac{2}{\gamma-1} \left[ \left( \frac{P_{t_{b_1}}}{P_{s_{b_1}}} \right)^{\gamma-1/\gamma} - 1 \right]}$$

The pressures and temperatures used were the numerical average of the values obtained by the individual bleed ports. Data are shown on the figure enveloping the thrust range covered during the bleed flow calibration.

The curve shows a decrease in the bleed flow ratio at low Mach numbers and appears to remain at a nearly constant value of about 0.82 at the moderate and higher Mach numbers. The fact that the bleed flow ratio is less than unity indicates that the static pressure measurements are somewhat lower than the actual static pressures at the bleed ports and can be viewed as a decrease in the effective area of the bleed ports. Flow impingement on the static taps would have the effect of increasing the static pressures measurements above the isentropic value, i.e., the opposite trend present in the figure. Based on this fact and the trend noted in the figure, it appears that local flow separation near the static taps was present, as separation could induce the static pressure measurements to be lower than the corresponding isentropic values. This figure also shows that for single nozzle operation, the manifold system pressure losses were somewhat dependent on which supply line was used to deliver the bleed flow to its respective measuring nozzle. This is shown in Figure A.3 by noting the higher bleed flow ratios obtained when using supply line 1 alone in comparison to using supply line 2 or both supply lines in combination.

As mentioned previously, the maximum bleed flow may be limited by the manifold system pressure losses and not by choking of the flow at the bleed ports. This statement is founded on the information that is presented in Figure A.3. At the maximum bleed flow conditions the associated Mach number is approximately 0.90 for all thrust levels presented in the figure. Physically, this is the Mach number required to pass the flow through the effective area of the bleed ports if the flow process was purely isentropic. This information implies that the flow at the bleed ports is nearly, but not entirely, choked. However, the maximum bleed flow values obtainable from the engine, if not limited by the manifold system pressure losses, could only be a small fraction greater than those values obtained during the investigation. This is substantiated by noting that for an isentropic flow process, the actual flow rate is relatively insensitive to changes in Mach number near the sonic condition. For a Mach number of 0.9, the isentropic flow rate is within 1 percent of the isentropic choked flow rate.

#### BLEED FLOW MEASUREMENT TECHNIQUE

The method for determining the quantity of bleed flow taken from the engine was the use of a calibrated convergent nozzle. It has been experimentally determined (Reference 7) that for a nozzle convergent half angle of 8 deg, the nozzle discharge coefficient ( $C_n$ ) becomes independent of the backpressure (ambient pressure during this investigation) if the nozzle pressure ratio is maintained at a value of three or more. Under these conditions  $C_n = 0.988$ . The fact that  $C_n$  is constant in this region allows the elimination of a static pressure measurement at the nozzle exit as the airflow passing through the nozzle can be determined solely by the total temperature ( $T_{t_n}$ ), total pressure ( $P_{t_n}$ ), and the area ( $A_n$ ) of the nozzle. The calibrated convergent nozzle measuring technique was quite applicable for the measurement of bleed flow in this investigation as nozzle pressure ratios greater than three could be maintained (except at the very low thrust setting and low bleed flow rates).

As  $C_n$  represents the ratio of the actual airflow passing through the nozzle to the value obtained by a one-dimensional isentropic analysis, the

bleed flow ( $W_b$ ) is thus computed from the one-dimensional isentropic choked flow equation as:

$$W_b = C_n W_{b_1} = 0.526 A_n P_{t_n} / \sqrt{T_{t_n}}$$

where

$$W_{b_1} = A_n P_{t_n} \sqrt{\left| \frac{g\gamma}{RT_{t_n}} \right| \left( \frac{2}{\gamma+1} \right)^{\frac{\gamma+1}{\gamma-1}}} = 0.532 A_n P_{t_n} / \sqrt{T_{t_n}}$$

To accommodate the expected maximum bleed flow available from the engine, it was necessary to manufacture two convergent nozzles with an exit diameter of 3.1 in. (7.874 cm). The total area of these two nozzles is 15.10 in.<sup>2</sup> (97.37 cm<sup>2</sup>). To maintain a nozzle pressure ratio of three or more at low bleed flow rates, a smaller nozzle with a diameter of 1.875 in. (4.763 cm) was required. The area of this nozzle is 2.76 in.<sup>2</sup> (17.81 cm<sup>2</sup>) or approximately one-third the area of one of the larger nozzles. The larger nozzle is shown mounted to one of the ducting pipes in Figure 7; whereas, the relevant geometry of the small and large nozzles is shown in Figure A.4. In cases where two nozzles were used to pass the bleed flow, the total bleed flow is the sum of the individual flows from each nozzle as computed from the above equation.

Instrumentation devices used to measure the bleed flow exiting from each measuring nozzle were a chromel alumel total temperature probe and a Kiel total pressure probe. Immersion depth for these instrumentation devices was one third of the ducting pipe diameter. Because the flow at the measuring station was turbulent, and thus had a reasonably flat velocity profile, sensitivity of the immersion depth was not considered critical. The Kiel total pressure probe was chosen because it has the capability of accepting flow at high values of flow angularity before losing its accuracy. A probe of this type was deemed necessary, since the measurement station was located only 1.5-ducting pipe diameters downstream of the 90-deg bend in

the ducting pipe. At this location the possibility of flow angularity does exist. The nozzle exit plane was located 4.87-nozzle diameters downstream of the measuring station for the small nozzle and 1.53-nozzle diameters for the large nozzle. Based on these relatively short lengths, the total temperature and pressure conditions at the measuring station were representative of the conditions at the nozzle exit plane.

#### ENGINE INSTRUMENTATION

The performance and operating characteristics of the J52-P-8A engine were measured with off-the-shelf instrumentation devices developed specifically for engine performance evaluations. This section describes the types of instrumentation used to obtain the engine characteristics.

Engine airflow was computed using a Pratt and Whitney Aircraft 14000 bellmouth inlet. This inlet is shown installed on the engine in Figures 3-4. The most obvious feature seen is the bellmouth screen which provides protection to the engine from large particle ingestion. The bellmouth is believed to provide for a more uniform pressure distribution at the low pressure compressor face by the generation of a large number of small vortices. The bellmouth was instrumented with three total-static pressure probes located radially about the bellmouth near the compressor face. The static pressure from one of these probes was input to a 0 to 25 psia scanivalve and served as a reference for the remaining bellmouth pressures. The remaining pressures were input to a 0 to 5 psid scanivalve along with the reference to obtain the total and static pressures in the bellmouth. The bellmouth screen was instrumented with a thermocouple harness (see Figures 3-4) that allowed three bellmouth total temperatures to be measured. The average of the inlet total temperatures, total pressures, and static pressures were then used to compute the engine airflow from the one-dimensional isentropic subsonic flow equation as follows:

$$w_a = A_1 P_{t_2} C_i - \frac{2g\gamma}{(\gamma-1)RT} \frac{P_{s_2}}{P_{t_2}}^{2/\gamma} - \frac{P_{s_2}}{P_{t_2}} \frac{\gamma+1}{\gamma}$$

$$A_1 = 3.435 \text{ ft}^2 (3,191 \text{ cm}^2) = \text{bellmouth inlet area}$$

$$C_i = 0.993 \pm 0.001 = \text{bellmouth inlet pressure recovery factor}$$

The low pressure compressor-turbine unit speed was measured using an ILS-60 tachometer in conjunction with a Pratt and Whitney Aircraft reduction gear. The range of this unit is 0 to 11,500 rpm. The high pressure compressor-turbine unit speed was measured with an ILS-120 tachometer. This latter unit has a range of 0 to 12,300 rpm.

The high pressure compressor discharge total temperature and pressure were sensed using a five-finger total temperature rake and a five-finger total pressure rake, respectively. The outputs of the individual total pressures were input to a 0 to 250 psia scanivalve. An average of these five pressures was then computed. The individual outputs of the five thermocouples were averaged to obtain the temperature characteristics.

The fuel flow rate was monitored by using two 0.75-in. F&P sensors. Each of these units has a range of 0 to 10,000 lb/hr.

The burner pressure was measured by a static pressure tap used in conjunction with a 0 to 250 psia scanivalve.

The turbine exhaust total pressure and temperature characteristics were obtained by using a Pratt and Whitney Aircraft total pressure harness and temperature harness, respectively. The pressure harness has several total probes located radially about the engine just aft of the turbine. The outputs of these pressure pickups are ducted into a common pressure line to provide a pressure balanced average instead of a numerical average. The temperature harness has six thermocouple stations. The device can be

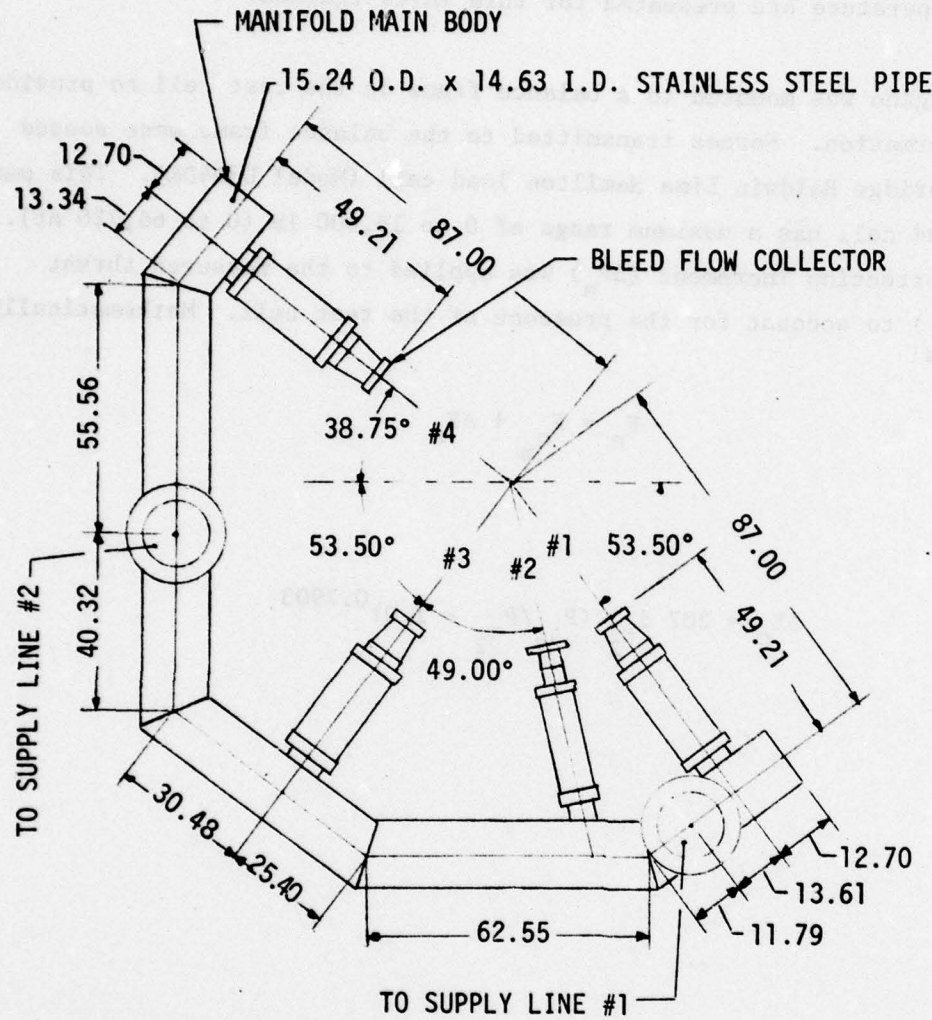
rigged to sense the individual outputs of each thermocouple and can also be wired to give an electrical average. The electrical average values of exhaust temperature are presented for this investigation.

The engine was mounted to a balance frame in the test cell to provide thrust information. Forces transmitted to the balance frame were sensed by a dual bridge Baldwin Lima Hamilton load cell (Model U3D4DR). This particular load cell has a maximum range of 0 to 15,000 lb (0 to 66,720 nt). A thrust correction increment ( $\Delta F_n$ ) was applied to the measured thrust forces ( $F_{n_m}$ ) to account for the presence of the test cell. Mathematically,

$$F_n = F_{n_m} + \Delta F_n$$

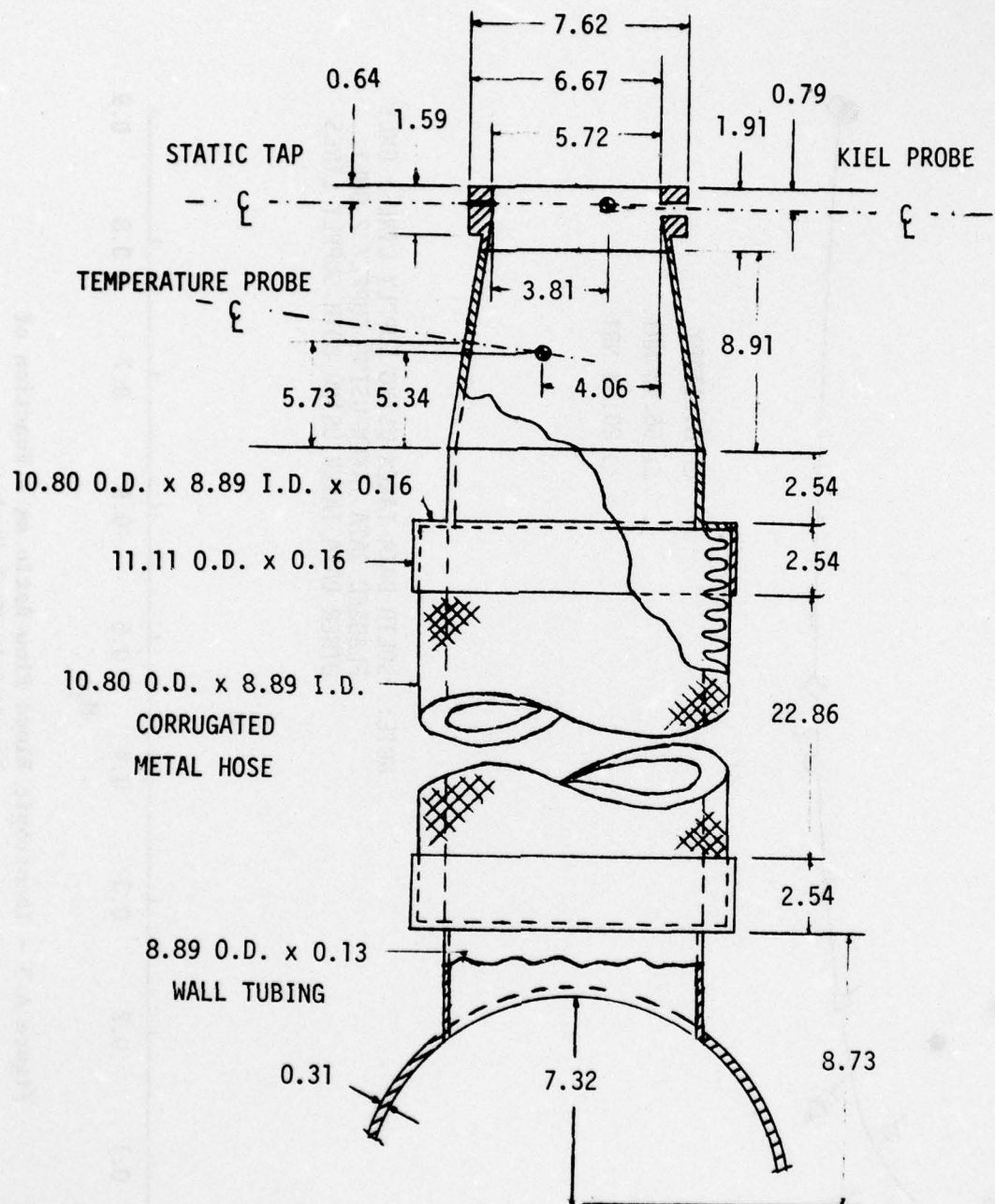
where

$$\Delta F_n = 207 \delta_{t_2} (P_{t_7}/P_{t_2} - 1.0)^{0.7903}$$



ALL DIMENSIONS IN CM

**Figure A.1 – Detailed Schematic of the Compressor Bleed Manifold**



ALL DIMENSIONS IN CM

Figure A.2 - Detailed Schematic of One of the Individual Bleed Port Collectors

AD-A057 325

DAVID W TAYLOR NAVAL SHIP RESEARCH AND DEVELOPMENT CE--ETC F/G 21/5  
AN INVESTIGATION OF THE PERFORMANCE OF A J52-P-8A ENGINE OPERAT--ETC(U)

AUG 77 R A HEMMERLY

DTNSRDC/ASED-387

NL

UNCLASSIFIED

2 OF 2

AD  
A057 325



END

DATE

FILMED

9-78

DDC

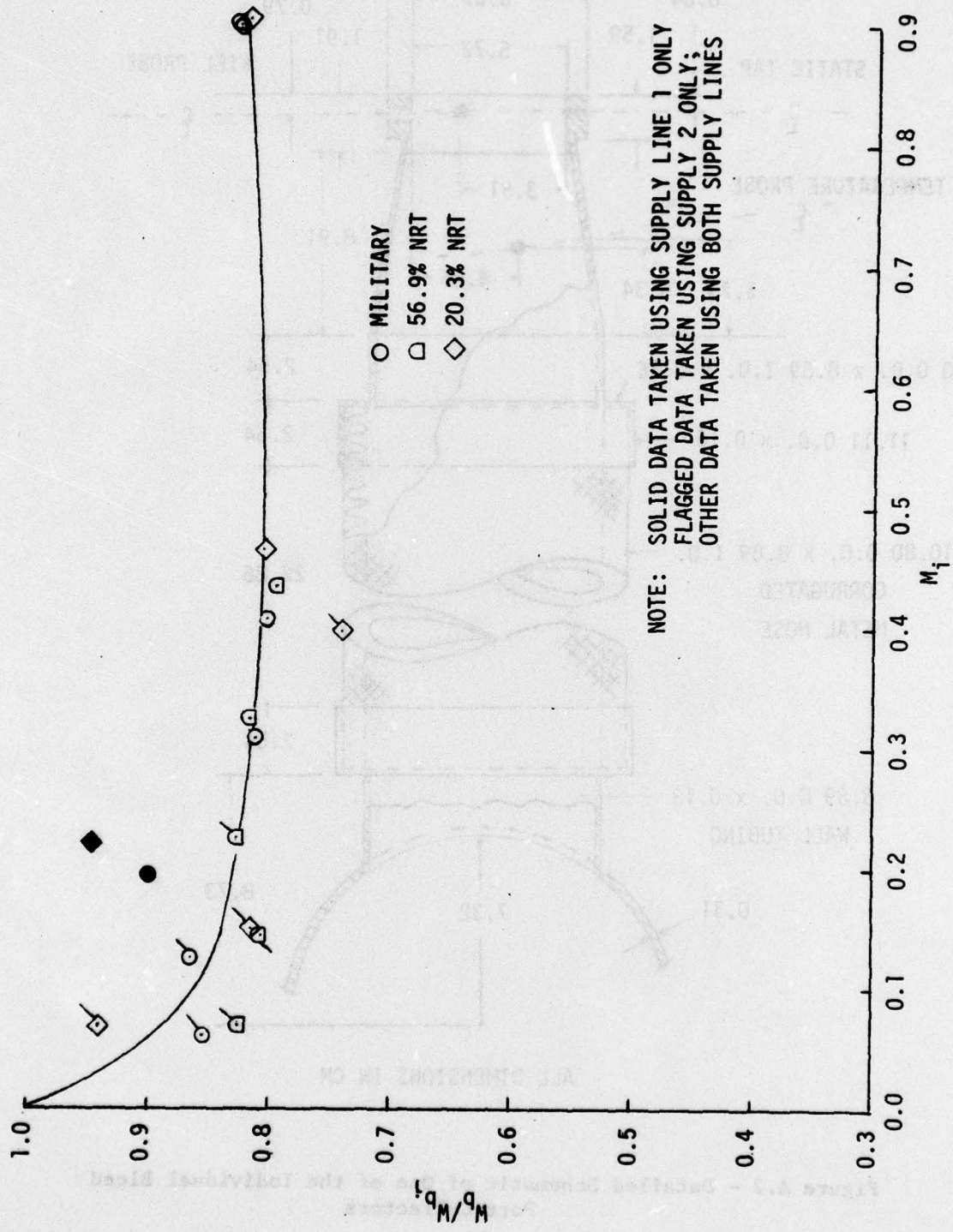


Figure A.3 - Isentropic Bleed Flow Ratio as a Function of Isentropic Mach Number

ALL DIMENSIONS IN CM

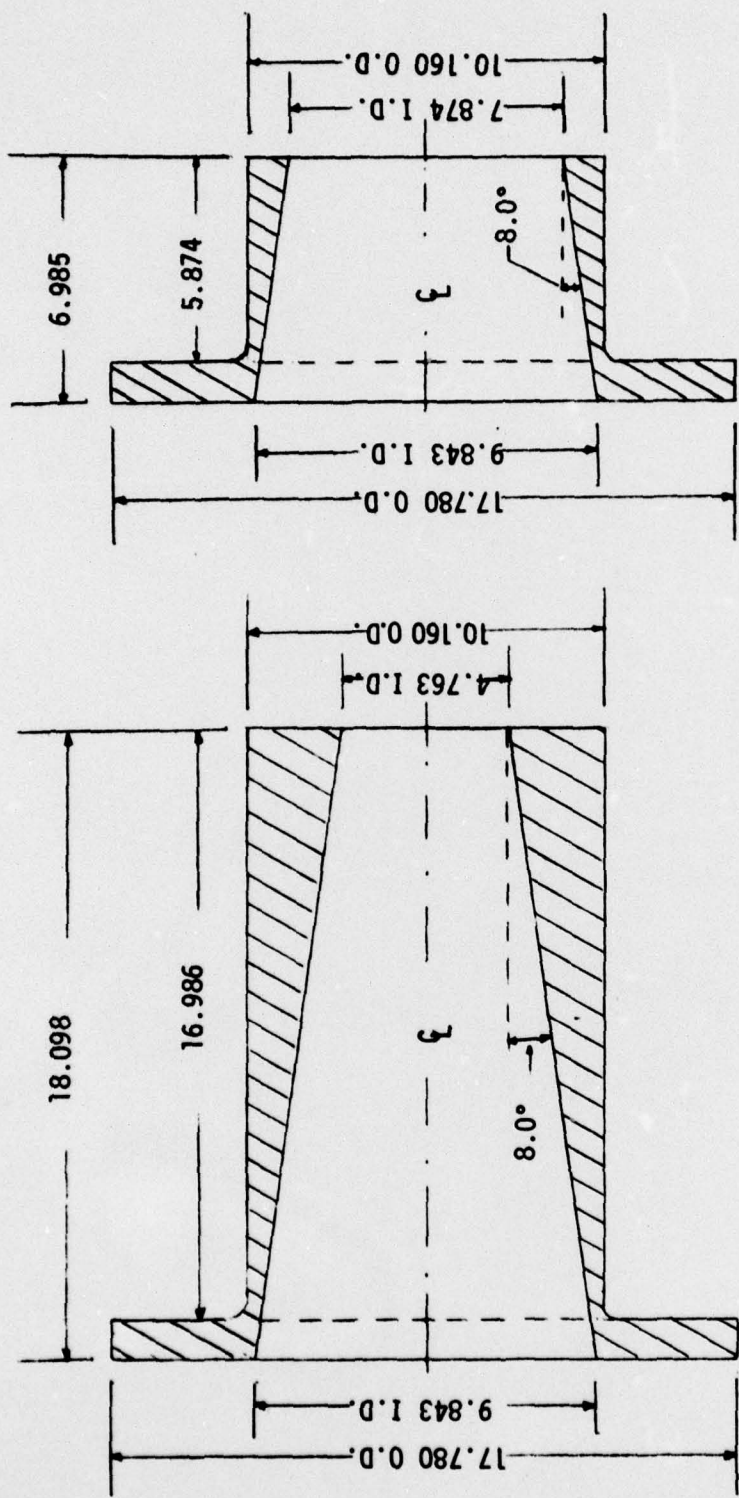


Figure A.4a - Small Diameter Measuring Nozzle

Figure A.4b - Large Diameter Measuring Nozzle

Figure A.4 - Cross-Section Views of the Small and Large Diameter Measuring Nozzles

**DTNSRDC ISSUES THREE TYPES OF REPORTS**

(1) DTNSRDC REPORTS, A FORMAL SERIES PUBLISHING INFORMATION OF PERMANENT TECHNICAL VALUE, DESIGNATED BY A SERIAL REPORT NUMBER.

(2) DEPARTMENTAL REPORTS, A SEMIFORMAL SERIES, RECORDING INFORMATION OF A PRELIMINARY OR TEMPORARY NATURE, OR OF LIMITED INTEREST OR SIGNIFICANCE, CARRYING A DEPARTMENTAL ALPHANUMERIC IDENTIFICATION.

(3) TECHNICAL MEMORANDA, AN INFORMAL SERIES, USUALLY INTERNAL WORKING PAPERS OR DIRECT REPORTS TO SPONSORS, NUMBERED AS TM SERIES REPORTS; NOT FOR GENERAL DISTRIBUTION.